THERMODYNAMIC MECHANISMS OF HELIX STABILIZATION IN A MODEL PEPTIDE AND PROTEIN

By

Ryan Murray

A Dissertation Submitted to the

Graduate School

In Partial Fulfillment of the

Requirements for the Degree of

DOCTOR OF PHILOSOPHY

Thomas J. Long School of Pharmacy and Health Sciences
Pharmaceutical and Chemical Sciences

University of the Pacific
Stockton, California

2022

THERMODYNAMIC MECHANISMS OF HELIX STABILIZATION IN A MODEL PEPTIDE AND PROTEIN

By

Ryan Murray

APPROVED BY:

Dissertation Advisor: Xiaoling Li, Ph.D.

Dissertation Co-Advisor: Bhaskara R. Jasti, Ph.D.

Committee Member: Xin Guo, Ph.D.

Committee Member: Liang Xue, Ph.D.

Committee Member: Narang, Ajit, Ph.D.

Graduate Studies: Bhaskara R. Jasti, Ph.D

THERMODYNAMIC MECHANISMS OF HELIX STABILIZATION IN A MODEL PEPTIDE AND PROTEIN

By

Ryan Murray

DEDICATION

To my wife, Toni Murray, and to my daughters, Ruby, Scarlett, and Hazel Murray

ACKNOWLEDGEMENTS

I would like to acknowledge Dr. Li for his support and giving me an opportunity to study in his and Dr. Jasti's lab. I appreciated his mentorship, suggestions, guidance, and support of my research, and enjoyed our discussions. I appreciate Dr. Jasti, his suggestions and guidance and for serving as my coadvisor. I'd like to thank Dr. Xue for allowing me to use his lab, his guidance and suggestions and serving on my committee. I'd like to thank Dr. Guo for serving on my committee and for his suggestions. I'd like to thank Dr. Ajit Narang for his support, encouragement, and suggestions, and for serving on my committee. I'd like to thank Dr. Mandeep Singh and Vanessa Rangel for helping run my DSC samples. I would like to thank Dr. Franz for running my NMR samples and for his suggestions and ideas. I would like to thank my lab mates Pramila, Sridivya, Jessica, and Jingda for their help, encouragement, and support. I would like to thank all the many other faculty and staff that have provided support and encouragement as well. I would like to thank Sonya for her help with forms, reminders, and support. I would also like to thank Lynda for her help in ordering supplies and her friendship. I am grateful for support for purchasing a differential scanning calorimeter from the National Science Foundation (MRI-1828179). Most of all, I would like to thank my wife and sweet children for their encouragement and support throughout my studies.

THERMODYNAMIC MECHANISMS OF HELIX STABILIZATION IN A MODEL PEPTIDE AND PROTEIN

Abstract

By Ryan Murray

University of the Pacific
2021

Biologics are large, complex therapeutic agents generally produced from living organisms. One group of biologics is peptide/protein based. Biological agents offer unique advantages over traditional therapeutics including longer half-lives, higher specificity, greater efficacy, and reduced off-target effects. However, protein/peptide based drugs suffer from both delivery and stability issues. The higher order of protein structures (secondary, tertiary, etc.) derive ~80% of their conformational stability from paltry hydrophobic effects, with net stabilization of 5-15 kcal/mole observed for many proteins. Loss of conformational stability can lead to increased aggregation, precipitation, and degradation; and reduced activity and side effects. To increase stability and improve other properties of the therapeutic agent, additives, referred to as excipients, are included in their formulation. Generally, stabilizing effects from excipients work by imposing enthalpic or entropic penalties on protein/peptide unfolding, increasing the free energy of the denatured state. How excipient stabilizes by what thermodynamic mechanism for a given protein/peptide is not always clear, requiring careful study and optimization for prospective agents. Much effort has gone into understanding excipient protection mechanisms and identifying potential liable regions like amino acid sequence and hydrophobic patches. One area that has received relatively little attention has been the effect of excipients on secondary structure (SS) thermodynamic stabilization/destabilization. SS features are major components of

biologic conformation in which deviations, even temporary, can lead to aggregation and precipitation. In this study, an experimental system is proposed to quantify and classify helix stabilization in a model peptide and protein. Thermodynamic stability was evaluated via helix unfolding in the peptide, or protein through use of circular dichromism (CD) and nuclear magnetic resonance (NMR) for model peptide polyL-lysine (PLL) and CD and differential scanning calorimetry (DSC) for model protein bovine serum albumin (BSA). The chosen molecular weight of the PLL polymer, adopts a helical structure, is neutral and a monomeric under tested conditions, making it an ideal model to evaluate excipient effects on helix stability. BSA is largely helical in nature, with most changes and aggregation behavior resulting from loss of helicity, making it a logical extension from the model peptide. Results showed stabilization from mannitol and trehalose being mainly enthalpically driven in both peptide and protein. Enthalpic destabilization was observed for PLL and BSA at low to mid concentrations but stabilizing for PLL and destabilizing for BSA at high concentrations, respectively. Moreover, use of entropy-enthalpy compensation (EEC) plots revealed primary stabilization mechanisms at varying excipient concentrations and types allowing for a classification system to be established under different conditions. Peptide/protein based therapeutics typically exist in a complex milieu of additives designed to enhance stability and performance, or allow novel delivery methods (oral, pulmonary, etc.) not typically available to such agents. Ultimately, this work provides a model for understanding excipient effects on helix stability in a complex system. Further work into other SS, higher order structures, as well as complex formulation systems in the model framework described in this work will help to improve the formulation optimization process.

TABLE OF CONTENTS

LIST OF TABLES

Table

LIST OF FIGURES

Figure

CHAPTER 1: INTRODUCTION

1.1 Biologics

Traditionally, the pharmaceutical marketplace has been dominated by what is now considered small molecule drugs. During the industrial revolution, dye manufacturing companies honed compound identification and organic synthesis techniques, allowing for the discovery and production of some of the earliest modern therapeutic compounds[1]. Well over a century later, myriad such compounds have been developed, produced, and used to treat various illnesses. Despite the significant number and sheer variety of small molecule drugs on the market, they share several similarities: i.e. a narrow size range on the order of 200-800 Da. Their absorption, distribution, metabolism, and excretion (ADME) behavior can often be predicable by a methodology similar to Lipinski's rule-of-five principles. Additionally, they are relatively non-selective and have the potential for off target effects[2]. Conversely, biologics are large complex macromolecules ranging in size from 3,000-300,000 kDa. They are generally produced through appropriately transfected cells, or other living organisms in the form of peptides, proteins, vaccines, DNA, or RNA rather than chemically synthesized. Moreover, they are very selective, posing less risk of off target effects[3]. This work will focus specifically on protein and peptide biologics.

Amino acid based drugs are a somewhat new class of therapeutics, having been first introduced in the form of vaccines in the late 19th century. However, with the advent of monoclonal antibodies, and an ability to express and produce a greater repertoire of peptides and proteins, the apparent benefits of biologics excited the pharmaceutical industry. This was due to their extreme specificity, lower risk of off target effects, and ability to address diseases less

accessible by small molecule compounds. While it is more difficult/expensive to develop and produce, generic biologic production and generic drug substitution of biologics is still in its infancy, potentially extending the revenue potential of any new biologic compound relative to synthetic drugs. Today there are hundreds of biologics on the market, with hundreds more undergoing clinical trials or development[3]. Applications for biologics range from cancers, infectious diseases, blood disorder, skeletal/muscle issues, eye, metabolic, skin, digestive, lung, and neurological disorders[3]. Currently, cancer, autoimmune, and infectious diseases comprise most of the treated ailments. In 2020 the total revenue from biologics are estimated to reached $313 billion dollars (relative $1,079.3 billion for small molecules)[4]. In 2016, six of the top eight revenue earning drugs were biologics[5].

Despite their increasing use and percentage of the market share, biologic therapeutics are often hamstrung due to their fragility. Slight deformation of their conformation or degradation during any of the production, formulation, or transportation steps can greatly affect efficacy, stability, and safety of this class of compounds. Moreover, due to these stability issues, biologics have short shelf storage times, complex transportation considerations (i.e. cold chain maintenance), and often require some form of extravascular administration. Because of this, optimizing biologic formulations to achieve required stability is of paramount importance.

Significant effort has gone into understanding stabilization mechanisms of biologics[6-13] to improve and expedite the formulation process. While excipient-biologic interactions are complex in nature, they can be broken down thermodynamically into two stabilizing/destabilizing components: enthalpic and entropic. In liquid formulation conditions, enthalpic and entropic protection mechanisms are described as preferential exclusion/hydration and crowding effects, respectively[9, 11, 14-18]. Overall increases from either component increases

the free energy of unfolding, thereby stabilizing the native conformation. Thermodynamically speaking, lyophilized and other solid formulations are also stabilized/destabilized enthalpically and entropically; however, the mechanistic protection mechanisms are more complex and debated[19, 20], but are typically described via water replacement and vitrification theory. A more detailed discussion on both liquid and solid formulation protection mechanisms will be discussed in later sections. It should be noted most solid formulations will need to be reconstituted prior to administration and will need adequate stability in the liquid phase as well.

Complicating the formulation optimization process is the specific interactions between various biologic agents and stabilizing additives. Buffers, disaccharides, crowding agents, surfactants, etc., can have different stabilizing/destabilizing effects depending on the protein/peptide agent being formulated, or the concentration of additive. Understanding how a given additive stabilizes a biologic therapeutic or specific component of the agent may help to improve the formulation process. Various studies have looked at factors such as hydrophobic patches[21], amino acid sequences[22] as a means to predict stability and excipient interactions; however, very little work has gone into understanding how secondary structure (SS) is stabilized in the liquid phase. This is important given that loss of secondary structure in even part, or temporarily can increase the risk of aggregation and precipitation. Having a general understanding and classification system to thermodynamically evaluate excipient interactions is proposed on SS features may help to improve the formulation process.

The present work explores the effects of various excipients on first a model helical peptide poly-l-lysine (PLL) and classifying said effects using an entropy-enthalpy compensation (EEC). Results from the PLL model were compared to a model protein bovine serum albumin

(BSA). Data from both peptide and protein are discussed and used as a means to evaluate and quantitate excipient interactions with helices in potential biologic therapeutics.

1.2 Characterization of Proteins and Peptides

Proteins are large complex molecules whose properties are largely determined through its amino acid (AA) sequence and chemical environment. Of the 20 naturally occurring AAs, it can be observed that there exists a large variance in size, pH, polarity, and hydrophobicity between them. Additionally, AAs and their accompanying peptide backbone bonds present no stable geometric features leading to their organization into SS and tertiary structures. The peptide backbone consists of an amide bond formed from the amine and carboxylic acid groups of two adjacent amino acids. For labeling purposes, (and because cellular machinery synthesizes proteins in this direction) the convention is to start numbering AAs from the N-terminal end and proceed to towards the carboxylic C-terminal in a given sequence. The resulting amide bond possesses approximately 60% sp^2 character making rotation about amide bond impossible[23, 24]. As a result, only two conformations are possible between two amino acids: cis, or trans. The later occurs in nearly all cases, except in the presence of proline in a sequence. Moreover, this lack of rotation means there is a formation of a plane between the backbone elements of two amino acids which possess an angle of 180^o and a torsional angle (labeled omega ω (see Figure 2.1)). The two other torsional angles phi ϕ and psi ψ describe the rotational angles between the amide and alpha carbon and amine and carbonyl atom, respectively (see Figure1.1).

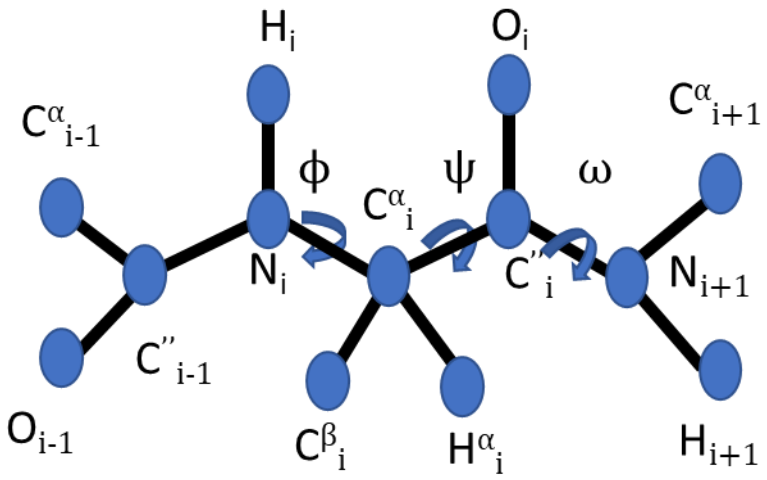

Figure 1.1 Anatomy of peptide/protein bonding and nomenclature.

Phi and psi angles can vary from -180^{o} to +180^{o} but are limited due to steric clashes between the carbonyl oxygen, amide hydrogen, and the alpha carbon hydrogen. Phi angles are calculated by looking down alpha carbon towards the amide bond and noting the angle between alpha carbon and *i*-1 carbonyl. Likewise, psi angles are determined through looking down the alpha carbon towards the *i* carbonyl and noting the angle between the *i*+1 and *i* amide.

Given the chemical properties of amino acids, peptide back bones, and the torsional angles they form, we can now discuss the formation of higher order structures such as secondary structure (SS), tertiary structure, and quaternary structure. As previously stated, the amide bond creates a plane between adjacent residues, and the phi and psi torsional angles are free to rotate 180^{o}; however, they are affected and limited by steric hindrance from other residue elements such as backbone features and side chain as well as any favorable/unfavorable solvent interactions. The angles adopted by the phi and psi are what give rise to SS features. SS elements such as helices and sheets allow for efficient hydrogen bond formation between

hydrogen donors and receivers[23] as well as minimize unfavorable hydrophobic interactions with aqueous solvents.

Tertiary structure comprises all SS elements and the overall folded conformation of the protein or peptide. Given the varied nature of AA side chains, the phi and psi dihedral angles, tertiary structure is greatly affected by AA sequences and environmental conditions. For globular proteins, solvent hydrophobic effect contributes 80% to protein folding[25]. Some proteins may even join other proteins creating a quaternary structure as is sometimes the case for some enzymes and cofactors.

1.3 The Protein Problem

Stability is of paramount importance in the preparation of fragile biologics. Stability can be classified in two ways: chemical and physical. The latter, physical (conformational) stability will be the focus of this work; however, physical and chemical stability are often inexorably linked.

1.4 Chemical Degradation

Chemical degradation is an important consideration for all protein-based therapeutics and can proceed through myriad pathways. These can be encompassed into broad classifications such as deamidation, hydrolysis, and oxidation.

Deamidation generally refers to the hydrolysis of an Asp or Gln residue amide side chain. Such reactions generally proceed via intramolecular cyclization, forming succinimide intermediate, then undergo amide cleavage[8, 9]. Deamidation rates are enhanced when the asp neighbor residues possess small side chains such as glycine, which reduces any steric hindrance that might otherwise interfere with the cyclization step. Additionally, pH conditions will factor

in deamidation propensity[9], requiring careful attention to pH conditions when preparing biologics with deamidation hotspots.

Hydrolysis proceeds via acid/base catalyzed amide cleavage. Like deamidation, it is enhanced by asp residues, especially when said residues are adjacent to a proline. It is especially common in the hinge region of monoclonal antibodies (mAbs), and can be catalyzed with poorly chosen buffers, radical species present in solution and metal catalysis[9].

Oxidation occurs through free radical generation, forming reactive oxygen species (ROS) which can damage most residues. Sources include metal catalyzing oxidation (MCO) species, as well as light exposure are common culprits[9]. Certain residues such as Met and Trp are most vulnerable to oxidation[9].

While degradation types may vary, molecular motion is a common contributor factor among them. Movement exposes liable sites and the diffusion of degradant material to them. As such, conformation contributes significantly to degradation rates of proteins and can be a good predictor of liable hotspots on a biologic compound. Helices, and sheets, reduce molecular motion of a protein relative to random coils, or disordered regions. Folding and unfolding of a protein also increase degradation propensity. In light of this, formulations which enhance conformational stability will in many instances enhance chemical stability.

1.5 Physical Instability

Physical stability is associated with three broad categories: conformational, colloidal and interfatial[26]. Conformational instability can occur through thermal stresses, chemical denaturation, or dehydration. Protein stability is often associated with conformational stability defined by transition temperature T_m. Essentially, the greater the T_m the more stable the native structure (though there are many caveats to this axiom that shall be discussed later). Contrary to

the increasing T_m conditions mentioned above, where folding/unfolding is entropically driven, cold temperature denaturation at or below the freezing point reduces the hydrophobic effect as water movement decreases, becoming more ordered around hydrophobic patches as crystallization begins[27]. This reduction can stabilize the unfolded state and denature the protein. Chemical denaturation through contact with chaotropic substances lowers the surface free energy of protein, thus increasing the concentration of denatured protein states[28, 29]. Dehydration during lyophilization removes structure stabilizing water from the protein surface, leading to loss of SS[30, 31]. Proteins may possess various charges and dipoles over their surface, leading to attractive/repulsive interactions affecting their colloidal stability which can be predictive of both aggregation propensity and solubility[26, 29, 32, 33]. Surface absorption/interface interaction can occur under many circumstances such as liquid-ice interfaces, air-water interface from vortexing, shaking, and container-liquid surface. Such interfaces provide a hydrophobic surface, allowing for protein unfolding, increasing the risk of protein aggregation and precipitation[8, 28, 29, 34, 35].

Protein aggregation can proceed through a variety of mechanisms with varying degrees of seriousness and is often a product of conformational change. Ultimately, it can lead to irreversible association, precipitation and inactivation of the desired compound[28, 29]. Many mechanisms attempting to explain aggregation have been put forward, and a basic model illustrating typical aggregation steps and pathways is shown in Figure 1.2.

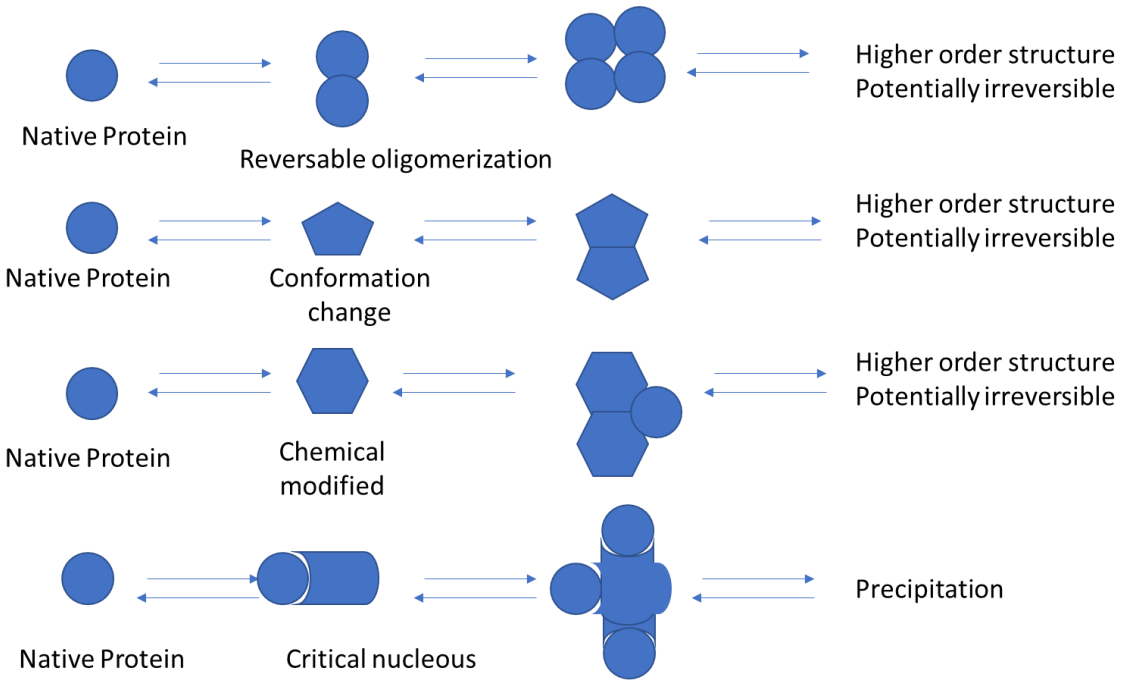

Figure 1.2. Peptide/protein aggregation and precipitation pathway.

Essentially, proteins can aggregate from the native or conformationally modified monomer to bi, tri, tetra and higher oligomers that have the potential to be reversible/irreversible. At a certain point, nucleation can occur, leading to large, insoluble aggregates.

1.6 Thermodynamic Principles

As previously discussed, chemical and physical degradation are major hindrances in the stability and delivery of biologics. Regardless of pathway, conformation maintenance is critical towards preserving form and function of such compounds over extended periods of time. Being large macromolecules with complex and environmentally sensitive features, understanding the principles behind stabilization is essential for successful formulations strategies. Traditionally, stabilization can largely be described from well-established thermodynamic principles.

Thermodynamics concerns itself with the relationship of different forms of energy as described by the three laws of thermodynamics. The first law states that energy is conserved

when undergoing different interconversion processes. The second law introduces entropy, followed by the third law which quantifies it[36]. Energy is a product of intensity factors (independent of material quantity i.e. temperature and pressure) and a differential of extensive property (mass and volume) of the system[36]. Taken together, thermodynamics allows for the quantification of work done by a system on its surroundings, heat transfer, whether a specific process/reaction is spontaneous or not, and can describe phase transitions of different substances under various environmental conditions. An ability to quantitate such factors is invaluable in evaluating formulation optimization of protein/peptide drugs. Of interest in the stabilization of proteins is determining the enthalpy, entropy, and Gibbs free energy of unfolding.

1.7 First Law of Thermodynamics

The first law of thermodynamics states that energy is conserved regardless of process or form that it takes; that it is a state function and can be expressed via equation 1 where E_2,and E_1, refer to the final and internal energy of the system, respectively, while *Q and W* refer to heat and work, respectively.

$$\Delta E = E_2 - E_1 = Q + W \quad (1.1)$$

Further examination of equation 1 allows the observation that work and heat are two equivalent ways of energy form interchange of a system. Being able to describe and quantitate the internal energy of a system is important in that it allows an understanding of how a system is behaving. For example, internal energy encompasses the microscopic motion of atoms, ions, molecules, and other relevant components of the system[36, 37]. Being able to account for such motion can shed light onto how molecules are rotating, vibrating, what energy state their electrons may be at, and to decipher various spectroscopic and thermographic spectrums.

To fully appreciate the first law, the other two laws and associated properties, a brief explanation of the state of a system, state functions and properties is required. A state system exists when all necessary variables to describe the system are defined[37]. The number and type of variables required to define a system will be system dependent, but in classical thermodynamic discussions typically are defined by P, V, T and n, representing pressure, volume, temperature and number of moles of a substance, respectively. A state function, on the other hand, describes the state of a system, and its properties depend only upon its current state, not how it got there; thus, a state function is path independent[37]. Finally, the thermodynamic properties and variables generally follow under two general categories, intensive and extensive properties. Intensive properties depend only on magnitude and are independent of quantity (i.e. temperature, pressure, density, etc.). Extensive properties do depend on amount (i.e. mass, volume).

For the first law it is observed that energy of a system is dependent on heat and work, two non-state path dependent parameters. However, if a system is allowed to infinitesimally change so that any change occurs under equilibrium conditions, the process can be considered reversible. Under such circumstances Q and W are represented as dq and dw, respectively.

While heat transfer and work are what determine the internal energy of a system, it is generally more convenient to measure other properties such as pressure, volume, and temperature. Taking an exact differential of internal energy ΔE of equation 1.1 as a function of temperature (T) and volume (V), we can establish the following relationship.

$$\Delta E = dq + dw = \left(\frac{\partial E}{\partial T}\right)_V dT + \left(\frac{\partial E}{\partial V}\right)_T \quad (1.2)$$

Under the first law, equation (1.1), it should be noted that specific conditions can create unique relationships between energy interconversions. For example, under constant heat (adiabatic conditions) dq goes to zero and changes in internal energy are equivalent to work done

by/to the system on its surroundings i.e. dE=dw. For constant temperature and constant volume, change in heat is equivalent to change in work done by the system (dq=-dw).

Under ideal gas conditions, work is defined as pressure (P) multiplied by surface area and change in height or volume (ΔV). $W = -P * \Delta V = -P(V_2 - V_1)$. Under reversible conditions where pressure increases by an infinitesimal amount, maximum work can be defined as illustrated by equation 1.3

$$W = \int_{V_1}^{V_2} dw = -\int_{V_1}^{V_2} Pdv = -nRT \int_{V_1}^{V_2} \frac{dV}{V} = -nRTln(\frac{V_2}{V_1}) \text{ (1.3)}$$

Alternatively, equation 3 can be expressed in terms of pressure due to Boyle's law $V_2/V_1=P_1/P_2$ leading to equation 1.4

$$W = -nRTln(\frac{P_1}{P_2}) \text{ (1.4)}$$

In the case of constant volume, change in energy is equivalent to change in heat, as can be deduced from equation 1.2. Under such conditions, equation 2 can reduce to $dqv = (\frac{\partial E}{\partial T})_V dT$ and can be expressed as the molar heat capacity at constant volume as:

$$C_V = \frac{dqv}{dT} \text{ (1.5)}$$

Molar heat capacity relates heat transferred during a change of state at constant volume.

We can explore the same relationship under constant pressure. Under such conditions, $W = -P\Delta V = -P(V_2 - V_1)$. Under these circumstances, the first law can be expressed by equation 1.6:

$$\Delta E = Q_P = -P(V_2 - V_1) \text{ (1.6)}$$

Where heat is absorbed under constant pressure. Rearranging equation 1.6 leads to equation 1.7 and an important new term, enthalpy.

$$Q_p = (E_2 + PV_2) - (E_1 + PV_1) \text{ (1.7)}$$

Enthalpy, H, encompasses the term $E + PV = H$. An increase in enthalpy is equivalent to heat absorbed by the system at constant pressure and the amount of heat needed to increase internal energy sufficiently to perform work of expansion by the system[37] as shown in the following equation:

$$\Delta H = \Delta E + P\Delta V \text{ (1.8)}$$

Enthalpy is a factor of state functions and as such is a state function as well. Taking the differential with respect to pressure and temperature yield the following relationship (equation 1.9):

$$dH = (\frac{\partial H}{\partial T})_P dT + (\frac{\partial H}{\partial P})_T dP \text{ (1.9)}$$

Since pressure is held constant, the second right hand term disappears, leaving the change in enthalpy with respect to temperature at constant pressure term. Because $dq_p = dH$ at constant pressure, we can define the molar heat capacity C_P as stated in equation 1.10:

$$C_P \equiv \frac{dq_p}{dT} = (\frac{\partial H}{\partial T})_P \text{ (1.10)}$$

For a change in enthalpy between products and reactants, or change between folded vs unfolded, Kirchhoff's equation may be used (equation 1.11):

$$\Delta C_P = [\frac{\partial(\Delta H)}{\partial T}]_P \text{ (1.11)}$$

ΔC_P is perhaps the most abstract of the commonly quantitated thermodynamic properties, yet it is one of the most informative quantities. ΔC_P through its shape and sign can indicate polar, or polar solvation, measure solvation effects, and illustrates the temperature dependence of entropy, enthalpy, and free energy on a system[38]; moreover, for the unfolding of a peptide/protein it represents the change in heat capacity between native and unfolded states[39-43] and correlates strongly with exposed surface area[44].

1.8 The Second Law of Thermodynamics

The second law of thermodynamics provides an explanation of why natural phenomena generally proceed only in one direction. The reason arises from the Carnot derived system property, entropy. From the second law as it will be shown, states that the entropy of the universe always increases. The result is that any natural phenomenon is highly unlikely to spontaneously reverse conditions back to the preceding state. This is typically proven in two ways: One, using a theoretical steam engine under reversible and non-reversible conditions; two, using the Boltzmann distribution equation in a statistical mechanical approach.

For the first method, engine efficiency is defined as work done divided by heat transferred (Efficiency=W/Q). We can see that engine efficiency will improve with greater temperature differential between a hot engine and its cold sink. This is expressed mathematically in equation 1.12:

$$\frac{W}{Q_{cold}} = \frac{Q_{Hot}-Q_{Cold}}{Q_{Hot}} = \frac{T_{Hot}-T_{Cold}}{T_{Hot}} = Efficiency \quad (1.12)$$

If T_{Cold} were to approach absolute zero, W/Q=1 and maximum efficiency would be achieved. If such a perfect engine operated under reversible conditions, then summing hot and cold heat over T_{Hot} would result in zero over an engine cycle (see equation 1.13):

$$\frac{Q_{Hot}}{T_{Hot}} + \frac{Q_{Cold}}{T_{Hot}} = 0 \quad (1.13)$$

As discussed earlier, heat is a path dependent variable; however, when divided by a state function such as temperature, a new path independent property is created, termed entropy. It can be expressed in terms of heat, or enthalpy (for infinitesimal changes) in equations 1.14 and 1.15, respectively.

$$\Delta S = \frac{Q_{Hot}}{T} \quad (1.14)$$

$$dH = (\frac{\partial H}{\partial T})_P \, dT \text{ (1.15)}$$

Q_{Hot}/T_{Hot} and Q_{Cold}/T_{Hot} are termed the entropy change at hot and cold, respectively, for reversible processes. Under such conditions, a cyclic process will result in a $\Delta S=0$. The significance means whatever entropy gained/lost in the system will be matched equally and oppositely by the surrounding environment and entropy of the universe remains unchanged. However, for an irreversible process this is not so, and universal entropy increases according to equation 1.16

$$\Delta S_{Univ} = \Delta S_{Syst} + \Delta S_{Surr} \geq 0 \text{ (1.16)}$$

Alternatively, a statistical mechanical approach using Boltzmann distribution can be used to describe entropy. Entropy by Boltzmann distribution is defined by equation 1.17:

$$S = kln(\Omega) \text{ (1.17)}$$

Where Ω represents the number of microstates, or configurations a system might adopt. Change in entropy is then defined by equation 1.18:

$$\Delta S = S_2 - S_1 = kln(\frac{\Omega_2}{\Omega_1}) \text{ (1.18)}$$

1.9 Third Law of Thermodynamics

The third law of thermodynamics states that the entropy of a pure crystalline substance is zero at absolute zero, due to this condition being the most orderly configuration possible[36]. Entropy can be calculated at any temperature and may be calculated by the following relation (equation 19):

$$S_T = \sum \frac{dq_{rev,i}}{T_i} + S_0 \text{ (1.19)}$$

Where S_0 is the entropy at absolute zero and S_T the absolute molar heat at any temperature. Additionally, $dq_{rev,i}$ under constant pressure conditions can be replaced with $C_P \, dT$, meaning S_T

values may be obtained from heat capacity and enthalpy changes during phase changes as the temperature increases[36]. This is evident from the equation 20:

$$S_T = \int_0^{T_m} \frac{C_P dT}{T} + \frac{\Delta H_m}{T_m} + \int_{T_m}^{T_V} \frac{C_P dT}{T} + \frac{\Delta H_v}{T_v} + \int_{T_v}^{T} \frac{C_P dT}{T} \text{ (1.20)}$$

The third law makes it possible to calculate absolute entropy of a pure substance as evidenced from the preceding equations.

1.10 Free Energy Applications

An ability to determine if a reaction will proceed spontaneously is critical for biologic stability assessment. In thermodynamic considerations, predicting spontaneity requires knowledge of system and surrounding entropy. However, it is desirable to have a parameter dependent only on the system. To do this, consider equation 15 where change in entropy of an isolated system is greater than or equal to zero, providing the relationship $\Delta S_{Surr} = -Q_{rev}/T$. Replacing entropy and heat terms with S and Q, respectively, and rearrangement of the equation, the following relationship is presented in equation 1.21:

$$Q - T\Delta S \geq 0 \text{ (1.21)}$$

For a process at constant pressure, a frequent condition of most benchtop experiments and biologic formulations, we can establish the following relationship by replacing heat Q, with ΔH and combining first and second law conditions as illustrated by equation (1.22):

$$\Delta H - T\Delta S \leq 0 \text{ (1.22)}$$

Where the left-hand side of equation is termed the Gibbs free energy and expressed as

$$G = H - TS \text{ (1.23)}$$

Gibbs free energy, *G*, is a new state function, because it is based off state properties H, T, and S. Under non-equilibrium conditions

$$\Delta G = \Delta H - T\Delta S \text{ (1.24)}$$

When ΔG=0 no net work can be gained from the system and has reached equilibrium. However, when ΔG≤0 then the reaction will proceed spontaneously, while the opposite is true when ΔG≥0 and the reaction will only proceed if energy is added to the system. What drives whether change in free energy is negative or positive and will proceed spontaneously or not, depends on change in sign and magnitude of enthalpy, entropy, and temperature. For example, at room temperature, ice will spontaneously melt despite its large heat of absorption due to the greater effect of entropy at that temperature.

1.11 Chemical Potential and Activity Coefficients

Thermodynamic principles have been discussed while examining behavior of pure substances and a single phase; however, this is rarely the case for systems of interest. For biologic formulations there are at a minimum three components (solvent, biologic, cosolvent) and potentially multiple phases. This will impact their stabilization and will be discussed in detail in later sections. For now, consider the free energy of an open, two component system under constant pressure and temperature as described by equation 1.25:

$$dG = (\frac{\partial G}{\partial T})_{P,n1,n2}dT + (\frac{\partial G}{\partial P)_{P,n1,n2}dP}) + \mu_1 dn_1 + \mu_2 dn_2 \text{ (1.25)}$$

Where the partial derivatives $(\partial G/\partial n_1)_T$ and $(\partial G/\partial n2)_T$ are defined as the chemical potential μ_1 and μ_2, respectively. Using the Maxwell relationships $(\partial G/\partial P)_T=V$ and $(\partial G/\partial T)_P=-S$, equation 1.25 is re-written as

$$\Delta G = -SdT + VdP + \mu_1 dn_1 + \mu_2 dn_2 + \cdots \text{ (1.26)}$$

Chemical potential, or partial molar volume, under constant pressure and temperature, components (n_j) held constant, the chemical potential of component *i* is proportional to the change in free energy due to infinitesimal changes in the number of moles n_i as described by equation 27:

$$\mu_i = (\frac{\partial G}{\partial n_i})_{T,P,n_j} \text{ (1.27)}$$

At constant pressure and temperature, the first two right hand terms of equation 25 disappear, and free energy change is solely dependent on change in molar concentration of components n_j as shown in the expanded and integrated equation 1.25 resulting in equation 1.28:

$$dG_{T,P,N} = \mu_1 n_1 + \mu_2 n_2 + \cdots \text{ (1.28)}$$

Chemical potential and its departure from ideal behavior can be described by activity coefficients. If we consider the vapor pressure of a pure substance above its respective pure liquid form, its chemical pressure can be described by equation 1.29:

$$\mu = \mu^o + RT \ln P \text{ (1.29)}$$

Where μ° is the standard, or reference state chemical potential. Using Raoult's law, P can be replaced with X (partial pressure of solvent) yielding the following relationship:

$$\mu = \mu^o + RTln\ X \text{ (1.30)}$$

Departures from ideal behavior are described by the "activity" of the solvent to replace the mole fraction[36] and labeled *a*. Here $a=\Upsilon X$, where ϒ is the activity coefficient and can be used to modify equation 3.28, 3.29, and 3.30 to derive the following relationships illustrated equations 1.31 and 1.32:

$$\mu = \mu^o + RTln\ a \text{ (1.31)}$$

$$\mu = \mu^o + RTln\ \gamma X \text{ (1.32)}$$

1.12 Equilibrium Constant and van't Hoff Equation

The conformation of biologic substances is capable of folding/unfolding, often in multiple ways. As previously stated, the energy to do so is minimal. To understand the amount of unfolded vs folded states, we must establish a relationship between free energy and equilibrium.

If we consider a model equation $aA + bB \rightleftarrows cC + dC$ where the left and right-hand sides represent reactants and products, respectively, and define the change in free energy in terms of chemical potential, the following relationship can be defined as follows:

$$\Delta G = (c\mu_C + d\mu_D) - (a\mu_A + b\mu_B) \text{ (1.33)}$$

Which we can then substitute in equation 3.29 into 3.31 and rearrange the equation to give an equation to relate chemical potential to activity

$$\Delta G = \Delta G^o + RTln[\frac{a_C^c a_D^d}{a_A^a a_B^b}] \text{ (1.34)}$$

Here, the natural log of the activity of the products/reactants can be represented K. Under constant pressure and temperature conditions, when change in free energy is zero (i.e. at equilibrium) equation 3.34 becomes equation 1.35:

$$\Delta G^o = -RTlnK \text{ (1.35)}$$

Equation 1.35 relates the standard free energy change to the equilibrium constant *K*, allowing the calculation of standard free energy or *K* if one of the two is known. This is significant as we shall soon see, as the conformational free energy change from either folding/unfolding, or equilibrium constant can be readily determined from analysis of experimental data. Moreover, from further observation, equation 1.35 and 1.22 can be combined, meaning that at any temperature the equilibrium constant K (of any appropriate observable) can be used to determine free energy, enthalpy, and entropy changes of any sort of reaction in a properly defined system. This, as we shall see, has major implications in the analysis of protein stabilization. Rearrangement of equation 1.35 makes obvious the relationship of equilibrium constant and temperature that can be rearranged as follows:

$$lnK = \frac{\Delta G^o}{RT} \text{ (1.35)}$$

If we differentiate with respect to temperature, equation 1.35 becomes

$$\frac{dlnK}{dT} = \frac{1}{R} * \left(\frac{d\left(\frac{\Delta G^o}{T}\right)}{dT}\right) \text{ (1.36)}$$

The Gibbs-Helmholtz equation relates the change in free energy with respect to temperature and may be combined with equation 3.36 to give the familiar van't Hoff equation[37] 1.37:

$$\frac{dlnk}{dT} = \frac{\Delta H^o}{RT^2} \text{ (1.37)}$$

Where ΔH^o is the standard enthalpy of reaction. This relationship may be combined with equation 1.37 and 1.22 to yield another useful relationship that shall be exploited in understanding protein stability in equation 1.38:

$$lnK = -\left(\frac{\Delta H^o}{RT}\right) + \Delta S^o/R \text{ (1.38)}$$

In equation 1.38, $\Delta S^o/R$ is the intercept of the line lnK of the plot of lnK over $1/\mathrm{T}$.

1.13 Peptide/Protein Stabilization Principles (Liquid State)

Proteins and peptides are stabilized through thermodynamic properties. Building from equation 1.33, the free energy change from native to denatured is quantitated from the following relationship.

$$\Delta G = G^D - G^N{}_D = -RTlnK = -RTln[D]/[N] \text{ (1.39)}$$

where D is the concentration of the denatured structure, N, native concentration. A driving force behind folding is the hydrophobic effect [25, 45]. Water, accumulating around hydrophobic side chains and patches, orders itself reducing the overall entropy of the system, leading to the folding and burying of hydrophobic side chains, while exposing the more hydrophilic amino acid backbones. Indeed, folding of proteins is relatively tight, with Pace and associates reporting radius of gyration (R_g) for model proteins as approximately 0.75 angstroms. For reference, R_g of water, ethanol, and closed pack spheres are 0.35, 0.47, and 0.71 angstroms, respectively [25]. Additionally, the same authors demonstrated that the larger the protein, the higher percentage of

residues were folded [25]. Earlier work by Pace and others demonstrated burial of -CH_2- groups contributed 1.2 kcal mol^{-1} per ang^3 and through other models estimated the hydrophobicity contributes 80% to the hydrophobic effect [25]. Other important contributions are those of hydrogen bonding and van der Waals interaction with polar groups [25].

1.14 Mechanism of Protection Through Direct Ligand Interaction (Wyman Linkage)

As can be seen from equation 1.1, free energy of native vs denatured states is critical to protein stability, with solvent, co-solvent and various additives, all potentially altering the equilibrium of the species. Stabilization occurs through two general categories: one, increased stability of the native state through Wyman type linkage; two, increased free energy potential for the denatured state. For the former, an endogenous ligand or stabilizing metal ion, buffer, etc., can increase stabilization of the native state (see Figure 1.3) [26, 46, 47].

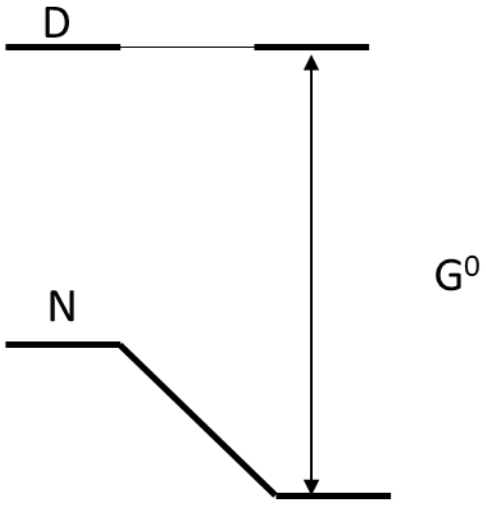

Figure 1.3. Wyman linkage stabilization of protein.

For the latter, preferential exclusion, increased hydration through osmolytes is the mechanism of action and an explanation will be given presently. Alternatively, the reverse can also be true; binding of an excipient to protein can stabilize the unfolded state.

1.15 Mechanism of Protection (Preferential Exclusion)

Osmolytes in nature (at the cellular level) and in biologic formulations are typically found in the hundreds of mM range [8, 35, 46-49]. In these concentration ranges osmolyte compounds act as co-solvent and can associate around the protein surface at concentrations similar to, lower and higher than that of the bulk solution and described as the interaction parameter [6, 7, 35, 46, 47, 49-51] in equation 1.40:

$$\xi_3 = \partial_3/\partial_2 = A_{3-}\, g_3 A_1 \quad (1.40)$$

Here, g_i is the concentration of component *i* in grams per gram of water and A_i is the amount of component *i* interacting with protein in grams per gram, the numbers 1, 2, 3 refer to water, protein, and osmolyte, respectively. Changes in the composition of the solution around the protein relative to the bulk solvent changes the activity coefficient of water, giving rise to changes in osmotic pressure across the surface area of the protein. The consequence being a change in the free energy of the native vs denatured states from our thermodynamic discussion given, a free energy relationship can be surmised in equation 1.41:

$$-RTln\left(\frac{k}{k_w}\right) = (G^D - G_W^D) - (G^N - G_W^D) = \Delta\mu_2^D - \Delta\mu_2^N \quad (1.41)$$

Which describes the free energy transfer of the denatured and native protein and can be related to the interaction parameter through the following relationship (equation 1.42).

$$\left(\frac{M_2}{M_3}\right)(\partial g_3/\partial g_2) = \left(\frac{\partial m_3}{\partial m_2}\right) \quad 1.42$$

$$(\partial\mu_2/\partial\mu_3) = -(\partial m_3/\partial m_2)(\partial\mu_3/\partial m_3) \quad 1.43$$

Where M_i is the molecular weight of component *i*, m_i is the molality of the *i* component. This means the interaction parameter $(\partial m_3/m\partial_2)$ if negative, increases the energy of the protein; if positive free energy decreases[46]. The transfer free energy can be obtained through integration of $(\partial\mu_3/\partial m_3)$ to yield equation 1.44:

$$\Delta\mu_2 = \int(\partial\mu_2\partial m_3)dm_3 \quad (1.44)$$

If the co-solvent is excluded to a greater degree from the denatured state (i.e. $(\partial m_3/m\partial_2)^D < (\partial m_3/m\partial_2)^N < 0$ then $(\partial\mu_2/\partial m_3)^D > (\partial\mu_2/m_3)^N$), the protein will be stabilized by the co-solvent because the resultant transfer free energy of the denatured conformation will exceed the native conformation. The compounds that preferentially bind to protein (left) and those that are excluded have on the hydration shell of a protein, as shown in Figure 1.3. The effects on conformation and stability are shown in Figures 1.2.

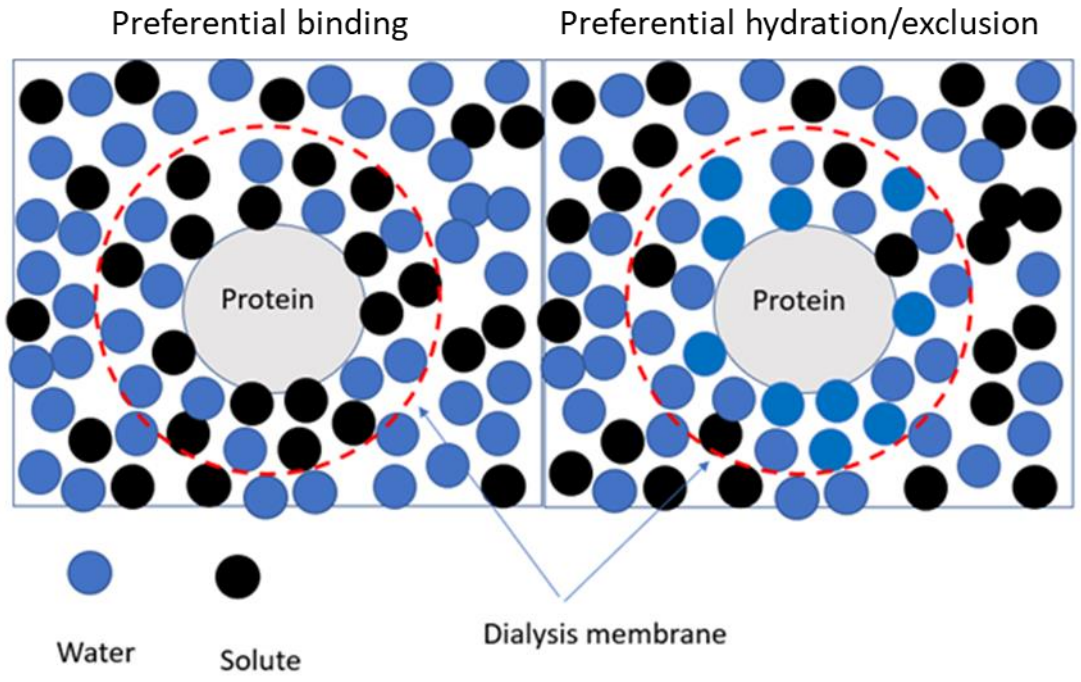

Figure 1.3. Preferential binding/exclusion by solutes.

An unfolded protein will have a greater surface area than the folded, native version of the protein. Cosolvents, which are preferentially excluded from a protein surface, create an enhanced hydration shell around said protein, increasing surface tension and osmotic pressure than it would experience in their absence. This increased pressure causes a protein to adopt a compact/native structure to minimize surface area and overall osmotic pressure. Denaturants have the opposite effect; they can bind to protein surfaces, reduce the hydration shell, and can decrease the ordering of water around protein and promote unfolding [46, 52, 53],

There are exceptions to these rules. Polyethylene glycol is an excellent osmotic, strongly excluded from the surface of proteins, but can have destabilizing effects on protein conformations in the liquid state [51]. While PEG is excluded from the surface, it has hydrophobic regions that can stabilize hydrophobic regions on a protein and reduce the energy difference between the native and denatured conformation. Indeed, PEG can lower the T_m of proteins [51], but can have other stabilizing and desirable factors as well.

1.16 Excluded Volume

It is well known that cellular environments are exceptionally crowded[14, 16, 35, 54, 55], and this crowding effect impacts both form and function of the local protein and peptide denizens[14, 16, 49, 54, 56, 57]. Unlike osmolytes and other preferential exclusion excipients, which have negative interaction with a proteins surface and stabilize native conformations enthalpically[16, 49, 56], crowders have minimal interaction with protein. Molecular crowders, as the name implies, occupy significant portions of the limited volume in a system, inhibiting peptide/protein unfolding of native structures, as the larger denature state would experience greater entropic loss than compact native structures[14, 16, 56, 57]. (Figure 1.4).

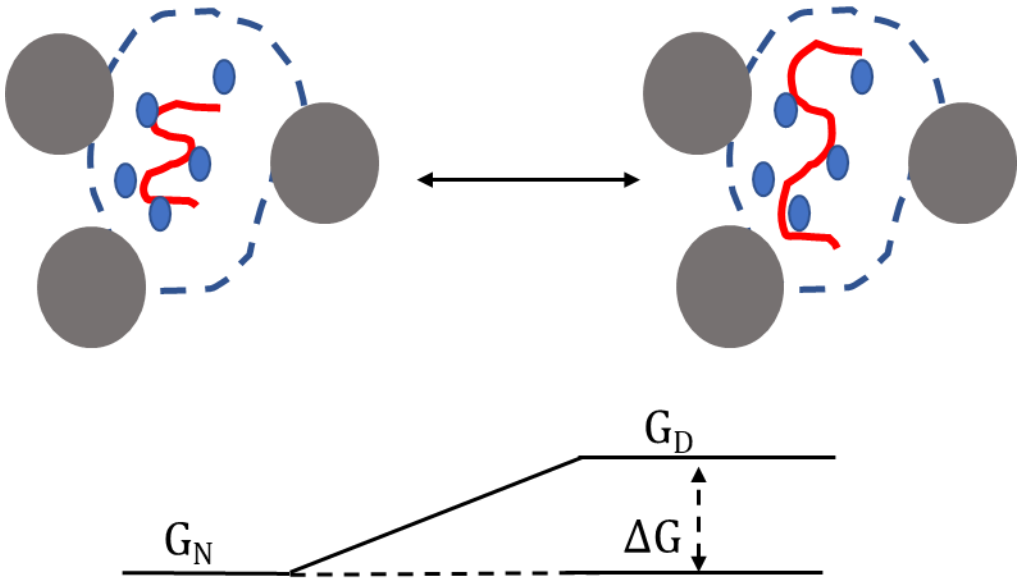

Figure 1.4. Effects of crowding agents on free energy of peptide/protein unfolding.

As can be seen from Figure 1.4, free energy of unfolding increases due to decreased volume available for the expanded molecule to move, reducing its entropic component. Molecular crowders such as dextran and other polymeric excluders typically demonstrated stabilization through increased T_m with minimal enthalpic change[14, 16, 54] observed. Here, entropic forces dominate stabilization[16] and a decrease in entropy tracks with crowder concentration. As might be expected, crowder size often matters, as two molecules at minimum occupy the sum of their radii implying a larger crowder is often a more efficient excluder (Figure 1.5). In Figure 1.5, R_P and R_e are the protein and excipient radii, respectively, and the shaded gray area is the hydrated portion of the protein.

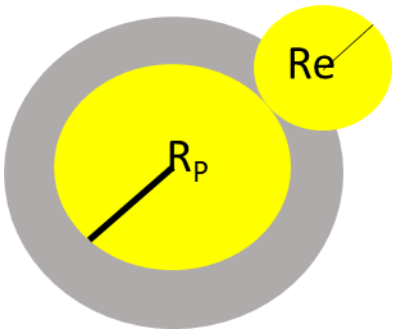

Figure 1.5. Visualization of crowder size and exclusion effect.

Crowding agents may, of course, also interact favorably or poorly with a protein surface and may alter the solvent surrounding the biologic agent in a kosmotropic/chaotropic fashion. Such behavior would impart preferential exclusion/interaction properties to an excipient and may thus enhance or reduce the stabilizing behavior of the cosolute. Polyethylene glycols are known to sometimes behave in such a way; however, it is often protein specific when doing so.

1.17 Interfacial Protection

As mentioned, another primary conformational destabilization pathway is that of absorption. Biologics can be exposed to various hydrophobic surfaces such as air, glass, silicon oil, etc. Mechanical stresses such as vibrations while transporting, shaking/vortexing to reconstitute a lipolyzed biologic can increase the amount of protein exposed to air/liquid interface. Contacting such surfaces decreases the free energy between folded/unfolded species, increasing the probability of denaturation. To combat these issues, surfactants are employed to reduce biologic/interface exposure. While myriad surfactants are commercially available, they are generally composed of the same elements, namely a hydrophilic head, aliphatic tail, and are amphipathic in nature. Like all stabilizing excipients, surfactants can have complicated and varying effects on protein stability, solubility, viscosity, aggregation propensity and so forth depending on the protein/peptide to stabilize and amount and type of surfactant used [8, 13, 28, 34, 35,

[46, 58-62]. The most common surfactants employed are polysorbate 20, polysorbate 80 (tween 20 and 80 respectively) and Poloxamer 188.

There are two primary protection mechanisms provided by surfactants: One, displacement from and preferential absorption to hydrophobic surfaces; two, favorable interaction with the protein's native conformation, or temporary binding and stabilization of unfolded regions until displacement of surfactant and refolding occurred [13, 59-61].

The former mechanism, displacement, is a function of concentration. Depending on concentration, surfactants have varying effects on a solution (see Figure 1.6). At low concentration, surfactants absorb to any available surface, displacing higher energy solution components, reducing the interfacial surface energy of the system (see region 1). As the surfactant concentration increase, surfactants will populate air, container, protein, and other surfaces to a greater degree, reducing the surface tension of water in a concentration dependent manner (region 2). As surfactant concentration increases, surface tension remains constant as much of the air/water sites are occupied, but due to thermodynamic considerations, continues to bind to the protein (region 3). If surfactant is increased further, it will begin to displace protein from the surface, reducing the surface tension, which again will plateau (region 4). Addition of more surfactant will result in complete displacement of protein and form micelles (region 5)[28].

Interfacial protection is critical, given the likelihood of protein exposure to these hydrophobic surfaces. Often proteins will be exposed to various mechanical stresses, oils, and of course air; therefore, protection is critical[8, 9, 26, 63]. PS 80 has shown to be a more potent displacer and better absorber of proteins than PS 20 or PXO 188; however, the latter is somewhat less likely to degrade into toxic, or denaturant material[9, 26, 63].

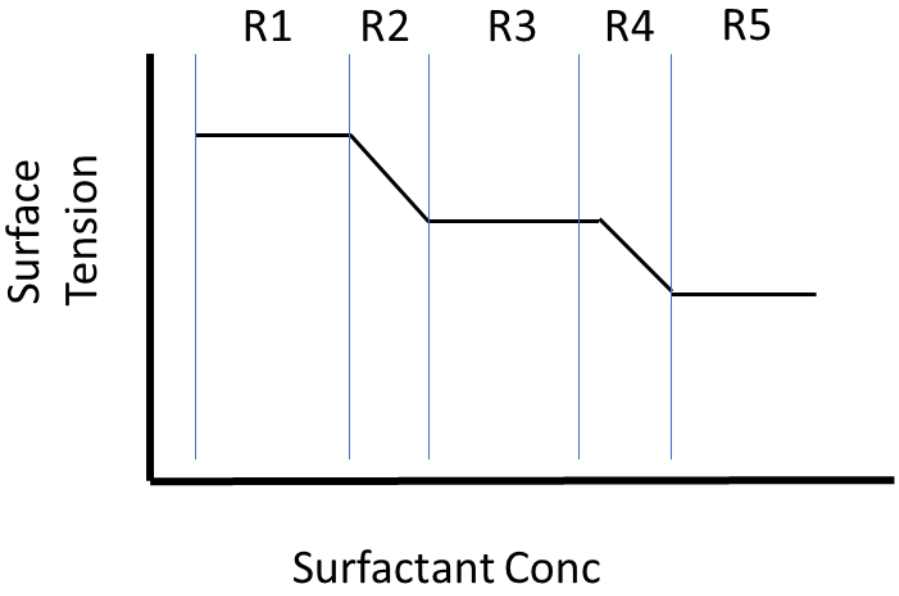

Figure 1.6. Effect of surfactant concentration on surface tension[28].

Interfacial protection is critical given the likelihood of protein exposure to these hydrophobic surfaces. Often proteins will be exposed to various mechanical stresses, oils and of course, air; therefore, protection is critical[9].

Surfactants can favorably interact with protein surfaces [13, 28, 34, 61, 62], though often in a much more attenuated manner than charged polymers such as SDS[9]. For example, Hoffman and company demonstrated tween 20 and 80 binding to BSA, mild interaction with lysosome and no binding with IgG1, while Chou through ITC demonstrated albutropin had a 10:1 binding ratio of surfactant to protein and moderate binding affinity relative to ionic polymers [60]. Similarly, Bam and Tandor demonstrated the ability of surfactants to stabilize partially unfolded peptides by preventing aggregation, and help in refolding [59, 61]. In a partial explanation of this behavior, a recent study by Arisoco through MD simulations demonstrated the ability of tween 20 to bind to unfolded portions of rHGH with the hydrophilic heads orientated towards the hydrophobic

patches of the protein. It was postulated that these interactions occupied sites prone to aggregation, yet through unfavorable interaction encouraged refolding[64].

1.18 Colloidal Stability, Solubility and Viscosity

Given the size and chemical make-up of proteins, they may possess various charges and dipoles potentially causing attractive/repulsive interactions between molecules. Such interactions can affect solubility, viscosity, and aggregation of a biologic therapeutic.

Colloidal stability results from the balancing of the various protein charges resulting in solution, thus reducing risk of aggregation, and optimizing the competing properties of solubility and viscosity. Colloidal stabilizing excipients function via screening protein charges, or similar to surfactants, occupy hydrophobic interactions of the proteins[33, 65], reducing aggregation potential.

Enhancing conformational stability through use of osmolytes is often done; however, stabilization through such compounds can decrease solubility and increase viscosity. Briefly, solubility is governed by the thermodynamics of the protein solution (i.e. transfer free energy in this case from solid to liquid), as well as the activity and ionic strength of the solution [7]. For example, denaturants and other conformational destabilizers can lower the surface transfer free energy of the protein relative to pure water and improve solubility. Electrolytes can improve solubility via suppression of electrostatic interaction at appropriate concentrations but reduce solubility due to specific protein-ion interactions (salting out) when concentrations become too high[52, 53, 66].

Viscosity, like solubility, is often another casualty when seeking conformational stability, especially at high concentrations desired in many formulations. It depends on several factors, some long range and some short range forces, the importance of which will change depending on

the nature of the protein and co-solvent. Overall solution characteristics are often determined by electrostatic repulsions as these are long range effects [66]. As protein and excipient concentrations increase, so do excluded volume, van der Walls, hydrophobic (protein-protein interaction), charge-charge and other electrostatic effects. Figure 1.7 illustrates some of these interactions; namely, volume exclusion, electrostatic repulsion/attraction, and hydrophobic attraction. Use of various excipients for screening the latter three will be detailed, and from previous discussion on stability it can be seen highly excluded stabilizing agents will limit solubility[66].

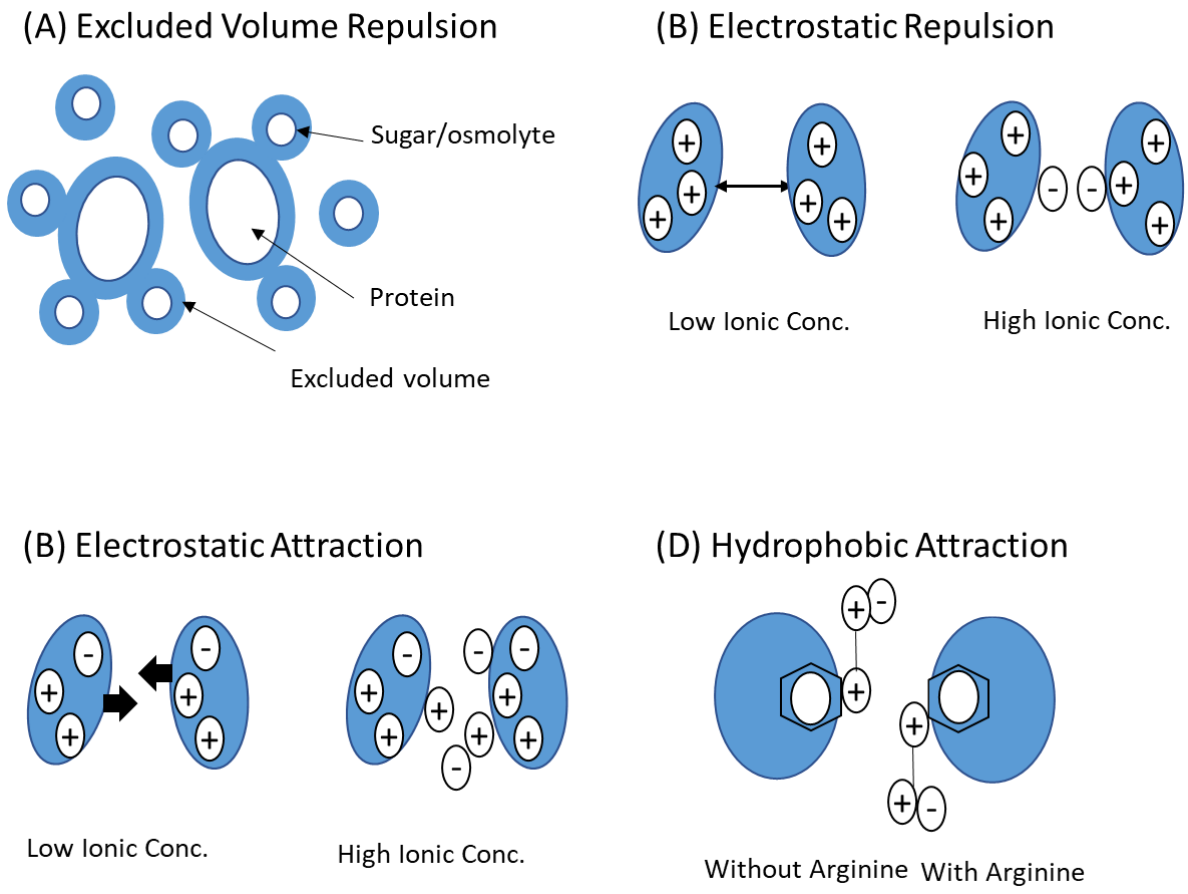

Figure 1.7. Effect of different interaction parameters on viscosity. Modified from Current Protein & Peptide Science 2018**,** 19 (8), 746-758.

Several viscosity models have been purposed for various situations. When considering the volume exclusion effect only, the Einstein equation and derivatives are widely used, the general formula described by equation 1.45:

$$\eta = \eta_0(1 + 2.5\phi) \quad (1.45)$$

Where η, η_0 and φ represent the solution viscosity, the water viscosity, and volume fraction of the solute. The value 2.5 is a parameter for solid sphere and is a function of solute shape. As can be seen, increasing the solute concentration will increase viscosity independent of specific interaction.

Deviation from this behavior at high protein concentrations is observed. Many empirical derivates of the Einstein equation can be found in the literature, with two being discussed here by Kreiger-Doughter and Conley equations, 1.46 and 1.47, respectively.

$$\eta = \eta_0 \exp\left(1 - \frac{\phi}{\phi_m}\right)^{-[\eta]\phi_m} \quad (1.46)$$

$$\eta = \eta_0 \exp\left(\kappa C\right) \quad (1.47)$$

Where φ is the volume fraction of the protein, φ_m is the maximum volume fraction molecule, κ and C are a constant and protein concentration respectively [66].

It is obvious from these two equations and others like them, that protein viscosity does not increase linearly with concentration, rather it follows an exponential behavior. The two previously mentioned equations fit BSA, globular proteins and antibodies fairly well. The Conley equation, while simple, does show deviations for antibodies at concentrations exceeding 300 ng/ml [66].

Proteins, being large, have multiple and variably charged compounds, and the viscosity effects are not solely determined by exclusion effects. Electrostatic interactions play significant roles as well in the form of repulsion or attraction. For dominant repulsion forces, maintaining a

pH near the isoelectric point (pI) will reduce such charge interactions as the molecule will be in its most neutral form, lowering viscosity. Additionally, a low concentration of salt will shelter such repulsions. Higher concentrations may increase exclusion effects especially with chaotropic ions typically employed in formulation. For electrostatic attraction, the opposite principle applies; moving away from the pI will decrease solubility.

An additional factor to consider is hydrophobic and clustering potential of proteins and their effect on viscosity. As discussed earlier, protein association brings risk of aggregation and more distressingly, irreversible aggregation. Arginine and amino acids with aromatic side chains and substances are often used here to reduce viscosity and risk of aggregation. Arginine and similar molecules can interact weakly with aromatic and hydrophobic sections, buffering these portions of the protein from associating with other proteins, preventing an increase in viscosity, and reducing the risk of aggregation.

1.19 Chemical Stabilization (Liquid Phase)

Chemical instability of proteins tracks strongly with amino acid sequence with degradation of product occurring via some form of hydrolysis or oxidation[8, 9, 18, 67]; and chemical degradation can have a significant effect on physical conformation and aggregation propensity[68]. Excipients such as buffers, osmolytes and surfactants can greatly mitigate degradation. For example, at low pH, the rate of deamination and other hydrolysis routes are greatly enhanced[8, 67, 68]. Aside from the use of proper buffers and concentration (type and amount are critical[67]) to mitigate degradation, osmolytes can stabilize native conformation, limiting movement, slowing hydrolysis. This has been observed in different antibodies when replacing NaCl with trehalose or mannitol, which reduced chemical degradation and enhanced overall stability while under storage at 25 and 40^{o}C[67]. Wang and the coworkers observed increased deamidation of 1gG1

antibodies formulated with phosphate buffers relative to citrate buffers[67]. While no mechanism was proposed, Zbacnik noted PBS and citrate buffers enhanced conformational stability in a concentration dependent manner, and suggested it proceeded through a Wymann ligand binding mechanism[26]. Indeed, many proteins are affected differentially by phosphate vs citrate buffer. If preferential binding stabilization is a factor, then it would not be surprising they would impart varying protection based on protein composition.

1.20 Solid Phase Stabilization

While focus of this work will deal with stabilization of biologics in liquid formulations, many compounds undergo lyophilization formulation, as it greatly enhances product shelf-life and eliminates the cold-chain requirement. However, lyophilized compounds will have to be reconstituted and be stable in the liquid form. Moreover, many of the same excipients utilized in liquid formulations are found in lyophilized products but may vary in their function relative to the enumerated mechanisms for the liquid state.

Briefly, lyophilization is composed of three steps: Freezing, primary drying then secondary drying. During the freezing step, water molecules freeze first, increasing the protein concentration and viscosity of the solution, inhibiting further crystallization. As the temperature continues to decrease, the remaining solution will harden to an amorphous, crystalline, or combined amorphous/crystalline solid (see Figure 1.8). Primary drying removes the water and is performed at a temperature below the collapse temperature also referred to as the glass transition temperature T'_g, or T_{eut} (eutectic point) for amorphous or crystalline compounds, respectively. Below this temperature, the compound will remain in a glassy, solid state[27, 31]. Further dehydration (secondary dehydration) is carried out at a higher temperature to increase the rate of water removal.

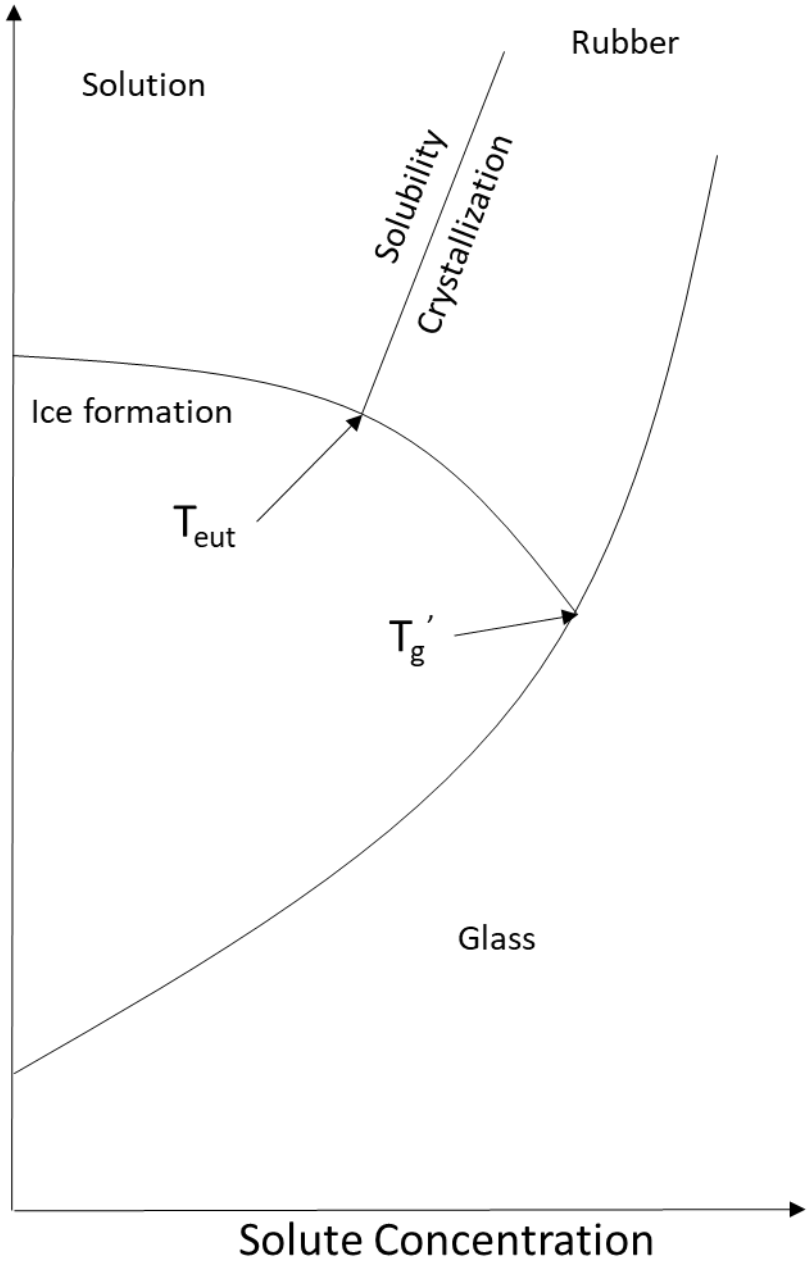

Figure 1.8. Effect of solute concentration on physical state of protein/biologic formulation.

Lyophilization exposes delicate compounds to two new stresses, freezing and dehydration. As the formulation freezes, ice-water interfaces are created that can cause absorption and denaturation of proteins, leading to potential loss of activity, aggregation, and

precipitation. Sublimation removes water, resulting in a loss of hydrogen bonds between the residues and structures in protein, another potentially denaturing factor [20, 46, 69].

Much like liquid formulations, excipients are utilized to stabilize lyophilized formulations and are purported to do so by two main mechanisms: vitrification and water replacement. According to vitrification, excipients stabilize protein through the formation of glassy state that immobilizes the protein. Water replacement functions through replacement of water-protein hydrogen bonds with those of a suitable excipient, thereby stabilizing the protein structure. Several FTIR studies have demonstrated the effectiveness of disaccharides in maintaining the secondary structure of protein after dehydration [46, 70].

Mobility of protein is often associated with stability and propensity for aggregation [20]. It has been purposed those combined effects of vitrification and water replacement can play a primary role in protection depending on the protein, type of movement, and conditions of the formulation at particular temperatures [20, 69]. Vitrification is best at protecting when global movement restriction is the predominant destabilization pathway, while water replacement can have a dominant effect for local movement [20]. Physical degradation may be more affected by global movements (vitrification), whereas chemical pathways are more likely governed by those of local motility (water replacement). It is important to remember that although protein glass transition temperatures are above the freezing temperature of water, it can still have significant mobility 10-20^{0}C below the T_g [20].

Immobilization is the goal for stabilizing lyophilized products. Properly designing such formulations can be very protein specific, depending greatly on the active ingredient's composition and excipient components. While optimization is very often a case by case endeavor, there are common principles and considerations that can be applied broadly. Chief

among these concerns are selections of proper cryoprotectants and lyoprotectants. Cryoprotectants, such as surfactants, protect the product during the freezing process by reduction in exposure to ice-water interfaces [20, 31, 35]. Lyoprotectants, such as disaccharides, protect against dehydration in the form of water replacement (hydrogen bond with the protein), but also form a glass state and vitrification protection properties. T_g temperature is another important consideration and directly related to cyro and lyoprotectant excipients chosen [20, 31]. Generally, the higher the T_g the better; however, many cryoprotectants such as tween 20 and tween 80 are plasticizers, and will lower the T_g, thus a balance needs to be maintained and evaluated when selecting type and amount of cryoprotectant. Other considerations include buffer selection (buffer pH can change drastically such as phosphate buffer; tris and citrate buffers are generally used), reconstitution times, and bulking agents [30, 31].

1.21 Chemical Degradation (Solid Formulation)

As in the case of liquid formulations, chemical degradation remains an important consideration, with pH, mobility, and interface interactions playing central roles in degradation rates. Solid phase formulations, due to the freezing and dehydration phases are especially important during the processing steps. During freezing, pH can change dramatically as the liquid phase decreases and concentrates product and excipients. Thus, careful consideration needs to be given to buffer type as said changes may exceed its protective range[10]. Other excipients including sugars, amino acids and various surfactants have been shown to decrease degradation, presumably from conformation maintenance and buffering capacity[67]. For the later consideration, histidine, arginine, and glycine have been proposed to be effective in this role[67].

1.22 Excipient Types, Classification, and Purposes

An excipient is any substance other than the active pharmaceutical ingredient added during the manufacture or finished product[71]. Excipients are added for a variety of reasons such as stabilization, increased solubility, viscosity reduction, pH control and many others. For our purposes here, excipient classes used in parenteral and lyophilized formulations will be discussed briefly, in terms of osmolytes, surfactants, and buffers, with a few examples given.

1.23 Molecular Crowders

Some common molecular crowders are dextran's, PEGs, polyvinylpyrrolidone (PVPs), Ficoll-70000, and hydroxyethyl (beta) starch and more recently, glycopolymers and functionalized dextrans[72]. As previously discussed, they interact minimally with the API, instead of stabilizing the native confirmation entropically through volume exclusion. However, volume exclusion may not be the only effect on the compound, as certain crowders may interact with local regions of a protein in a preferential manner, causing local instability.

1.24 Surfactants

Surfactants serve to protect compounds from interfacial stress in either the liquid or solid state. During freezing, transportation, reconstitution, or administration, biologics are exposed to mechanical stress, mixing, cavitation, and denaturizing substances such as oil and glass. Common surfactants include polysorbate 20 or 80, PLX 188, cyclodextrins, amino acids glycine, and histidine to name a few. In the liquid phase, they protect by aggregating onto unfolded portions of the protein surface, at various interfaces and protect protein from aggregation. During the lyophilization process, interfaces form between ice crystals and the remaining solution, creating potentially denaturative surfaces. Here surfactants will serve as cryoprotectant and lyoprotectants, minimizing surface interactions[10, 30, 64]. Careful consideration needs to be

given to surfactant selection when preparing a lyophilized formulation. Surfactants generally will reduce the collapse temperature of the resulting cake and vary in their hydroscopic nature. Generally, the less surfactant needed, the better.

1.25 Buffers and Salts

One of the most ubiquitous excipients, buffers play an important role in biologic formulation in liquid or solid state. At the most basic level, they serve to maintain an appropriate pH for the therapeutic. Mechanisms behind conformational stabilization range the big three: conformational, colloidal, and interfacial. Given the relatively low concentrations of buffers in formulations to those of commonly used osmolytes, conformational stability is generally believed to occur through ligand binding rather than preferential exclusion, though there are examples of the latter protection mechanism as well[26]. Additionally, buffers can function as a surfactant with charged ions accumulating at air or ice interfaces. Colloidal stabilization through charge screening and hydrophobic blocking is possible too[26, 33]. An important consideration for buffer use is temperature. During the lyophilization process, low temperature and dehydration can greatly change the solution pH, potentially outside a buffer's protective range; however, other protective benefits may negate this behavior[26]. In addition to physical stability, chemical stability can be enhanced with maintenance of appropriate pH.

Common excipients include phosphate buffer, acetate, and tris buffers (the former two are often used in lyophilized formulations). Amino acid buffers such as histidine, glycine, and arginine are also commonly used and are popular in lyophilized products. With regards to amino acid buffers, arginine performs multiple functions, acting as a buffer, surfactant, and viscosity reducing agent (the latter is believed to occur through screening of aromatics[8]).

Salts can function as charge screeners and osmolytes depending on whether it has salting in/out characteristics[52, 73]. As such they can be used to improve solubility, viscosity, or conformational stability.

1.26 Analytical Method

1.26.1 Thermal Course of Heat Capacity and Enthalpy

Measuring protein/peptide stability is generally considered in thermodynamic terms and often assessed through monitoring unfolding under thermal, chemical, other stresses. Unfolding is generally measured using certain assumptions/approximations like two state and reversibility, or a justification of why such approximations are valid. Additionally, data is generally fit to specific mathematical models to determine the desired parameters. In this section, a brief explanation of change in enthalpy determined through change in heat capacity (Kirchhoff's relationship) and how it is used to measure thermodynamic changes due to unfolding is discussed. Ultimately, data from CD, DSC, NMR was fitted using the discussed equations and models.

Unlike traditional melting temperatures of many substances where a phase transition occurs at a single temperature, protein unfolding occurs over a temperature range and its temperature dependence tracks the change in heat capacity (equation 1.48):

$$\Delta H_{cal}(T) = \int_{T_{ini}}^{T} C_{p,NU}(T)dT \quad (1.48)$$

The DSC determined enthalpy ΔH_{cal} (T), incorporates the conformational enthalpy (ΔH^{o}_{NU}) and the increased heat capacity of the unfolded heat capacity due to increased water binding to the larger protein surface area[42]; as shown in the relationship shown below:

$$\Delta C^{0}_{p,NU} = C^{0}_{P,U} - C^{0}_{P,N} \quad (1.49)$$

This increase in heat capacity has direct bearing on the discussion at large, given that excipients will directly increase the enthalpic cost of an unfolded protein. Therefore, it is important to account for this increase in heat capacity in a temperature dependent manner as shown in equations 1.50:

$$\Delta H_{NU}(T) = \Delta H^0_{NU} + \Delta C^0_{P,NU}(T - T_m) \text{ (1.50)}$$

Transition temperature T_m is chosen as reference temperature as it is easily deduced when ΔG=0, since in this scenario the protein/peptide is half denatured regardless of the number of steps (equation 1.51). The experimentally determinable enthalpy is determined by multiplying $\Delta H_{NU}(T)$ by the fraction unfolded ($\Theta_U(T)$) (equation 1.52). The predicted heat capacity is determined by taking the derivative of the enthalpy with respect to temperature (equation 1.53)

$$\Delta H^0_{NU} = T_m \Delta S^0_{NU} \text{ (1.51)}$$

$$\Delta H(T) = \Delta H_{NU}(T)\Theta_U(T) = [\Delta H^0_{NU} + \Delta C^0_{P,NU}(T - T_m)]\Theta_U(T) \text{ (1.52)}$$

$$C_{P,NU} = \frac{d\Theta_U(T)}{dT} + \Delta C^0_{P,NU}\Theta_U dT \text{ (1.53)}$$

The first term on the right side is conformational change contribution, the last the increase in heat capacity. Thus, the enthalpic contribution from heat capacity is given by equation 1.54:

$$\Delta H^0_{Cp} = \int_{T_{ini}}^{T_{end}} \Delta C^0_{P,NU}\, \Theta_T dT \text{ (1.54)}$$

$\Theta_U(T)$ can be calculated using either a two-state or multi state model.

From the equation 1.35 ($\Delta G = -RTln(K(T)) = \Delta H - T\Delta S$) it can be seen ΔG is affected by temperature protein folding. Accounting for changes in heat capacity, folding entropy can be determined by equation (1.54)

$$\Delta S_{NU}(T) = \Delta S^0_{NU} + \Delta C^0_{P,NU} \ln\left(\frac{T}{T_0}\right) \text{ (1.54)}$$

The predicted free energy can thus be described by equation 1.55 or shortened to equation 1.56 when heat capacity cannot be measured.

$$\Delta G_{NU}(T) = H^0_{NU}\left(1 - \frac{T}{T_m}\right) + \Delta C^0_{P,NU}(T - T_m) - T\Delta C^0_{P,NU}\ln\left(\frac{T}{T_m}\right) \quad (1.55)$$

$$\Delta G_{NU}(T) = H^0_{NU}\left(1 - \frac{T}{T_m}\right) \quad (1.56)$$

Heat capacity is generally not measurable through spectroscopic techniques but can be determined through tracking the enthalpic change with respect to transition temperature T_m (equation 1.57).

$$\frac{d\Delta H}{d\Delta T} = \Delta C_P \quad (1.57)$$

1.26.2 Two-State Model

The simplest and most often employed model[42], two-state unfolding assumes a protein adopts only two conformational states, native (N) and unfolded (U). The fraction of N vs U is determined by temperature dependent equilibrium constant K(T) as seen in equation 1.58, where [N] and [U] are native and unfolding concentrations, respectively, and equation 1.59 relates $\Theta_U(T)$ to equilibrium constant.

$$K(T) = \frac{U}{N} = \frac{\Theta_U T}{1 - \Theta_U T} \quad (1.58)$$

$$\Theta_U(T) = \frac{K(T)}{1 + K(T)} \quad (1.59)$$

From equations 1.58 and 1.59 the relationship between free energy and equilibrium constant becomes clear i.e. $\Delta G = -RTln(K(T))$.

Likewise, chemical denaturation can be described by relationship given in equation 1.60

$$K(C_D) = C_{U/}C_N = \Theta_U(T) = \frac{C_U}{C_U + C_N} = \frac{K}{1+K}, therefore, \Delta G_{NU} C_D = -RTlnK(C_D) \quad (1.60)$$

Where C_N and C_U refer to native and unfolded species concentrations, respectively, and C_D the denaturation concentration.

Changes in free energy due to chemical denaturation can also be described by equation 1.61

$$\Delta G_D = \Delta G_D^{H2O} - m[D] \quad (1.61)$$

Where [D] is denaturant concentration and *m* is the slope and measure of the change in free energy with changing denaturant concentration and corresponds directly to the amount of protein solvent exposed surface area[74, 75].

1.26.3 Multi-State Folding (Zimm-Bragg theory)

Protein unfolding often occurs in a sequential manner and is inadequately described by a two-step model. Several ideas have been put forward over the years to account for the multi-step process of coil-to-helix transition[76, 77]. One model, Zimm-Bragg (ZB) theory, has demonstrated utility in describing protein unfolding and thermodynamic parameters in globular proteins with not only helical content, but varying SS composition [39-42].

For the simplest iterations of the ZB model, unfolding proceeds in a sequential manner were local equilibria between native "(n)" and "(u)" residues exist. Interactions proceed through nearest neighbor effect, and heterogeneous residues are averaged enthalpicaly[39, 41, 76, 78]. The lowercase is used to delineate between individual residues rather than the whole molecule of a two-state model. For the original models, "n" refers to helical residue while "u" is a coil amino acid. For reasons that will be discussed later, "n" and "u" will be used to describe folded/unfolded, respectively of any SS feature. Though specific backbone interactions govern SS formation and geometry, i.e. i and i+3 for helices, this is adequately accounted for in ZB since cooperative changes between adjacent residues leads to the proper torsional angles between peptides resulting in the defined SS[40, 42].

ZB is governed by two parameters, nucleation σ and propagation s. The former describes the penalty of forming helix-coil junctions in a helical strand and defines the sharpness in

conformational change near the transition temperature. In most cases it is relatively constant under various thermal and chemical stresses and is often treated as such. Typical values range from 10^{-3}-10^{-6}. The propagation factor, on the other hand, is sensitive to both the temperature and chemical environment and described by equations (1.62 and 1.63) respectively:

$$s(T) = e^{-\frac{h}{R}*(\frac{1}{T}-\frac{1}{T_m})} \text{ (1.62)}$$

$$S(C_D) = e^{-K_D(C_D-C_m)} \; where \; n + D \rightleftarrows u \; and \; \frac{C_u}{C_n} = K_D c_D \text{ (1.63)}$$

Here, *h* is defined as the enthalpy of unfolding per residue, D the denaturant, K_D the binding constant of the denaturant, C_m the chemical denaturant concentration at the transition point. σ and s are often determined through fitting data to the defined ZB model, h can be fitted, or calculated as well, but is often estimated from literature sources and will be discussed in greater detail shortly.

The mathematical explanation of ZB can be surmised as follows. A polypeptide chain of length N units can adopt 2^N conformations (helix or coil), with combinations of i+1 for a continuation of a sequence leading to cc, hc, ch, and hh possibilities. The probabilities of all occurrences can be described by matrix M (see equation 1.64)

$$M = \begin{pmatrix} 1 & \sigma s \\ 1 & s \end{pmatrix} \text{ (1.64)}$$

Where s is given by equation 24, and M can be used to calculate partition function Z (equation 1.65).

$$Z(\sigma, s, N) = \begin{pmatrix} 1 & 0 \end{pmatrix} \begin{pmatrix} 1 & \sigma s \\ 1 & \sigma \end{pmatrix}^N \begin{pmatrix} 1 \\ 1 \end{pmatrix} \text{ (1.65)}$$

Taking the derivative of the natural log of Z with respect to temperature fractional helicity at any temperature can be determined (equation 1.66).

$$\Theta_{helix}(T) = \frac{s}{N} * \frac{d(lnZ(\sigma,s,N))}{dT} * (ds/dT)^{-1} \text{ (1.63)}$$

Combining equations 1.58 and 1.59 thermodynamic properties of sequential unfolding can be determined. Free energy of unfolding is governed by propagation factor s(T) or s(C_D) for thermal or chemical denaturation, respectively, and is given by equations 1.64 and 1.65:

$$\Delta G_{NU}^{0} = -NRTln(\frac{s(T_{end})}{s(T_{ini})}) \text{ (1.64)}$$

$$\Delta G_{NU}^{0} = -NRTln(\frac{s(C_{end})}{s(C_{ini})}) \text{ (1.65)}$$

An additional feature of ZB theory is the probability determination of any conformation. One feature of interest is that of the number of helices in a sequence, which is described by equation 1.66:

$$\eta_{\sigma}(T) = \frac{\sigma dlnZ(\sigma,s,N)}{d\sigma} \text{ (1.66)}$$

An alternative to matrix methods, when N is large, or N is greater than $1/\sigma^{0.5}$ Z and Θ simplifies to equation 1.67 and 1.68, respectively.

$$Z = \frac{s+1+\left(\left(1-s)^2+4\sigma s\right)^{\frac{1}{2}}\right)}{2} \text{ (1.67)}$$

$$\Theta = \frac{1}{2} - (1-s)/(2 * \left((1-s)^2 + 4\sigma s\right)) \text{ (1.68)}$$

Helix and beta-sheet formation is primarily driven by van der Waals and hydrophobic interaction, not hydrogen bond formation[79]. Enthalpy of helix formation is generally reported to be 1.1 kcal/mol and assumed to be the average enthalpy of residue unfolding in a protein[39, 40, 42]. This will not be the case of PLL peptides, where the h parameter will be fitted to data.

1.26.4 Circular Dichroism

With the advent of extensive protein structural libraries starting in the 1980's (due to a combination of various recombinant DNA technologies, X-ray crystallography, and NMR techniques), greater insight into the role of structure played in protein function became much

more apparent[80]. The two analytical techniques mentioned, however, can be time and resource consuming. Moreover, they are sometimes untenable in the case of a protein not being crystallizable (X-ray crystallography), or if it is too large (NMR). CD, on the other hand, is extremely robust, relatively less resource intensive, and much more amenable to rapid analysis[81-83]. For these reasons, CD has become a primary method for characterization of protein and peptide structures. Applications include evaluating SS features and content[80, 83, 84], higher order features[80], amino acid residue identification[80], protein-protein interaction[82], cofactor and ligand binding[80, 82, 85], kinetics of folding/unfolding and other kinetic processes[82, 85], and most importantly for this work, measuring the thermodynamics of SS unfolding[80, 85-87].

A CD instrument is composed of five components: light source, monochromator (for wavelength selection), polarizer, sample compartment, and detector (See Figure 1.9).

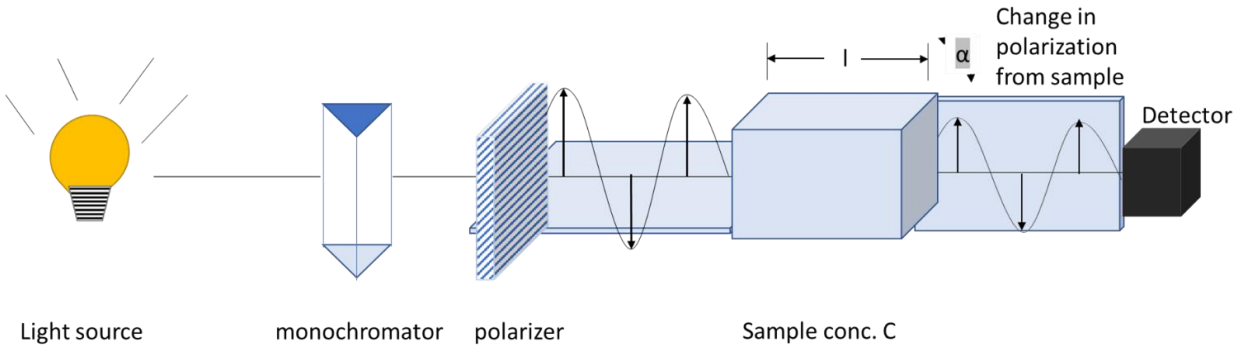

Figure 1.9. A schematic of a circular dichroism spectrometer.

Useful CD analysis is a function of the cotton effect, where an optically active substance absorbs light and polarized light differentially. Figure 1.10a illustrates this phenomenon in two cases: case (I) the equal absorption of left handed (counter-clockwise) and right handed (clockwise) light when passed through an optically inactive, symmetric sample. Case (II), left

and right handed light are absorbed differentially due to passing through an optically active substance. Differential absorption can be caused by multiple factors. Carbon atoms form four bonds, potentially yielding an optically active center. Some bonds such as C-S-S-C create dihedral angles that will produce cotton-like effects[80], or an absorbing agent will be connected to chiral center eliciting unequal absorption of polarized light. Finally, any condition in which a chromophore is part of an asymmetric environment with different polarized light passing through it, differential absorption will occur. In the cases of proteins and peptides, this unequal absorption (depending on wavelength) is due to SS features (240 nm and below)[80, 85], tertiary/quaternary aggregation, and binding effects (260 nm and above)[80, 82].

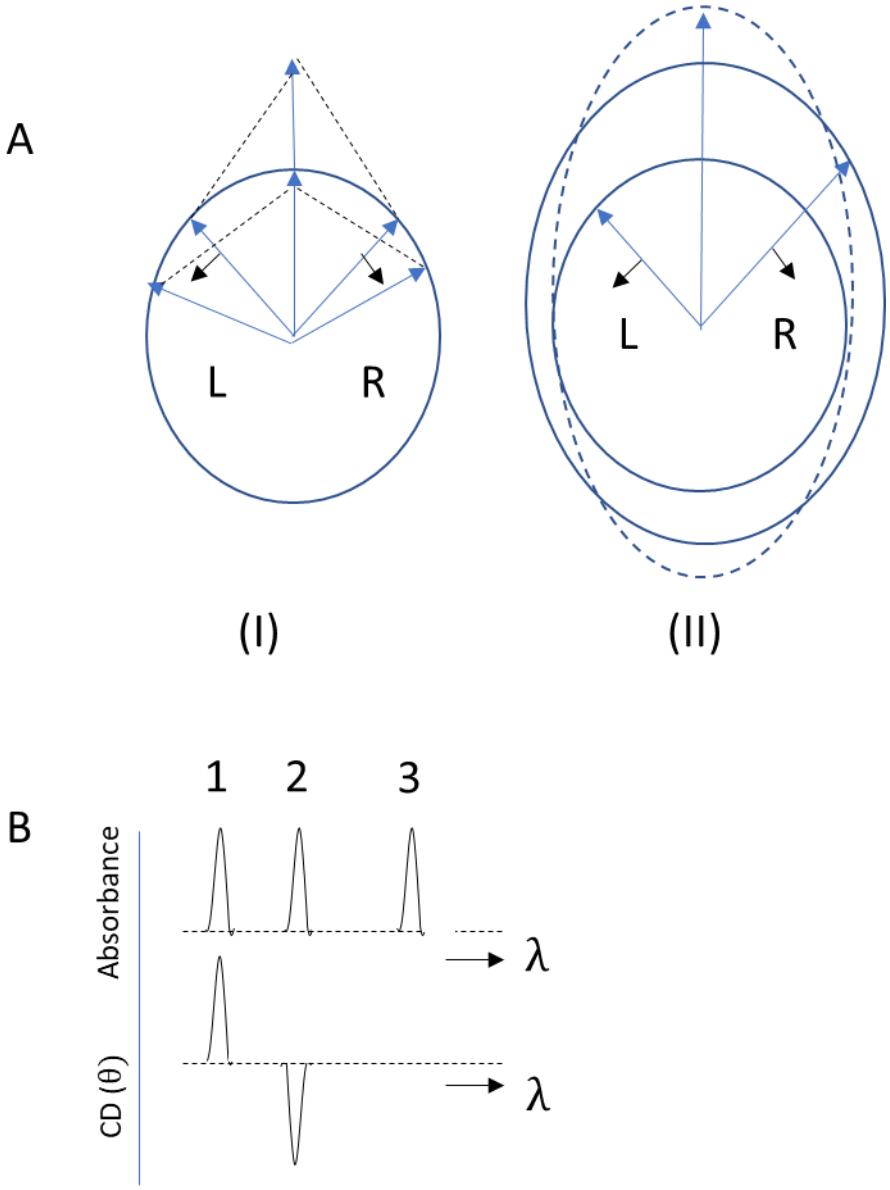

Figure 1.10. Differential absorption of polarized light from CD. In Figure A case (I) polarized light passes through a optically inactive sample with no difference in absorption occurring, resulting in plane polarized light radiation as evidenced by resultant vector shown above. Case (II), polarized light passes through an optically active light source resulting in unequal absorption of L and R light, generating polarized radiation illustrated by the elliptical dashed line. (B) a comparison between ordinary absorption of a chromophore and CD absorption of same chromophore at identical wavelength. Band 1 for CD shows positive absorptions, band 2 negative and no absorption for optically inactive band 3.

Secondary structural analysis of peptides and proteins measured in the far UV spectrum and generally proceed through the election transitions $n \rightarrow \pi^*$, and $\pi \rightarrow \pi^*$[81, 84, 85, 87] with the former transition, forbidden electronically, but allowed magnetically[87] and primarily responsible for the large negative absorption band at 222 nm in alpha helices[87]. In addition to the strong, negative 222 nm peak, helices show a strong negative 208 nm ($\pi \rightarrow \pi^*$) and positive peak at ~198 nm, giving the characteristic negative double peak chromatogram. Beta sheets show a strong negative 216-218 peak. Random coils show positive and negative peaks at approximately 216 and 203 nm, respectively sheets[84]. Figure 1.11 provides a classical CD chromatogram of helix, sheet, and coil SS features. Another useful feature of CD is using the combination of CD libraries and algorithms allow breakdown SS content of complex proteins and peptides[83] further expanding its application.

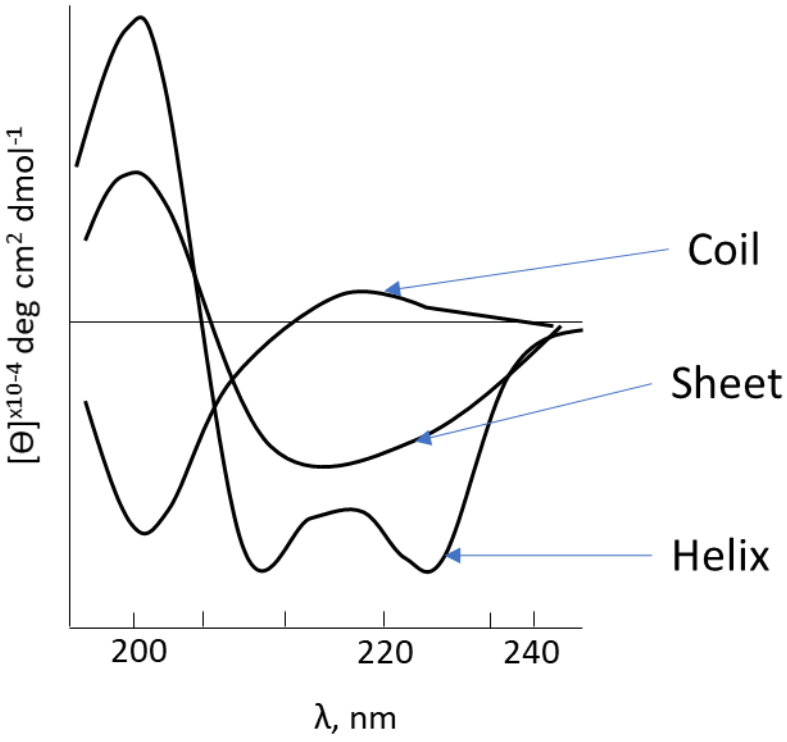

Figure 1.11. A CD spectrum of helix, coil, and beta-sheet secondary structure features.

Like other absorption methods, CD absorption follows Beer's law (under appropriate concentrations ranges) concentration dependent absorption as detailed in equation 1.69:

$$[A] = \varepsilon * l * C \text{ (1.69)}$$

Where *A* is the measured absorption, ε, the extinction coefficient, *l*, the optical path length, and *C* is the molar concentration. In the case of molar ellipticity, the Beer's like behavior is adapted to difference in polarized light absorption described in equation 1.70:

$$\Delta A = A_L - A_R = \varepsilon_L * l * C - \varepsilon_R * l * C = \Delta\varepsilon * l * C \text{ (1.70)}$$

Where L and R refer to the left and right handed light. The difference in absorption results in light that is elliptically polarized forming an angle θ, measured in millidegrees. Ellipticity and absorption are related by the equations:

$$\Delta A = \frac{\theta}{32980} \text{ (1.71)}$$

$$\theta = \frac{2.303(A_L - A_R)}{4l} \text{ (1.72)}$$

While most CD spectrum are recorded I in millidegrees (mdeg) most data is reported in the concentration normalized mean residue ellipticity (MRE) which possesses the units deg.cm^2/mol. Conversion of mdeg to MRE proceeds via equation 1.73:

$$MRE = \frac{mdeg * 100 * M}{C * l * n} \text{ (1.73)}$$

Where *M* is molecular mass, *C* is concentration in mg/ml *l* is path length in cm, and *n* is the number of residues in the protein/peptide samples.

CD methods are very amenable to protein/peptide thermodynamic studies due to its sensitivity to secondary structure changes that allows for changes in fraction folded/unfolded due to chemical/thermal denaturation to be measured. In the case of recording changes in fraction helicity there are numerous methods. For proteins, the most common method is to monitor changes in ellipticity at 222 nm and assume max helicity of a given protein at 222 nm is -36,000

MRE (deg.cm^2/dmol), while measured MRE for a coil is taken as -3,000 deg.cm^2/dmol[87]. Fraction helicity is then calculated according to equation 1.74:

$$fH = \frac{[\theta]-3{,}000}{-36{,}000-3{,}000} \quad (1.74)$$

Where θ is the measured MRE value. Other estimations include monitoring changes at 208 nm. In that instance equation 45 holds, though max helicity and coil MRE values are changed to -33,000 and -4,000 deg.cm^2/dmol, respectively. For peptides monitored at 222 nm, equation 45 is often used as well, however, more accurate measurements can be made using equation 1.75:

$$fH = (-36{,}000(1 - \frac{2.57}{n}) \quad (1.75)$$

Where *n* is the number of peptide residues.

As illustrated in equation 1.68, fraction helicity can be used to determine the equilibrium constant *K* from equation 1.68, free energy can be determined at any temperature. However, from relationship of equation 1.64 and 1.66 (relating enthalpic and entropic free energy to the equilibrium constant *K),* a new useful relationship between the two can be deduced[88]

$$K = e^{-\frac{\Delta G_O}{RT}} = e^{-\frac{\Delta H_O}{RT}+\frac{\Delta S_O}{R}} \quad (1.76)$$

Provided the molar heat capacity is constant, equation can be re written as:

$$K = e^{-\frac{\Delta H_m}{R}*\left(\frac{1}{T_m}-\frac{1}{T}\right)+\frac{\Delta C_p}{R}*(\frac{T_m}{T}-1+\ln(\frac{T}{T_m})} \quad (1.77)$$

For CD there is often insufficient information to properly fit molar heat capacity and it is generally set to zero, further reducing equation 1.77 to the following:

$$K = e^{-\frac{\Delta H_m}{R}*\left(\frac{1}{T_m}-\frac{1}{T}\right)} \quad (1.78)$$

Here ΔH_m refers to the van't Hoff enthalpy and T_m refers to the transition at the temperature, the latter is defined as the observed midpoint thermal transition. Here curve fitting routines utilizing Levenberg-Marquardt algorithm are used to fit the enthalpy and transition temperature.

Alternatively, equation 1.78 can be expressed in the non-exponential form as a function of free energy when convenient and fitted in the same function:

$$\Delta G = \Delta H(1 - \frac{T}{T_m}) \text{ (1.79)}$$

At the T_m point free energy is zero and the equilibrium constant is 1; from equation 1.64 it can be observed that entropy is determined from enthalpy divided by the transition temperature

$$\Delta S = \frac{\Delta H_m}{T_m} \text{ (1.80)}$$

Thus, all transition temperatures of interest can be determined from CD techniques.

While molar heat capacity, ΔC_p usually cannot be measured from single scans, it is often determined though chemical denaturation at multiple concentrations according to equation 1.81:

$$\Delta C_p = \frac{dH}{dT_m} \text{ (1.81)}$$

CD requires additional sample preparation considerations. For instance, many buffers are not compatible with CD as they absorb UV at the tested wavelength. Therefore, careful consideration must be given when choosing buffering agents. In cases where buffers with unfavorable characteristics are needed, complications can be mitigated through minimizing the buffer component concentrations, and/or choosing another suitable scanning range with less UV absorbance for said compounds.

1.26.5 Differential Scanning Calorimetry (DSC)

DSC provides valuable insight into the thermodynamic properties of peptide/protein folding and stability of both liquid and solid formulations such as free energy, enthalpy, entropy, molar heat capacity and the transition temperature. For solid formulations, glass transition temperature can be determined as well.

DSC functions by measuring heat absorption from a protein/peptide as it undergoes thermal unfolding. This is accomplished using a reference cell with identical solvent conditions

to the sample cell minus the protein/peptide (see Figure 1.12). As heat is applied to both cells, unfolding occurs in the sample cell resulting in heat absorption by the protein and a differential temperature between reference and sample. Heaters on the sample cell then raise supply the additional electric power to the cell, eliminating the temperature differential. This generally occurs as a single peak for simple proteins. After corrections for the instrumental and transition baselines as well as concentration normalization to the resulting thermogram, the calculated enthalpy ΔH_{cal}, ΔC_P, and T_m can be directly determined (see equations 1.55-1.56). Additionally, van't Hoff enthalpy (ΔH_{HV}) can be determined and compared ΔH_{cal}. Under van't Hoff, a two-state unfolding model is assumed when $\Delta H_{cal}/ \Delta H_{HV}=1$. Changes in free energy, enthalpy, entropy, molar heat capacity, and transition temperature were determined from equation 5.9 to assess changes in overall stability.

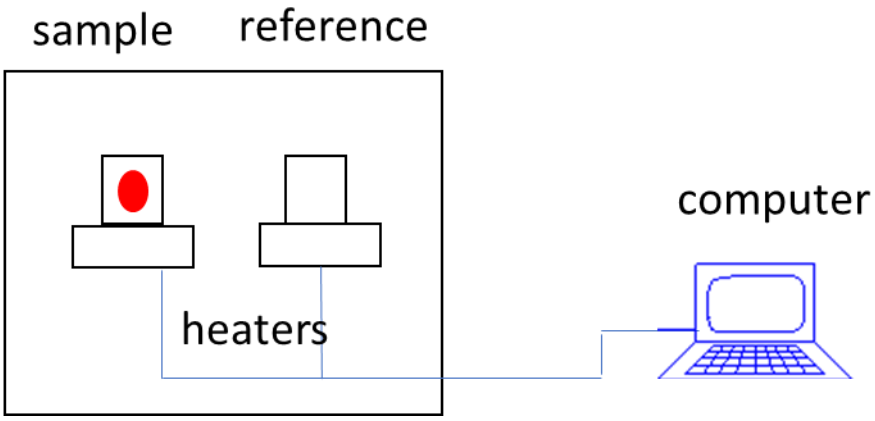

Figure 1.12. A schematic of a DSC set-up.

1.26.6 Nuclear Magnetic Resonance (NMR)

One of the most important and structurally elucidating analytical techniques, NMR operates on the absorption of radio waves by the sample ranging from 4-900 MHz[89]. NMR

differs from other traditional electromagnetic absorption techniques operating in the ultraviolet, visible, and the infrared portion of the spectrum. For such systems absorption involves interaction with the outer electrons of atoms as opposed to nuclei as is the case for NMR. Additionally, to make absorption possible, samples must be placed in an intense magnetic field to develop sufficient energy to allow absorption to occur. Figure 1.13 provides a brief schematic of an NMR system. There is a radio source, sample placed between two magnets, a detector and recorder.

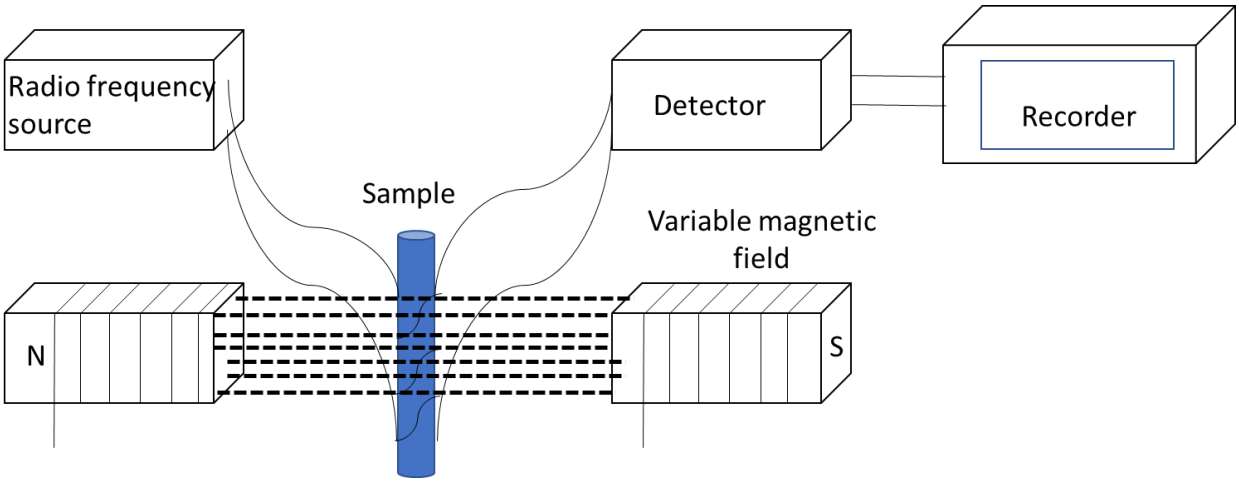

Figure 1.13. A schematic representation of NMR instrument components.

All charged particles in motion have an associated magnetic field, creating a magnetic dipole and a corresponding magnetic moment μ. When dealing with nuclei, the molecular moment is connected to nuclei's angular momentum quantum number, I, referred to as nuclear spin. Magnetic moment is proportional to the gyromagnetic ration ϒ as shown in equation 1.82

$$\mu = \gamma * I \quad (1.82)$$

Classically, NMR is often described as a spinning top precising around a uniform magnetic field (illustrated in Figure 1.14). The movement μ traces a circle around the magnetic field as described by the Larmor precession frequency in equation 1.83:

$$v = \frac{\gamma B_o}{2\pi} \quad (1.83)$$

Additionally, if a weaker magnetic field is placed perpendicular to B_o, it will cause the magnetic moment, μ to move away from B_o and the angle θ to increase. The change in θ corresponds to a change in resonance energy, *v*, which is the same as the field B_1 and must equal the Larmor precession frequency (equation 1.83)[90, 91]

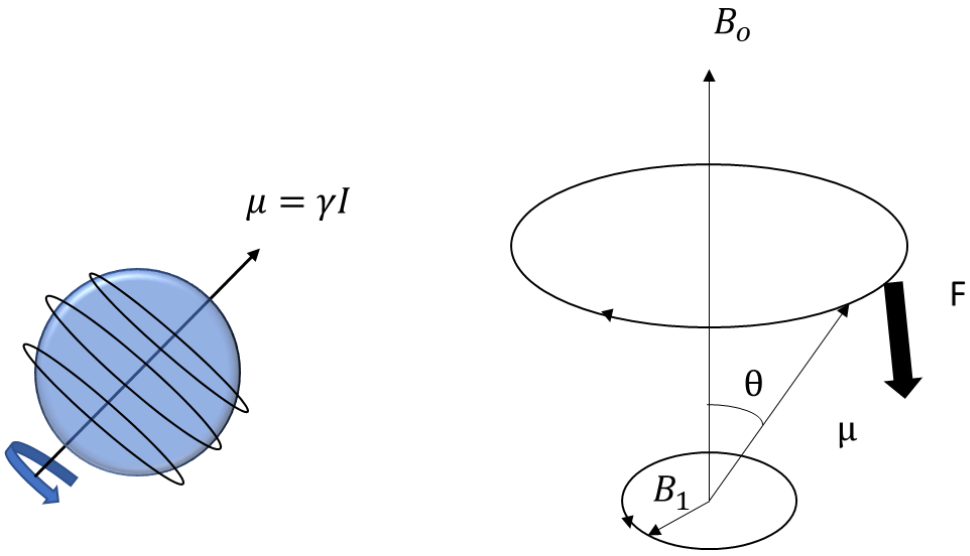

Figure 1.14. Angular momentum of the proton in NMR. The angular momentum μ is represented by the arrow through the spinning nuclei, B_o and B_1 represent the strong external magnetic field and the weaker, orthogonal magnetic field, respectively, while θ represents the angle between B_o and μ.

Typically, atomic nuclei are viewed as spheres, rotating about an axis, and possess intrinsic angular momentum, *P*. Angular momentum, like most other atomic properties, are quantized as detailed in equation 1.84:

$$P = \hbar\sqrt{I(I+1)} \quad (1.84)$$

Where ħ=h/2π (h is Planck's Constant). The maximum number of spin states, or P values is *I* the nucleus will then have 2*I*+1 discrete states[89, 91]. In the absence of an external field all states will of course be degenerate. In the case of ^{1}H, the only nucleus considered here, has an *I* value of ± ½.

As previously discussed, μ is proportional to the magnetogyric ratio and angular momentum *p* (equation 1.82). The relationship between observable magnetic moment and nuclear spin leads to observable magnetic quantum states *m = I, I-1, I-2,…, -I*; thus the ^{1}H proton will have a magnetic quantum state *m*=±1/2.

As stated earlier, in the absence of a magnetic field, all energy states are equivalent; however, once placed in a magnetic field the two *m* states possible of ^{1}H will split (see Figure 1.15), the magnitude of which is directly proportional to the strength of B_o as described by equation 1.85:

$$\Delta E = \gamma\hbar B_o \quad (1.85)$$

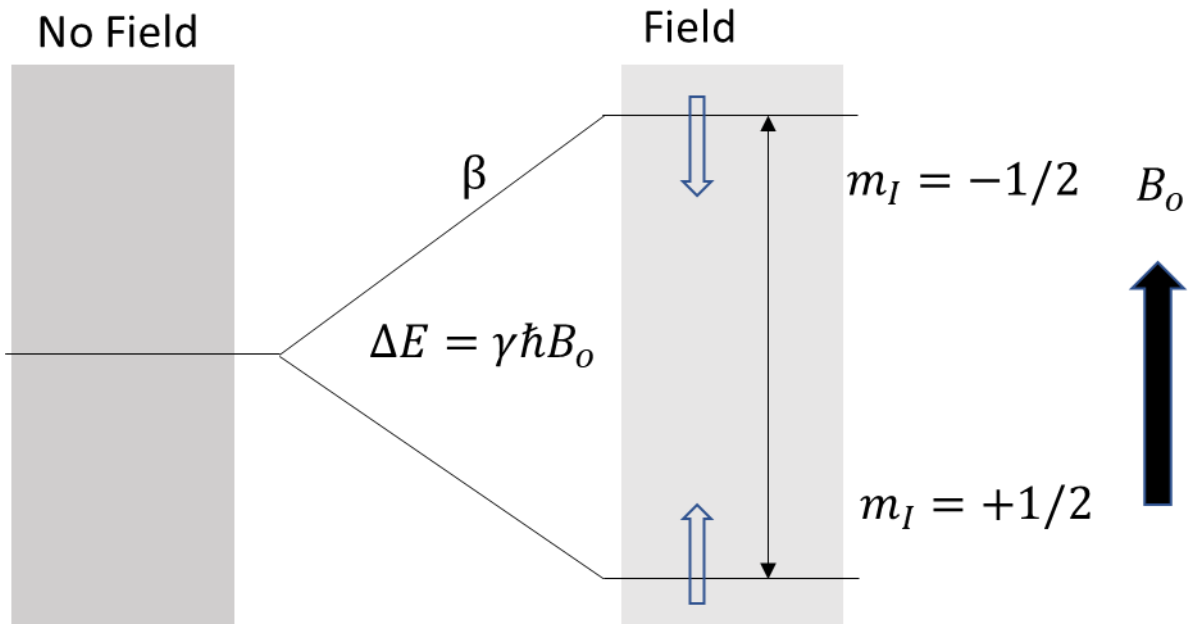

Figure 1.15. The nuclear spin energy levels of a spin-1/2 nucleus in a magnetic field.

When placed in the magnetic field, the *m*=±1/2 values are no longer degenerate and will be populated differentially with the lower energy state, *m*=+1/2 being more populated. By how many protons will occupy the lower relative to the higher is described using a modified Boltzmann equation (equation 1.86):

$$\frac{N_j}{N_0} = \exp\left(-\frac{\Delta E}{kT}\right) \quad (1.86)$$

Where N_j and N_0 are the population of higher and lower energy states, respectively, ΔE is the difference in energy of the two states, *k* is the Boltzmann constant, and *T* is the temperature. Generally, difference are very small, on the order of 10^{-6}, or parts per million, ppm[89].

Fortunately, nuclei are not only subject to artificial, external magnetic fields, but are very sensitive to nearby nuclei and their chemical environment. Given that a nucleus is surrounded by electron(s), when it is placed in a magnetic field, they too will have induced magnetic moments, causing them to circulate, generating a secondary, weaker magnetic field in opposition to the

applied field[90] (see Figure 1.16). This will cause the nucleus to be shielded in part from the external magnetic field and is described by equation 1.87:

$$B_{local} = B_o(1 - \sigma) \text{ (1.87)}$$

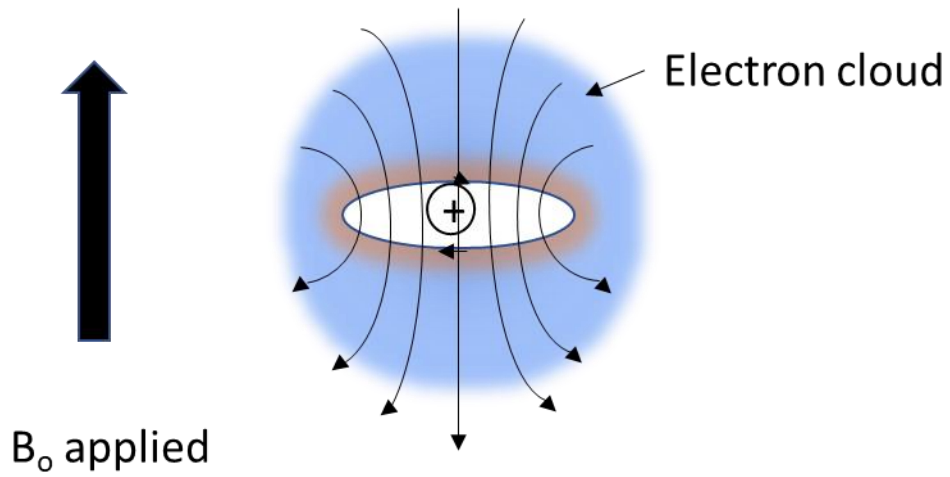

Figure 1.16. Magnetic field effect on electron motion and resultant induction of secondary, opposing magnetic field.

Equation 1.87 has important implications in identifying nuclei in a given molecule. Given ^{1}H in a molecule will experience a different chemical shift dependent on its neighboring atoms, a particular ^{1}H can be identified based on its chemical shift from a reference molecule such as tetramethylsilane (TMS).

When observing a proton NMR spectrum, the peak of a particular nucleus will often show a triplet or quartet signal. This often occurs because neighboring nuclei can contribute to the local magnetic field of the nucleus. Such behavior is referred to as the spin coupling constant, *J*, a scalar value. They are independent of field strength and much smaller in value than spin values. When two different nuclei delineated as A and X, respectively, both having spin ±1/2 and very different chemical shifts. When spins are positive or negative, they are

referred to as α and ß, respectively. For species X, if it is α; then the spin of A's Larmor frequency will be shifted by -1/2 *J* from its combined external and shielding magnetic effects. Likewise, if X is ß it would have a +1/2 *J* shift, creating doublet splitting for A, centered around the chemical shift features of A. X would also be a doublet, only it would be centered around the X chemical shift (see Figure 1.17a). The same process can be repeated for more similar nuclei and is also shown in Figure 1.17a. Combinations of nuclei can be explained in number and intensity using Pascal's triangle (Figure 1.17b).

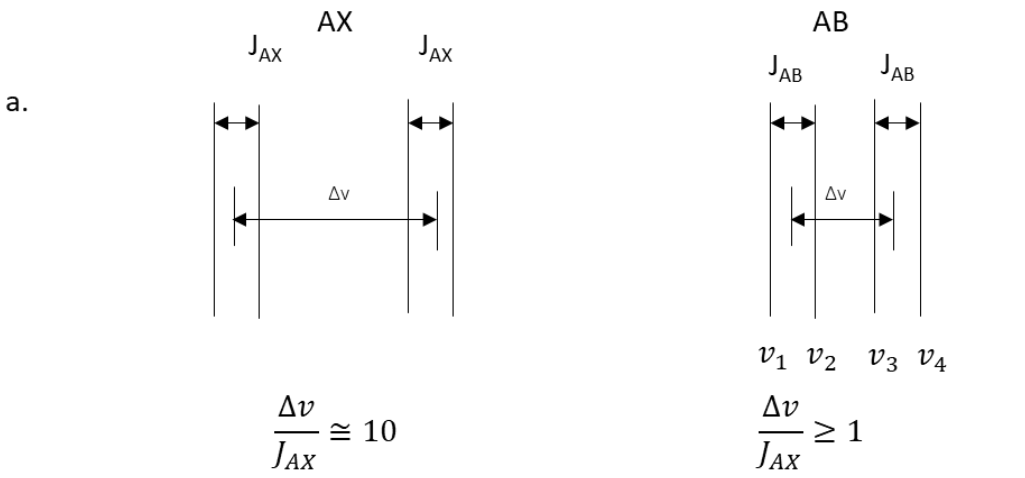

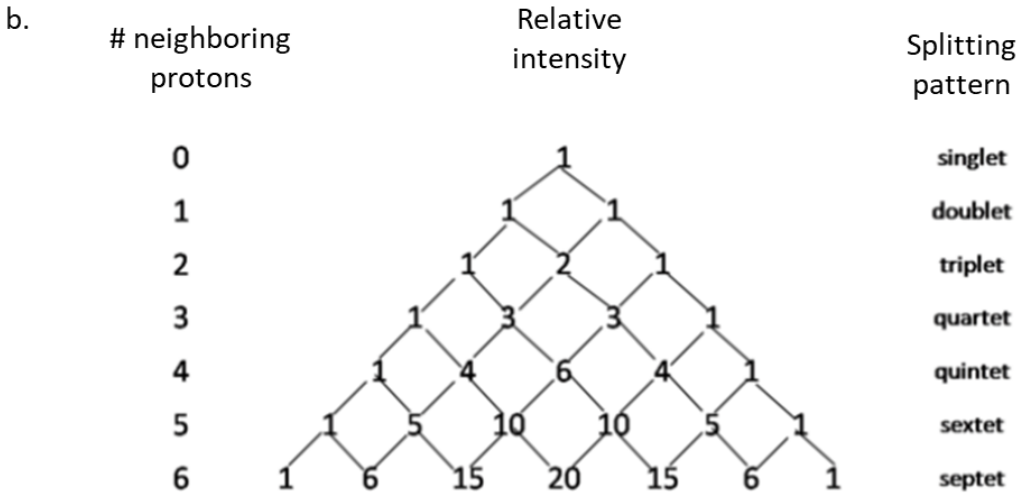

Figure 1.17. In part a. splitting patterns from two dissimilar (AX) and similar (AB) nuclei are shown. In b. splitting pattern and relative intensity based on the number of neighboring atoms are given.

1.26.7 Use for NMR and Peptide Secondary Structure Elucidation

Hα NMR chemical shifts in peptide backbones have long been known to be strongly affected by their torsional angles[92-95] and as such have been explored as means to elucidate SS content, ring effects, and hydrogen bonding in peptides and proteins[93, 96-98]. Chemical shift

estimations of peptide based and similar macromolecules are assumed to occur from independent and additive factors[92-94, 99] as described by equation 1.88:

$$\Delta\delta = \delta_{total} - \delta_{rc} = \delta_{tor} + \delta_{ring} + \delta_{HB} + \delta_{e} + \delta_{side} + \delta_{misc} \quad (1.88)$$

Here, *rc, tor, ring, HB, e, side, misc* refer to random coil or intrinsic, torsional, ring, hydrogen bond, electric field, side chain, and miscellaneous contributions, respectively. For Hα shifts, random coil "intrinsic" and torsional angle (ϕ/ψ) considerations contribute the most to observed chemical shifts, followed by ring currents, hydrogen bonding, and miscellaneous contributions[94]. The magnitude of contribution is enumerated in Table 1. Ignoring intrinsic, random coil effects, it can be observed that torsional factors make up over two-thirds of Hα variation[94].

Table 1.1.
Factors contributing to Hα chemical shift.2 RC refers to random coil, Tor, torsion angle, SC, side chain, HB hydrogen bonding, and ring, ring current.

Attribute	δ contribution
RC	25
Torr (φ, ψ)	50
Torr (φ, ψ_{i-1})	0
SC (χ)	0
SC $(\chi)_{i-1}$	0
HB	5
Ring	10
Local Charge	0
Misc	10

1.27 Statement of the Problem

Formulation optimization is a time consuming, complicated experimental process. To optimize formulations, excipients are often added to stabilize protein and peptide/protein based biologics. Thermodynamic mechanisms responsible for stabilization of secondary structure of biologics are not clearly understood.

1.28 Hypothesis

Excipients can thermodynamically stabilize/destabilize helix SS features in peptides and proteins. Thermodynamic mechanistic effects can be deduced from measuring changes in fraction helicity in SS of systems having excipients by comparing them with no excipient. Also, excipients stabilization or destabilization may be classified based on enthalpic or entropic dominant effects as preferential excluders/binders or crowders, respectively.

1.29 Aims

The current investigation has three specific aims: 1) Develop a model that can quantitate excipient thermodynamic stabilization of alpha helices in peptides through peptide unfolding using CD and verified with NMR. 2) Evaluate thermodynamic stabilization/destabilization mechanisms of PLL alpha helices. Aim 3) Extension of peptide model to model protein, BSA and its unfolding using DSC.

CHAPTER 2: DEVELOPMENT OF A MODEL SYSTEM FOR INVESTIGATING SECONDARY STRUCTURE OF PEPTIDE AND PROTEIN

2.0 Introduction

The objective of this aim is to develop a model that can evaluate excipient stabilization of alpha helix stability in peptides through peptide unfolding. Evaluation of excipient thermodynamic protection mechanisms, especially at different concentrations, will significantly improve the formulation process. As discussed in the thermodynamic and introductory sections, free energy of helix unfolding is directly linked to its stability. To determine stability enhancement/destabilization due to excipient effect, monitoring changes in fraction helicity due to thermal or chemical stress is needed. Briefly, this can be done through equating fraction unfolded vs native structure with the equilibrium constant *K*. From *K*, free energy and other thermodynamic parameters of unfolding can be determined. In setting up a suitable model, several factors need to be considered, such as the composition of the testing system, model peptide, solvent conditions, and types of excipients to evaluate. The general model will consist of three components: NaOH pH adjusted buffered solution (pH 11.7), a model peptide, and selected excipients at various concentrations. The model will then be subjected to thermal challenges and changes in fraction helicity and corresponding free energy recorded and plotted to evaluate changes in thermodynamic properties.

Few studies have looked at the thermodynamics of unfolding of specific SS features. The only studies that have looked at unfolding in specific SS unfolding are hydrogen deuterium exchange (MS_HDX) studies of lyophilized proteins/peptides[100]. To the best of my knowledge, no studies have directly measured change in thermodynamics of helix unfolding in peptides/proteins in liquid solutions.

PLL as a model peptide was chosen as it forms monomeric helix formation, chemical environments alter its SS, and its high solubility. PLL is a homo-polymer capable of adopting various SS depending on solvent conditions[101-103]. At pH less than 10.6, it adopts a random-coil extended helix structure but will transition to an alpha helix when the pH exceeds 10.6 due to the side-chains becoming deprotonated at high pH[101]. Upon heating above 55ºC for an extended period of time, then cooling, PLL will slowly and irreversibly form a beta-sheet SS[103]. Below55ºC heating is reversible[104] and two state. The degree of helicity at high pH is both a function of temperature and PLL size. Large PLL polymers will adopt a mostly helical structure at room temp, while smaller polymers will exist as partial helices at room temp and even 0 ºC[103, 105]. Here a 20-mer PLL polymer was chosen, as this represents the maximum length helix that would typically be found in a protein. Additionally, at this size, PLL fraction helicity will be more sensitive to solution conditions than larger analogs while also existing in monomeric form, simplifying results.

2.1 Excipient Selection

Excipients come in many classes and are included in formulations for a variety of protective and functional purposes. Here, three types of excipients are evaluated, polyols, disaccharides, and polymers represented by mannitol, trehalose, and PEG400, respectively. The former two are purported to be excluded from the peptide backbone, enthalpically stabilizing biologics[15, 16, 106, 107], polymer PEG400 is generally described as a crowder[108]. Mannitol, one of the most commonly used biologic excipients[109], has served many functions ranging from tonicity agent, bulking agent, lyoprotectant[110], osmolyte, and conformational stabilizing agent as previously mentioned. Trehalose likewise is found in a variety of formulations, a common lyoprotectant, kosmotrope, and osmolyte[9]. Like mannitol, it has been found to be excluded from

protein surfaces which effects may be concentration dependent[106, 111]. PEG400 is used in both liquid and solid formulations and has been is used as a crowding, or tonicity agent, or plasticizer. In liquid formulation it is often described as a crowding agent entropically stabilizing biologics[108]; however, due to its hydrophobic and enthalpic regions, it may preferentially bind to hydrophobic regions of a protein and peptide, thereby destabilizing it[51, 56, 108]. Urea was evaluated as negative control due to its denaturation effects which result from preferential binding and its chaotropic nature[74, 78, 112, 113]. Such destabilization will allow greater comparison of thermodynamic interaction mechanisms as well as a means to evaluate protective excipients against a chemical desaturating environment.

2.2 Model System for Thermodynamic Analysis

The model peptide system consists of three different systems: system #1, PLL in a buffered aqueous solution (pH 11.7) undergoing thermal stress. System #2 contains all components of the first in addition to tested excipients mannitol, trehalose, PEG400, and urea all at different concentration gradients. Like the previous system, system #3 contains PLL, buffered solution and excipients of system #2; however, mannitol, trehalose, and PEG400 are all held at constant concentration of 0.5M, individually against varying concentrations of urea while exposing to thermal denaturation (see Figure 2.1).

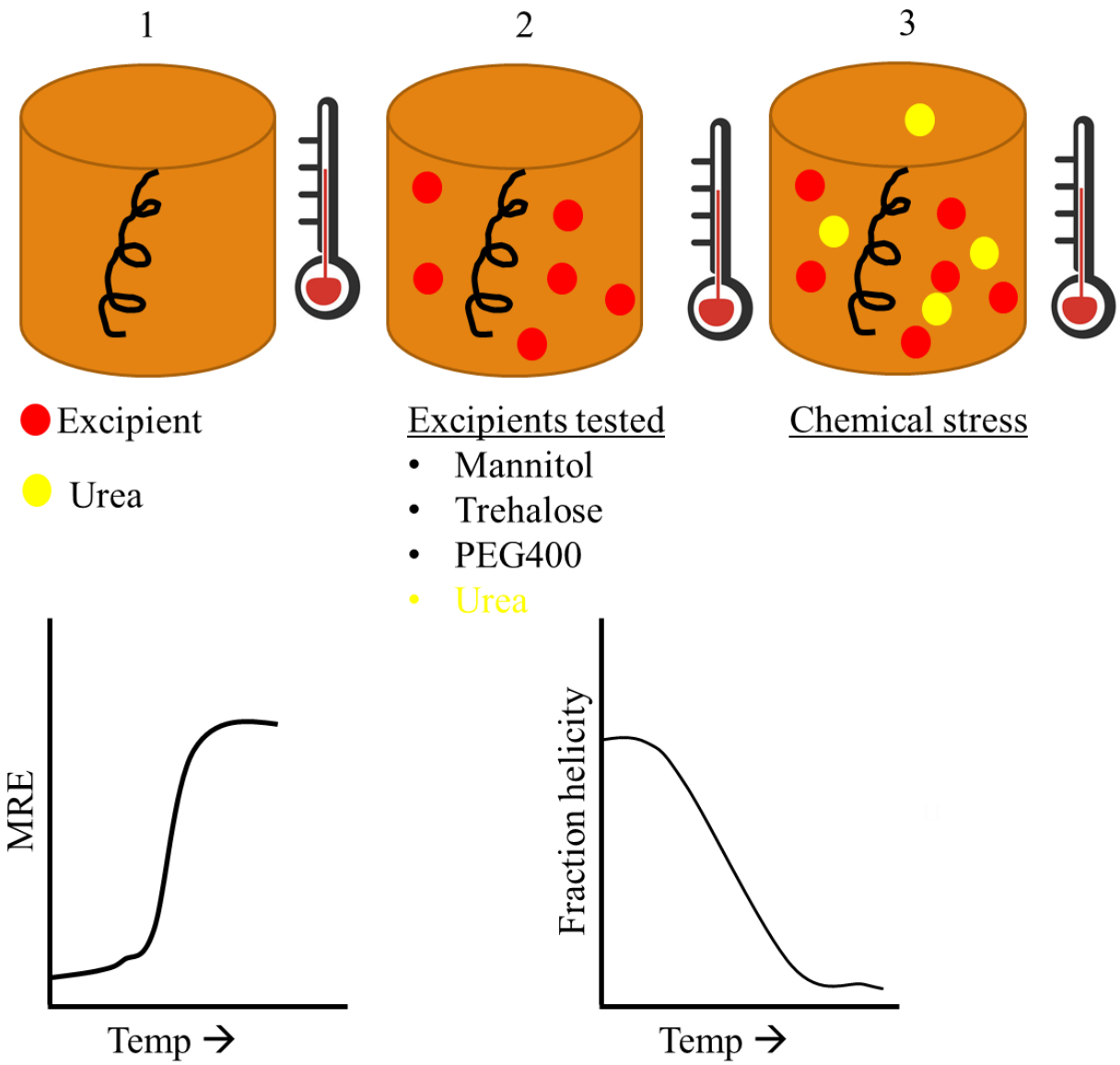

Figure 2.1. Peptide unfolding model. Red circles represent tested excipients, including urea in system #2. In Figure #3, yellow circles represent urea while red represent mannitol, trehalose, PEG400. Loss in peptide SS measured with CD is observed with loss in MRE absorption at 222 nm. The loss of MRE with increasing temperatures is correlated with corresponding loss of helicity using equation 1.79.

The thermodynamics of each system can be determined through monitoring changes in helicity using CD spectroscopy and NMR (used in system #3). As shown in Figure 2.1, thermal stress will induce loss of helicity (left figure). Excipients added will result in changes in the

enthalpy, entropy, and overall free energy of the system and will be determined through the following relationship:

$$\Delta\Delta X = \Delta X_2 - \Delta X_1 \text{ (2.1)}$$

Where *X* represents *G, H,* or *S,* allowing the quantification of helix stabilization to be measured. It should be noted that TΔΔS T = 298 K. Furthermore, from system #3, ΔC_p can be evaluated and used to monitor changes in ΔC_p with excipient type.

2.3 Materials and Methods

Materials were purchased from Alamanda Polymers with a purity greater than 95%. All excipients, urea, NaOH, and NaCl were purchased from Sigma Aldrich, St. Lois, MO, at 95% or greater purity and were used without further purification. PLL was weighed then diluted to stock concentration in NaOH solution with 10mM NaCl, to a concentration of 15 mM and adjusted to a final pH of 11.7. Excipient stock solutions were prepared at max desired concentrations then serial diluted to the desired concentrations of 0, 0.1, 0.25, 0.35, 0.5, 0.75, 1.0 M at pH 11.7. Stock PLL was added to each excipient dilution at a 100x dilution ratio for a final PLL concentration of 150 µM. All systems were then subjected to thermal stress as described in the CD analysis sections. Additionally, the effect of pH on PLL SS conformation was assessed. For conformational studies, PLL was prepared at 150 µM at pH 7.4 (10mM NaCl in PBS buffer) and at pH 11.7 in 00.5mM NaOH and 10mM NaCl. Blanks with buffers and excipients were run to later be used to subtract background noise from samples.

2.4 CD Analysis

CD-UV analysis was done on a Jaso-810 CD spectrometer with an attached Peltier and 0.1 cm quartz cuvette. CD spectra were recorded in triplicate with a scan rate of 100nm/min, 1mm slit width with excipient/buffer solutions as blanks. HT values did not exceed 600 V for

recorded data. Full scan spectra were acquired from 200-260 nm at 20°C. Thermal denaturation was carried by increasing the temperature from 20°C to 50°C at a rate of 0.5°C/min.

Data analysis: All data was collected in mdeg then converted to MRE using equation 5.29; fraction helicity was then determined from equation 5.30 while equilibrium constant *K* and free energy ΔG were determined from equation 5.30 and 5.23, respectively, for all data points using Excel 2016. Data was then plotted in Prism 6 using equation 5.36 and fitted with the Levenberg-Marquardt algorithm.

2.5 Results and Discussion

2.5 1 CD Analysis of Secondary Structure

Full scan CD spectra for neutral and basic pH solutions is shown in Figure 2.2. It can be seen at neutral pH (the orange line) the sample is indeed a coil, with positive peak in 210 to 225 nm range and negative peak at 198 nm. PLL at the high pH conditions (grey line) bears the trademark negative peaks at 222 and 208 nm, with trending large peak in the mid 190s range indicating a peptide helical in nature. At 194 nm the voltage exceeded 600 V and all data at lower wavelengths was not used. From Figure 2.2 it can be confirmed PLL does possess coil and helix SS features at the literature purported pH values.

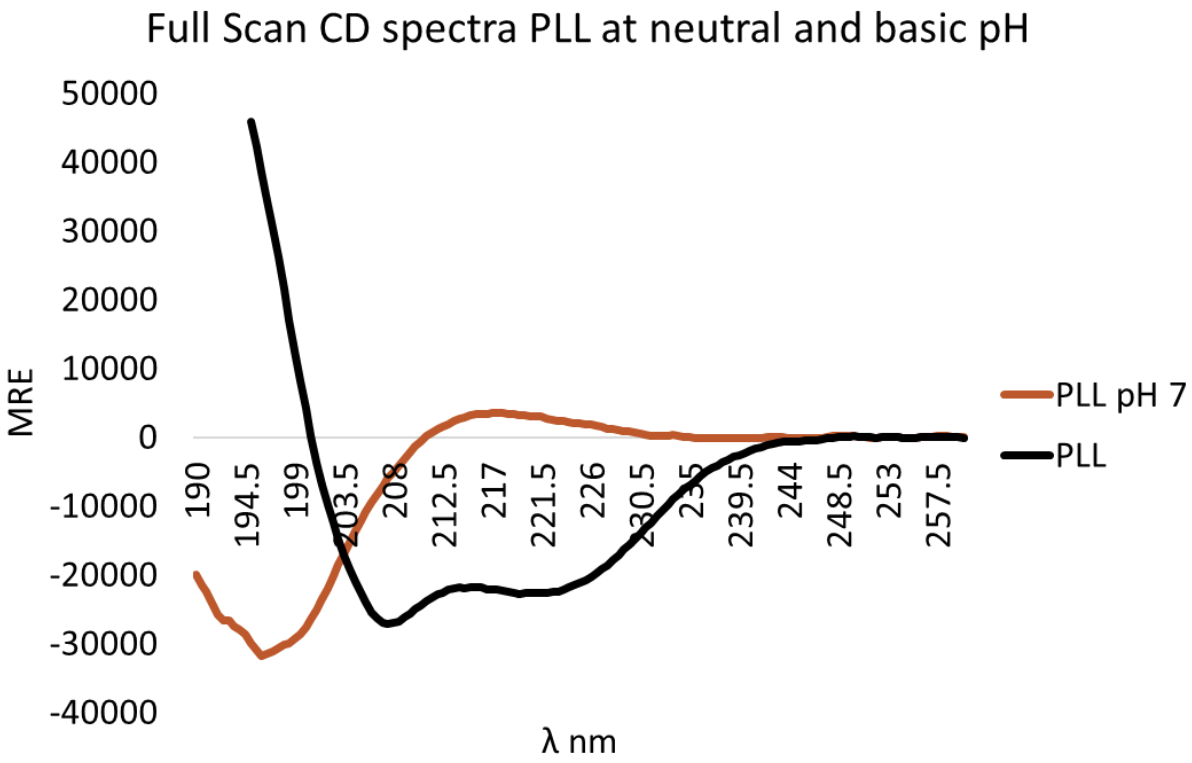

Figure 2.2. PLL full scan CD spectrum in neutral and basic solutions. The orange line represents PLL at pH 7.4 in PBS solution and the grey line, PLL at pH 11.7. The helix trademark double negative peaks are observed (black pH 11.7), while coil features are observed at pH 7 (orange) solution.

2.5.2 Effect of Temperature on PLL MRE and fH

Stabilizing additives can not only alter helical content due to preferential hydration or crowding effect but reduce unfolding due to thermal stress. CD thermal denaturation studies of PLL in increasing concentrations of mannitol were done (Figure 2.3) and monitored at 222 nm (as detailed in the methods section). Additionally, the effect of chemical and thermal denaturation via urea (0.75M shown in Figure 2.3) was done. From the figure it can be seen that mannitol concentration decreased MRE at 222 across all temperature ranges relative to PLL with no mannitol while 0.75M urea increased relative MRE of PLL (Figure 2.3a). MRE was

correlated with fraction helicity (Figure 2.3b) using equation 5.31, showing mannitol increased fraction helicity while urea decreased it.

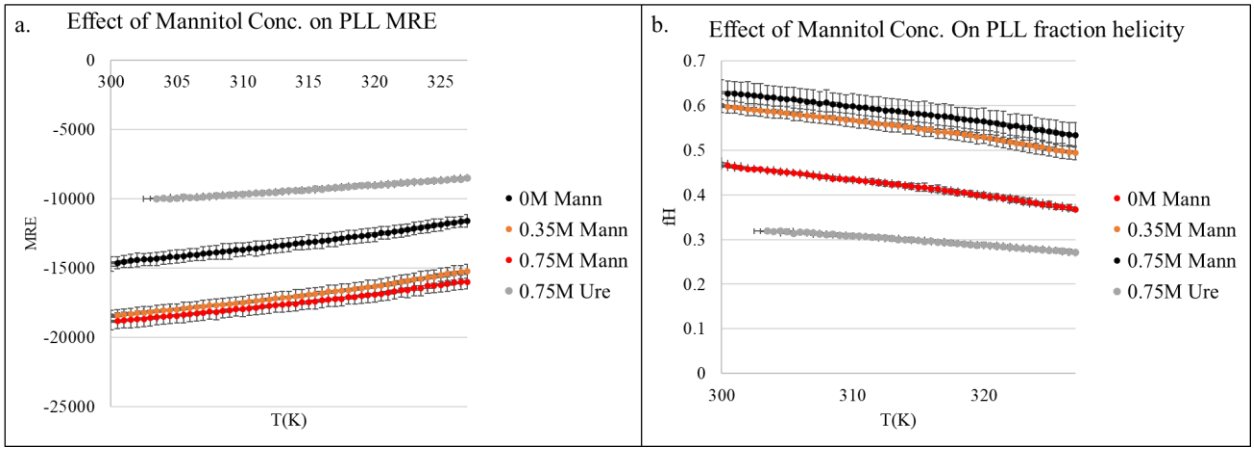

Figure 2.3. Effect of mannitol on PLL MRE (a) and fH (b).

It should be noted the slight sigmoidal shape of PLL while undergoing thermal denaturation and the reasons why. As mentioned earlier, PLL does display some unique unfolding properties. At temperatures exceeding 55°C it begins to fold into beta sheets irreversibly[104]. Below this temperature it interchanges between helix to coil structure, reversibly[104]. Complex interactions between helix to coil and coil to sheet may complicate the unfolding process due to poor cooperativity of peptide unfolding/folding[41, 114, 115], which can affect curve shape. Such behavior for example has been observed in certain slow unfolding helical peptides[114]. However, change in MRE and the corresponding fraction helicity are consistent with the expectation of the effects of excipient concentration and type, and gave consistent results through multiple experiments and analysis.

2.5.3 Effect of Excipients on PLL Unfolding Thermodynamics

Through thermal unfolding of PLL in the presence of various excipients at increasing concentration, changes in ΔΔH, TΔΔS, and ΔΔG were determined. Observations were recorded in Table 2.1 and Figure 2.4.

Table 2.1.
ΔΔX of PLL unfolding in the presence of mannitol.

Conc. [M] (n=3)	ΔΔH	TΔΔS T=298K	ΔΔG
0.1	14.3±0.478	12.6±0.462	1.67±0.0234
0.25	19.4±0.689	16.0±0.867	3.45±0.0751
0.35	20.2±0.938	16.7±0.867	3.42±0.0992
0.5	17.3±1.17	13.5±1.06	3.72±0.148
0.75	21.8±3.93	16.8±3.50	4.94±0.610

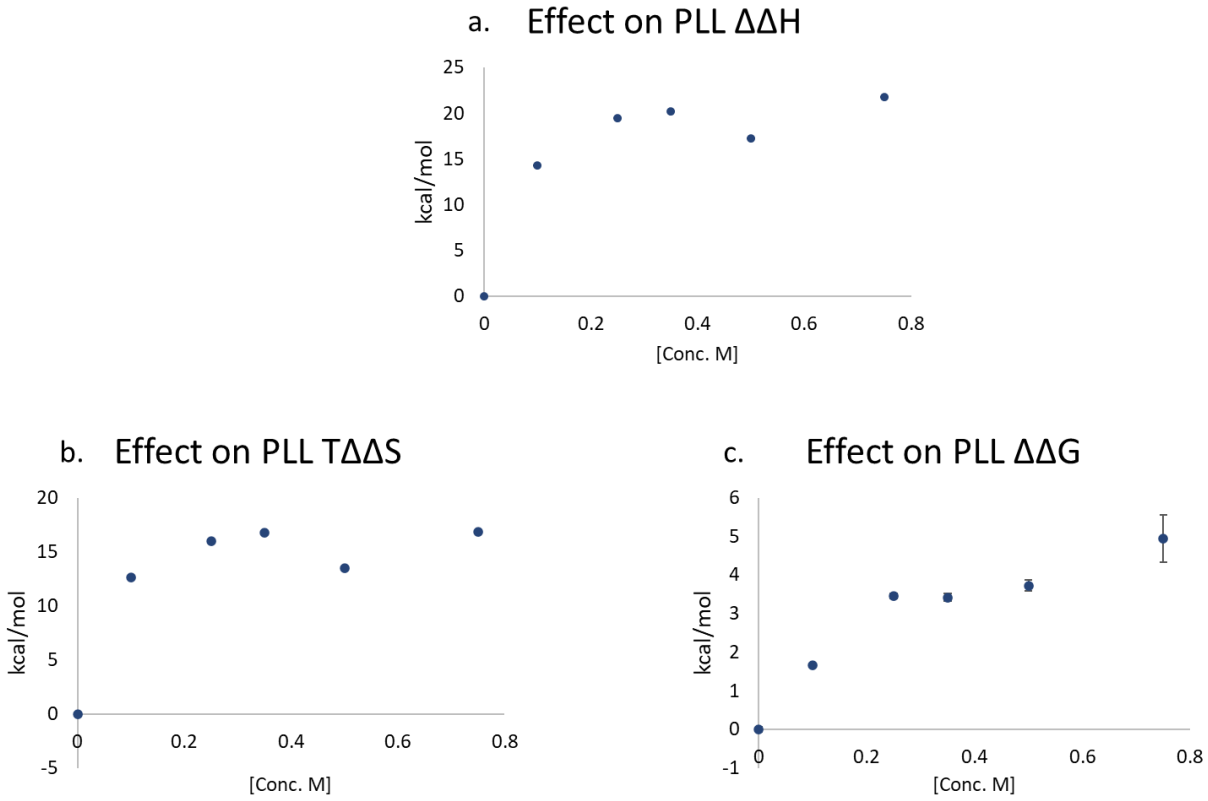

Figure 2.4. ΔΔX of mannitol on PLL a.) ΔΔH effects of mannitol on PLL unfolding. b.) Plot of TΔΔS PLL helix unfolding. c.) Plot of ΔΔG PLL helix unfolding.

An increase in ΔΔH is observed at all concentrations of mannitol; however, offsetting TΔΔS destabilization is observed reducing enthalpic stabilization. Near max enthalpic/entropic changes were observed at low concentrations creating an apparant plateau. However, net ΔΔG stabilization occured in a concentration dependent manner due to slight variations and increases in ΔΔH relative to smaller TΔΔS changes (Table 2.1 and Figure 2.4c).

Similar trends are observed with trehalose as shown in Table 2.2 and Figure 2.5 with increased enthalpic stabilization occurring at all trehalose concentrations, with a significant increase at the highest 0.75 M trehalose concentrations. Similar to mannitol, entropic destabilization is observed at all concentrations. Net stabilization of free energy is observed from 0.25-0.75 M trehalose. Surprisingly, trehalose thermodynamic parameter value changes were less in magnitude than mannitol. Trehalose was expected to be a stronger kosmotrope due to its larger size and greater number of oxygen atoms; however, mannitol effects were stronger. This is attributed to mannitol being a potentially stronger osmolyte than trehalose.

Table 2.2.
ΔΔX of PLL unfolding in the presence of trehalose.

Conc. [M] (n=3)	ΔΔH	TΔΔS (T=298K)	ΔΔG
0.1	6.79±0.535	6.90±0.125	$0.111\pm2.10\times10^{-2}$
0.25	4.16±1.23	3.40±0.0960	$0.758\pm1.00\times10^{-2}$
0.35	4.23±1.02	3.54±0.128	$0.691\pm2.00\times10^{-2}$
0.5	6.67±1.14	5.79±0.222	$0.882\pm8.00\times10^{-2}$
0.75	16.2±3.93	11.1±1.16	5.15±0.610

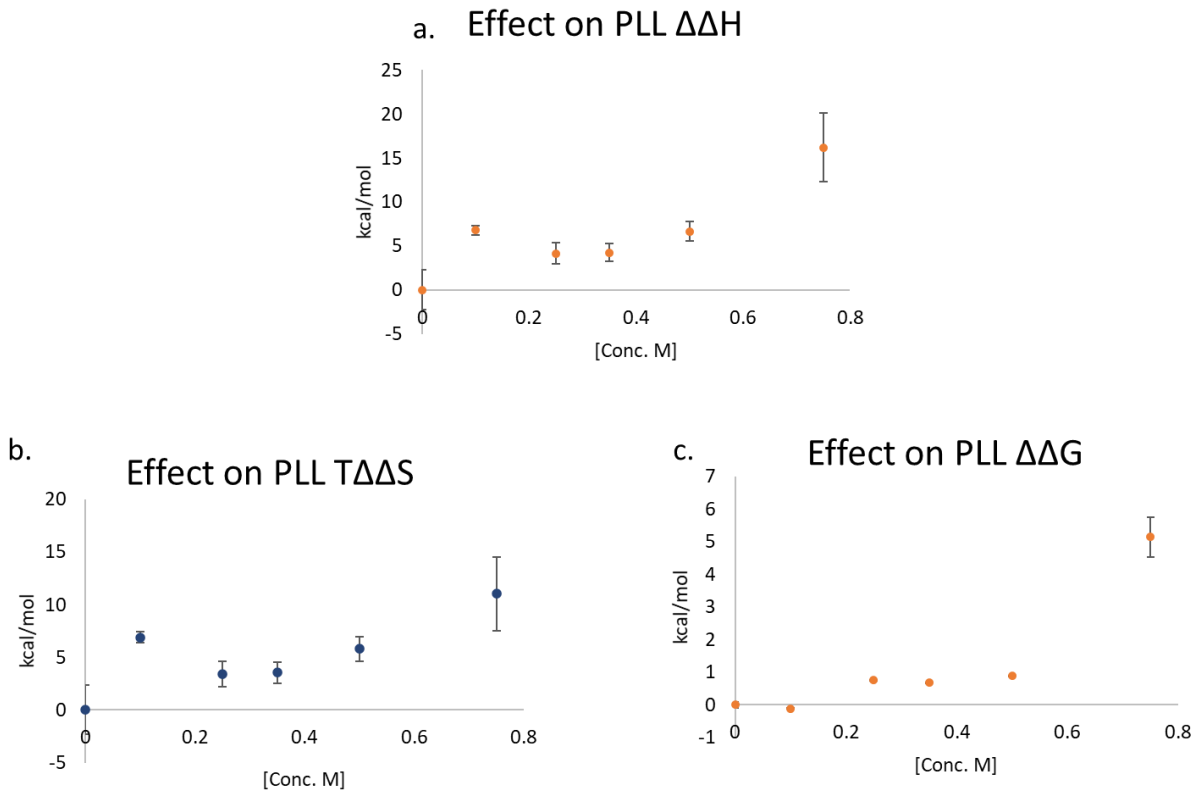

Figure 2.5. ΔΔX effects of trehalose on PLL a.) ΔΔH effects of mannitol on PLL unfolding. b.) Plot of TΔΔS PLL helix unfolding. c.) Plot of ΔΔG PLL helix unfolding.

PEG400 data, shown in Table 2.3 and Figure 2.6, differs from the mannitol and trehalose as there are minimal changes in the low to mid range concentration. Enthalpy stabilization is largely offset by entropy destabilization. At higher concentrations PEG increases ΔΔH significantly.

PEG400 has complicated, concentration-dependent effects on enthalpy, entropy, and free energy changes. The -CH_2 portion of PEG400 has the potential to preferentially interact with the peptide backbone and other hydrophobic portions of the ligand. Such interactions may be significant at the low to intermediate concentrations. Additionally, entropic stabilization was important at the low to intermediate concentrations. At high concentrations enthalpic concentrations dominate. Further discussion in later sections will explore these effects.

Table 2.3.
ΔΔX off PLL unfolding in the presence of PEG400.

Conc. [M] (n=3)	ΔΔH	TΔΔS (T=298K)	ΔΔG
0.1	-3.13±3.50	-1.31±2.02	11.8±0.381
0.25	0.460±1.38	1.13±0.734	$-0.672\pm6.10\times10^{-2}$
0.35	-3.88±1.07	-3.36±0.586	-0.517±0.0550
0.5	5.97±1.70	5.49±0.852	$0.477\pm3.00\times10^{-3}$
0.75	35.1±4.15	26.7±1.78	8.36±0.429

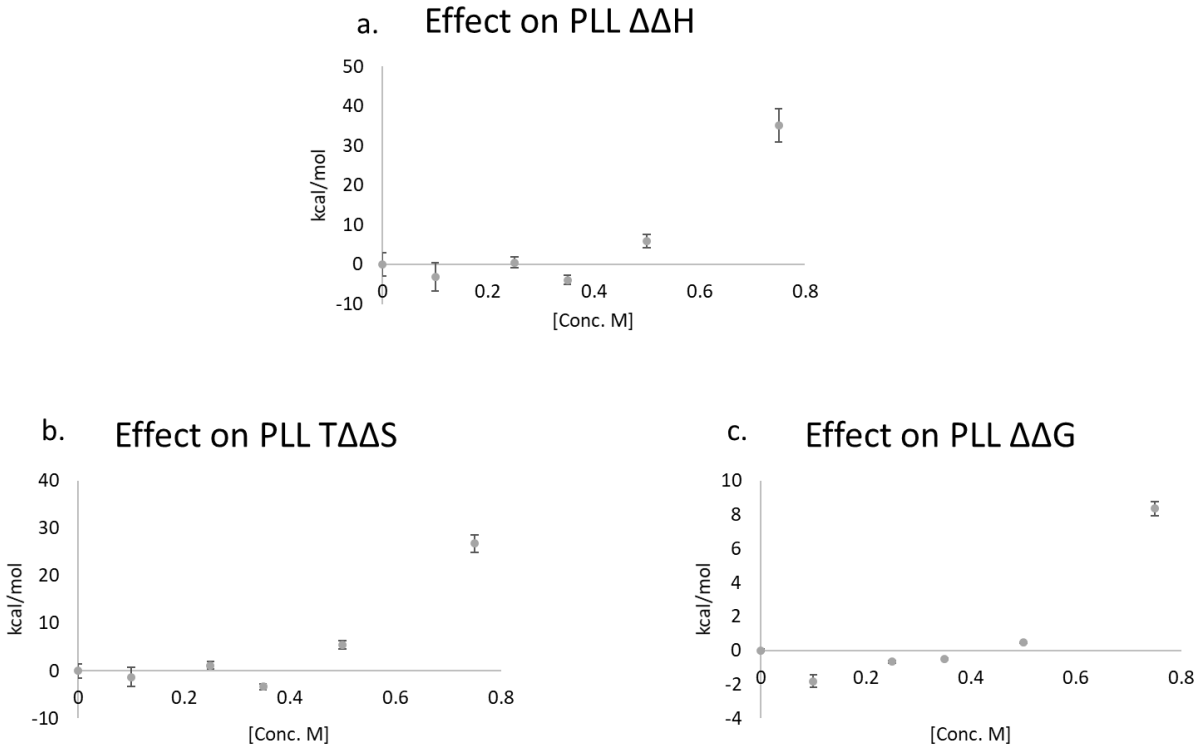

Figure 2.6. ΔΔX effect of PEG400 on PLL unfolding. a.) ΔΔH effects of PEG400 on PLL unfolding. b.) Plot of TΔΔS PLL helix unfolding. c.) Plot of ΔΔG PLL helix unfolding.

Urea decreases ΔΔH at all concentrations, plateauing at 0.35M with similar compensating TΔΔS stabilization increases with urea concentration, less so than enthalpic destabilization

(Table 2.4 and Figure 2.7). Overall, free energy destabilization was observed, plateauing at 0.335M urea concentration. Urea enthalpic destabilization was expected given its chaotropic nature. The plateau effects beginning at intermediate concentrations could be explained by the relatively small size of the PLL polymer being studied. Large globular proteins can show linear concentration dependent decreases in ΔΔG over large urea concentrations[74]. PLL, however, does not have tertiary and multiple SS features to unfold, and its smaller surface area may get saturated at lower concentrations. Smaller more incremental increases in urea concentration may have allowed for a linear effect to be observed.

Table 2.4.
ΔΔX of PLL unfolding in the presence of urea.

Conc. [M] (n=3)	ΔΔH	TΔΔS (T=298K)	ΔΔG
0.1	-1.69±1.52	-2.33±1.57	-0.641±7.53x10^{-2}
0.25	-8.85±1.23	-9.58±1.28	-0.732±7.78x10^{-2}
0.35	-25.0±1.17	-26.5±1.06	-1.45±0.175
0.5	-25.0±1.17	-26.5±1.38	-1.45±0.310
0.75	-25.0±0.265	-26.5±1.44	-1.44±2.24x10^{-2}

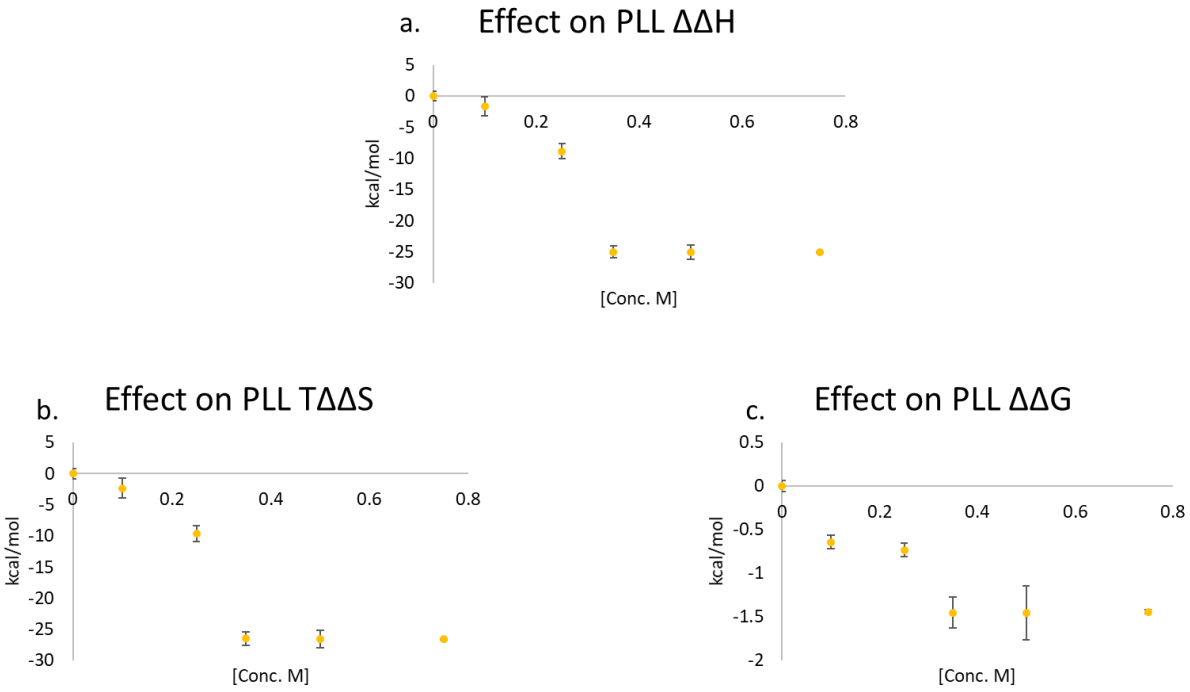

Figure 2.7. ΔΔX of PLL unfolding in the presence of urea. a.) ΔΔH effects of mannitol on PLL unfolding. b.) Plot of TΔΔS PLL helix unfolding. c.) Plot of ΔΔG PLL helix unfolding.

2.5.4 Effect of Chemical and Thermal Denaturation of PLL Unfolding Thermodynamics

PLL in the presence of 0.5M mannitol, trehalose, or PEG were chemically denatured using a urea gradient as well as thermally denatured at each urea concentration. Results from the preceding experiments are shown in Figure 2.8 for changes in enthalpy, entropy, and molar free energy. ΔΔH decreases linearly with urea concentration but remains positive for up to 0.5M urea. TΔΔS (Figure 2.8b and Table 2.5) likewise decreases in a concentration dependent manner, positive and destabilizing at lower concentrations; however, at higher concentrations it becomes negative and partially stabilizes PLL entropically, with overall destabilization observed. ΔC_p increases in the presence of mannitol; however, such increase is small and falls within the error range of PLL without mannitol.

Trehalose shows a linear decrease in enthalpy with increasing urea concentrations, with the only positive ΔΔH observed without the presence of urea. Entropic results mirror those of enthalpy, and overall trends follow those of mannitol, but less in trehalose. As with mannitol, there is no significant difference between trehalose stabilized PLL and no trehalose.

PEG400 shows similar behavior to system #2, where initial low/mid concentrations had minimal stabilizing effects or were slightly destabilizing. Here, enthalpy remains fairly constant until reaching 1M urea. Similar results are observed entropically where changes remain fairly constant while decreasing at the highest urea concentration. PEG400 effect on ΔC_p cannot readily be discerned due to significant standard deviation.

Table 2.5.
Effect of urea on ΔΔX in the presence of 0.5M excipient.

PLL Excipient Conditions	Urea Conc. M	ΔΔH	TΔΔS (T=298K)	ΔCP
No Excipient	0	$0.00\pm7.07\times10^{-2}$	$0.00\pm3.53\times10^{-2}$	$1.98\times10^{-2}\pm3.99\times10$
Mannitol	0	$0.823\pm5.54\times10^{-2}$	$0.124\pm2.49\times10^{-2}$	$2.35\times10^{-2}\pm1.90\times10$
(0.5M)	0.25	$0.397\pm4.99\times10^{-2}$	$-0.178\pm2.49\times10^{-2}$	
	0.5	$0.159\pm3.08\times10^{-2}$	$-0.249\pm2.40\times10^{-2}$	
	1	$-0.864\pm6.32\times10^{-2}$	$-1.08\pm3.16\times10^{-2}$	
Trehalose	0	$0.231\pm7.61\times10^{-2}$	$-0.255\pm3.81\times10^{-2}$	$1.59\times10^{-2}\pm4.04\times10$
(0.5M)	0.25	$-0.793\pm4.81\times10^{-2}$	$1.04\pm2.40\times10^{-2}$	
	0.5	-1.43 ± 0.171	$-1.43\pm8.55\times10^{-2}$	
	1	-1.64 ± 0.191	$3.93\pm9.53\times10^{-2}$	
PEG400 (0.5M)	0	$-1.06\pm6.88\times10^{-2}$	$-1.29\pm3.44\times10^{-2}$	-1.98×10^{-2}
	0.25	$-1.06\pm6.88\times10^{-2}$	$-1.29\pm3.44\times10^{-2}$	
	0.5	$-0.930\pm5.58\times10^{-2}$	$-0.941\pm2.79\times10^{-2}$	
	1.0	$-3.17\pm8.13\times10^{-2}$	$-3.21\pm4.04\times10^{-2}$	

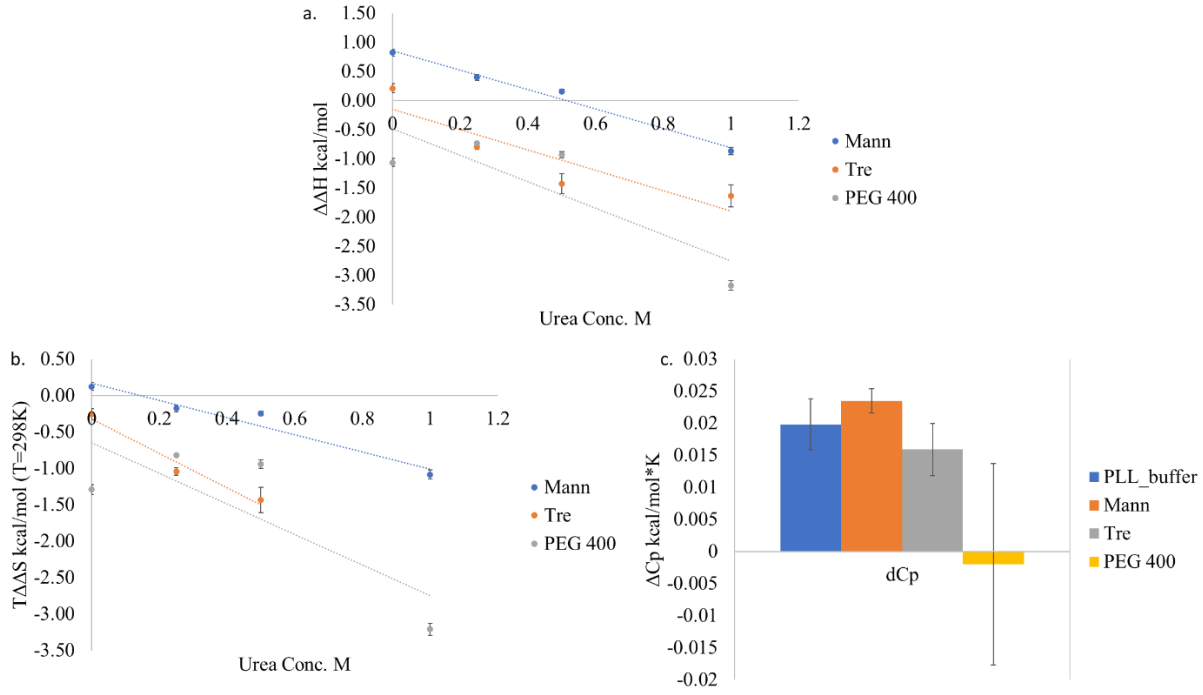

Figure 2.8. Urea and mannitol effect on PLL in the presence of 0.5M mannitol, trehalose, PEG400 with increasing urea concentrations a. ΔΔH against urea concentration, b. TΔΔS against urea concentration shown, and c. Table of ΔΔH, TΔΔS and ΔC_p shown.

Mannitol and trehalose both stabilized PLL alpha helices against thermal unfolding, increasing the enthalpic penalty of doing so with increasing concentration. While the ΔΔH effects were similar between the two additives, mannitol showed greater enthalpic stabilization than trehalose. Interestingly, enthalpic stabilization was offset partially by loss of entropy, somewhat negating the enthalpic stabilization; however, overall free energy stabilization was observed. PEG400 showed no significant effect (*p-value* 0.680) on PLL unfolding either entropically or enthalpically, except at the higher concentrations, ΔΔH increased. Urea significantly decreases ΔΔH but plateaued at the mid concentrations. Unlike mannitol and trehalose, enthalpic destabilization was offset entropically by urea; however, it was less in magnitude than enthalpic destabilization.

When holding mannitol, trehalose, and PEG400 concentrations constant at 0.5 M, while increasing urea concentrations, several effects on ΔΔH and TΔΔS were observed. Mannitol maintains its enthalpic stabilization up to 0.5M urea concentrations. Interestingly, urea seemed to stabilize PLL entropically despite the presence of mannitol, with stabilization increasing with urea concentration. Urea had this effect on all tested excipients. Like system #2, trehalose behaved in a similar manner to that of mannitol, but less in magnitude. PEG 400 was destabilized enthalpically at all concentrations, however such destabilization remained relatively flat, until 1M urea.

The effect of 0.5M excipients on PLL ΔC_p (estimated through chemical denaturation) was minimal and statistically insignificant; however, it was observed that mannitol ΔC_p may trend higher in heat capacity effects. Stabilizing excipients would be expected to increase ΔC_p as the difference in heat capacity of the native vs unfolded state would be higher in energy. Though excipients showed a trend in molar heat capacity increase, the effects cannot be stated due to the relatively small values and comparatively large error bars.

Overall, excipients showed concentration dependent effects on helix stability/instability depending on the type of excipient. Mannitol and trehalose stabilization increased with higher concentrations and PEG400 decreased with higher concentrations, though it was a stabilizing agent at low to mid concentration.

CHAPTER 3: CONFIRMATION OF ALPHA HELIX STABILIZATION USING NUCLEAR MAGNETIC RESONANCE

3.1 Introduction

CD is an excellent analytical technique to assess changes in secondary structure in proteins and peptides; however, NMR provides an orthogonal SS validation technique. Through use of chemical shifts of the alpha proton (αH), identification of SS features can be achived[116] as discussed in detail in the introduction sections.

Due to the significance of torsional effects, chemical shifts of Hα continue to be an area of interest to chemists seeking to quantitate SS of complex protein and peptide structures. Early studies were hindered due to the complex, convoluted spectrum in this region with little hope of resolution. Work shifted to small peptides, especially homopolymers as their spectrums presented less of an obstacle towards interpretation. However, such examples proved an insufficient model to whole proteins and peptides as they were generally analyzed in non-aqueous environments, possessed significant poly dispersion index (PDI) characteristics, and formed limited SS features under nonstandard conditions. As a result, such studies ceased. Instead, NMR analysis of protein structural features blossomed with the advent of more powerful NMRs, cross correlation techniques such as NOESY, and isotopically labeled proteins. Such techniques along with X-ray crystallography allowed for the compilation of large libraries of detailed protein and peptide structures. Protein databank libraries along with data mining and statistical analysis approaches allowed for the cataloging of Hα shifts of amino acids contributing to SS elements in proteins, establishing a chemical shift index (CSI) of said residues relative to their intrinsic random coil state. CSIs adjacent techniques have renewed interest in the analysis of $\Delta\delta_\alpha$ for protein/peptide characterization in a variety of disciplines. However, one area that has

received little exploration since Hα changes with homopolymers has ceased is its change with respect to denaturative conditions. Use of Hα shifts under such conditions would perhaps aid in evaluating local protein unfolding. To that end, studies of a homopolymers representative of proteins and peptides were carried out using NMR and CD for conformation.

Having an appropriate homopolymer peptide offers a significant advantage in this regard as peaks in the desired region are relatively simple to assign and provide a proof of concept, and clean, quantitative means to monitor unfolding of peptide and protein SS. Here a 20mer poly-l-lysine (PLL) was used as a model peptide as it can form helices, beta sheets and coil structures in aqueous environments within appropriate pH conditions. Additionally, it forms monomeric helices even at the relatively high concentrations required for adequate NMR signal strength and can be obtained without a large poly dispersion index (PDI), a problem for earlier studies[94]. Additionally, PLLs of this size form partial helices with increasing/decreasing helicity possible upon addition of cosolutes or change in temperature. CD is a common method for peptide/protein structure ellucidation[80, 83, 85, 117], and was used to determine the fraction helicity (fH) of PLL. Changes in $\Delta\delta_\alpha$ under varying temperature and cosolute conditions were recorded to evaluate the degree of correlation with fH as determined via CD. Studies assessing PLL fraction helicity (fH) were evaluated using chemical shift methods and compared against circular dichroism (CD). Moreover, effects of thermal and chemical denaturation on helix PLL unfolding were also performed and evaluated against fH as determined via CD. Such a model can provide useful insight in Hα changes with helicity in a small, simplified model and may be applied to larger proteins to better understand local protein unfolding through NMR.

3.2 Method

Samples were prepared the same as that of CD; however, concentrations of PLL ranged between 10-20 mg/ml in water with 30 ul D_2O (for signal locking). Samples were run on a JOLE 800MHz NMR using HNMR with Dante suppression of the water peak. Samples were analyzed at 5K intervals ranging from 300 K to 320 K. Sample analysis and peak assessment were evaluated using JOEL software.

Changes in chemical shift from random coil were first assessed through aligning all β, γ, δ, and ε proton peaks to the random coil PLL (pH 7) at 300 K, as these peaks did not significantly shift with temperature increases. From here, changes in αH were measured through comparing Hα peaks at pH 7 (coil) compared to helix solutions (pH 11.7) at varying temperatures. Max helicity was measured from a PLL solution of 50:50 MeOH and water at room temperature [118]. The fraction helicity was determined by dividing the difference between chemical shift coil and observed chemical shift and max helicity from the PLL methanol: water sample at each respective temperature. Data was plotted and evaluated in the Graph Pad Prism software, version 6 and Excel.

3.3 Results and Discussion

3.3.1 Identification of PLL Protons and Temperature Effects

Proton ^{1}HNMR of PLL is shown in Figure 3.1; where all protons are identified. From the most shielded to least shielded (ppm), each proton is listed as follows: γ at 1.1, δ 1.3, ß 1.6, ε at 2.9, α and α' at 4.15 and 4.05 ppm, respectively. The amide bonds are barely visible at ~8.0 ppm. Regarding the α peaks at 4.15 and 4.05, they refer to internal and external α protons, respectively[119]. The peaks for ß, δ and γ are poorly resolved as PLL is a polymer, and small

differences in the same proton type (due to its location in the helix/coil structure) cause only small chemical shifts and overlap with each other.

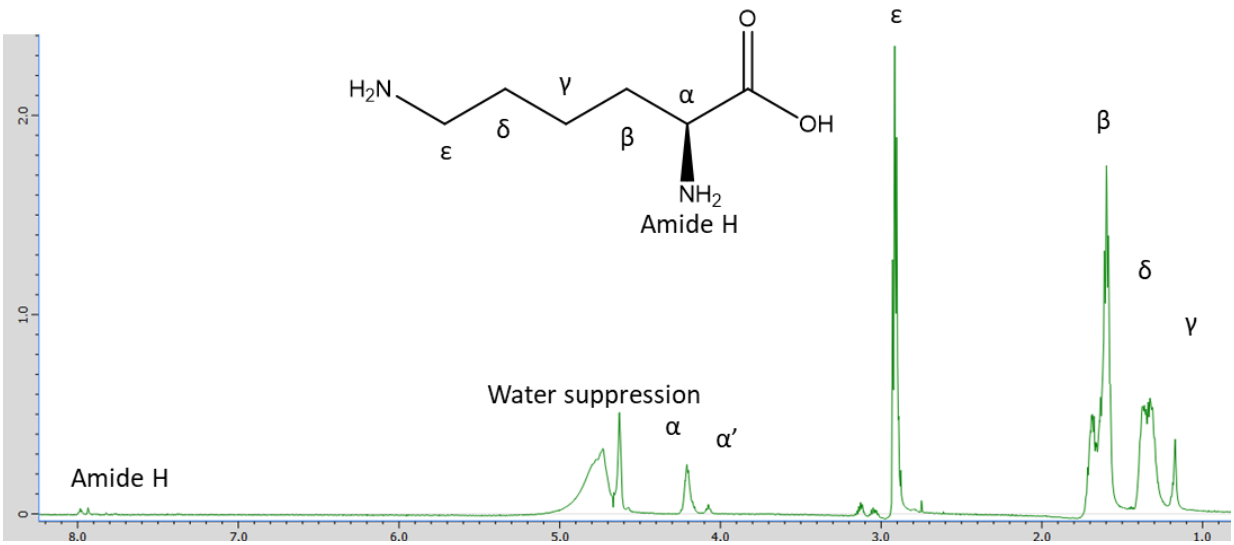

Figure 3.1. α[1]HNMR of PLL.

Effect of temperature on αH chemical shift was observed and recorded in Figure 10.2a. As can be seen from the Figure, chemical shifts for the ß, γ, δ, and ε do not change with temperature; however, αH chemical shifts do change with temperature (Figure 3.2b). For peptides, helices and coil chemical shifts are demarcated at 4.21 and 4.14, respectively[92, 96, 116, 120]. Thermal denaturation of PLL from 300-320K at 5K increments caused αH of the helical peptide to shift downfield with temperature increases (Figure 3.2b) due to deshielding from loss of the oxygen proximity to the alpha proton[121], while the 4.14 coil alpha proton remains constant.

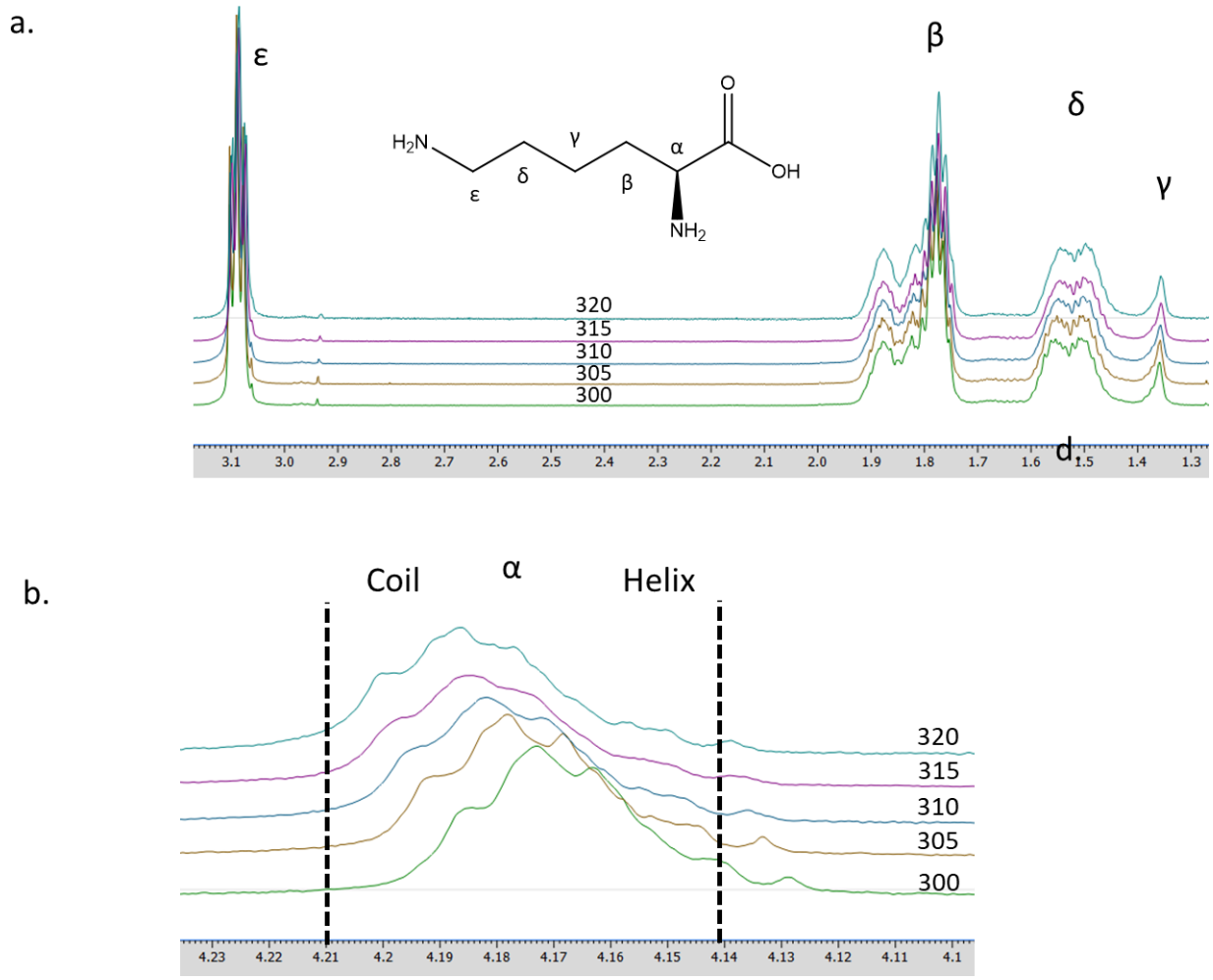

Figure 3.2. Temperature effects on the chemical shift of the different PLL protons.

3.3.2 Fraction Helicity Through NMR and Thermodynamic Effects of Excipients

Shifting of helix alpha protons downfield is associated with loss of helicity[92, 97, 121, 122]. To quantitate change in PLL helicity, comparison of αH chemical shift at max helicity vs coil structure was performed. PLL adopts its highest fraction helicity under MeOH:H_2O solvent conditions, while it exists in a coil configuration at pH 7 in an aqueous environment. A far UV full CD scan from 190-260 nm was carried out for PLL at pH 7, 11.7 (in buffered aqueous environment) and with MeOH:H_2O solvent conditions resulting in coil, partial helix, and helix

SS character, respectively (Figure 3.3a). It can be seen that helicity in the organic/aqueous environment is greater than that of the basic PLL solvent system, while neutral pH PLL solution is clearly coil. Normalizing all recorded αH chemical shifts at different temperatures to that of the organic/aqueous system was done to estimate fraction helicity and compared to that of CD.

The effect of 0.5M mannitol on thermal denaturation and chemical denaturation of helical PLL was then examined. (Figures 3.3b and Table 3.1). The data show with an increase in temperature, fraction helicity decreased as measured NMR, corroborating CD data; however, the extent of increase is different between the methods. For PLL systems, the rate of decrease is greater in CD with a slope of 0.363±0.237 and reasonably linear correlation of r^2 0.857 being observed. However, when in the presence of 0.5M mannitol and increasing concentration of urea, rate of PLL helix unfolding increased faster with NMR with slopes of 2.32±0.0321, 2.36±0.278 and 3.44±0.723 for 0, 0.5, and 1M urea concentrations, respectively. Mannitol as in the case of CD increased the helicity of PLL, and hindered unfolding. It was observed that mannitol protected PLL helix chemical unfolding up to 0.5M urea compared to PLL only at pH 11.7. Reasons for discrepancies likely stem from the slight changes in chemical shifts of alpha helices caused by helix unfolding (~0.1 ppm) compared to relatively large changes in molar ellipticity (measured as MRE) which can range in magnitude by tens of thousands of deg*cm^2/dmol. Measuring small changes in chemical shift are more likely to be subject to error and poor precision. While there was poor correlation between the two methods, trends in increased unfolding due to thermal and chemical stress were observed for both methods. Given CD is an established analytical method for protein and peptide unfolding, results obtained from CD were used to calculate thermodynamic parameters due to loss of helicity. However, having an orthogonal confirm loss of helicity was desirable.

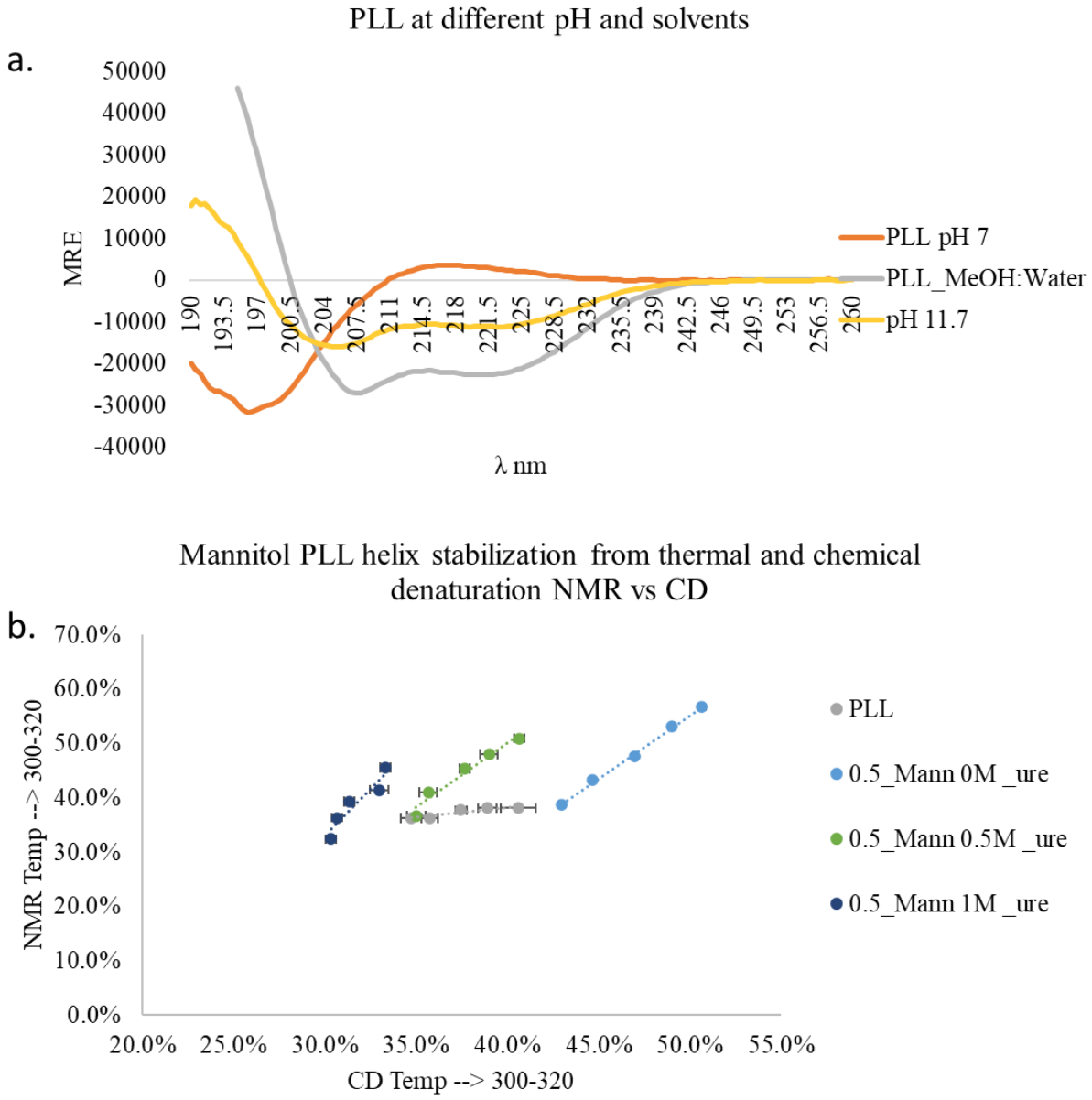

Figure 3.3. In a. a full far UV scan of PLL at different pH and solvent conditions is shown. In b. changes in helicity of PLL due to temperature and urea denaturation are shown. Here, gray is PLL at pH 11.7, no mannitol; light blue, PLL with 0.5M mannitol; green, 0.5M mannitol and 0.5M mannitol, and dark blue 0.5M mannitol and 1M urea.

Table 3.1.
NMR-CD plot slopes.

System Conditions	Urea Conc.	Slope	r^2
Buffer	0	0.363±0.237	0.857
Mann	0	2.32±0.0321	0.996
	0.5	2.36±0.278	0.960
	1	3.44±0.723	0.883

CHAPTER 4: AIM 2: ELUCIDATING EXCIPIENT THERMODYNAMIC STABILIZATION MECHANISMS OF HELICAL PEPTIDES

4.1 Introduction

Biologics are relatively large, complex, and fragile molecules, subject to physical and chemical degradation. Other factors such as solubility, viscosity, and pH need to be tailored to meet delivery conditions and improve patient comfort and compliance. At times, such factors may complicate the overall stability. For example, solubilization enhancement often reduces the free energy unfolding,[8, 9] increased concentration increases the risk of aggregation and increases viscosity, making injections more difficult. However, reducing viscosity increases the risk of aggregation. Biologics may demonstrate ideal stability at pH levels not acceptable to intravenous administration. Additionally, many small molecule pharmaceutics are formulated together to enhance therapeutic effects and patient compliance. No such strategies have been successfully achieved with biologics[123]. Meeting such formulation demands often requires complex excipient compositions with each component possessing stabilizing/destabilizing features. Excipient interactions may vary with type and concentration, thus being able to classify such excipient protection mechanisms under a variety of conditions is desirable.

The enthalpy-entropy compensation (EEC) is a phenomenon observed across a wide variety of chemical processes[107, 124-129], and is pertinent to drug design and protein folding/unfolding. The overall change in free energy of any chemical reaction is, of course, governed by compensating/competing components enthalpy and entropy[130]. Briefly, EEC occurs when enthalpy and entropy offset one another minimizing free energy change. This is classically observed with the transfer of alkanes and alcohols to aqueous solutions, which is enthalpically favored, but entropically unfavored by a factor of 2-3,[127] offsetting enthalpy and minimizing the

change in free energy. Many explanations for EEC have been provided, ranging from statistical mechanical models using many micro-states[128] to supplemented hydrophobic effect models[125-128, 130] i.e. solvent surrounding the protein/peptide and cosolute/excipient "feel different" relative to solvent of the bulk solution. For example, a protein surface where water is strongly ordered, comes into the vicinity of a relatively hydrophobic cosolute, energetic water surrounding the two species is released, increasing the entropy of the system, favoring the process; however, this comes at the expense of formerly strongly bound water at the surface being broken to less energetic bulk solution interactions. Moreover, loss of entropy of a solute/effective ligand upon binding also needs to be considered (this is especially relevant in the case of ligand design). This overall process is shown in Figure 4.1.

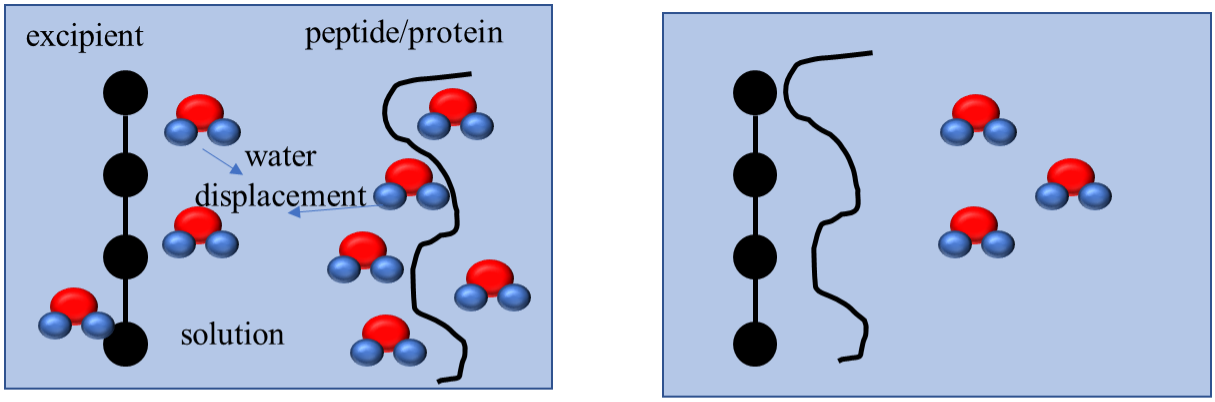

$$\Delta G_{solv-disp} = \Delta H_{solv-disp} - T\Delta S_{solv-disp}$$

For all solvent molecules: $\Delta S_{solv-disp}$ favors excipient binding
For non-energetic waters: $\Delta H_{solv-disp}$ opposes excipient binding
For energetic water: $\Delta H_{solv-disp}$ favors ligand binding

Figure 4.1. Enthalpy-entropy compensation effect of an excipient on a peptide/protein.

The opposite is true for protein/cosolutes when the two species repel (strong water ordering around each other, no interaction) creating a greater hydration shell that is enthalpically

driven, offset by the loss of entropy of the local water molecules. In both cases, folding/unfolding is hindered/helped through net enthalpic means while both are offset entropically. Thus, we see another molecular explanation of the exclusion/inclusion theory of protein/peptide stabilization. Such discussion can naturally be extended toward neutral crowders: lack of space for peptide/protein unfolding creates a stabilizing entropic penalty towards unfolding yet reduces the number of potentially high energy bound water molecules, creating net entropic stabilization overall. Given the complex nature of both biologic solute and excipient cosolute, determining which free energy component prevails in physical stabilization can be difficult to predict.

EEC generally follows a linear relationship towards whatever process is being monitored, i.e. ligand binding strength/size, protein stabilization through excipient addition, etc., and maintains this linear relationship through a wide temperature range (150-300K)[127]. From protein unfolding studies reported on by Liu et al, of 3,224 proteins, a strong correlation between enthalpy and entropy was observed with a correlation coefficient of (0.991) reported, a slope of (0.909), observed and $P<(0.001)$[126]. Moreover, with a slope so near unity indicates any change in enthalpy will be offset by entropy[131], resulting in small free energy changes. Free energy vs enthalpy, however, showed little to no correlation with changes in ΔH and ΔG, indicating their independence from each other[126]. Given the linear nature of EEC, plotting entropy of unfolding vs enthalpy of unfolding can provide insight into the entropic stabilization of peptides or proteins, especially when delineating said graph into quadratic regions via diagonals through the origin (see Figure 4.2).

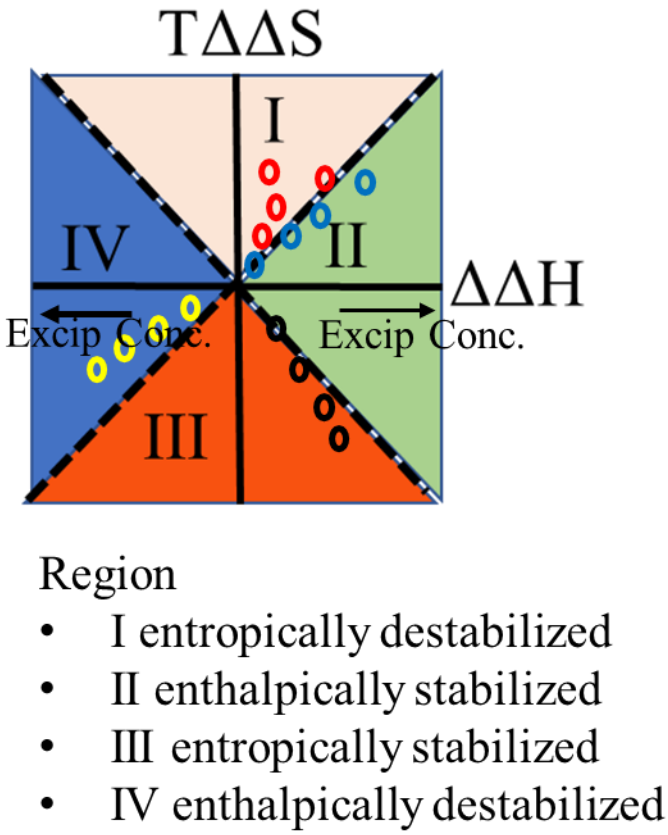

Figure 4.2. A generic graph of EEC for peptide is shown. Regions I-IV indicate if an excipient is stabilizing/destabilizing by primarily enthalpic or entropic means. Regions I and IV are entropically and enthalpically destabilizing, while conversely, regions II and III are likewise stabilizing. Arrows indicate excipient concentration gradient.

Figure 4.2 divides the EEC plot into four regions. The top half (regions I and IV) are entropy and enthalpy destabilizing, while the converse is true of regions II and III. The arrows indicate increasing excipient concentration. It is observed through the increasing blue circle excipient concentration in regions I and II that an enthalpic compensation is gained but stability is largely offset by loss of entropy. Black circles indicate concentration dependent excipient entropic stabilization as indicated from the non-unity slope. Increased distance from the diagonal indicates increased stabilization by entropic means. Such stabilization by excipients is

likely the result of crowding effects. Like region II, region IV possesses non-unity EEC effects and is enthalpically denatured.

EEC plots have several uses in studying protein/peptide behavior for many processes. Recently, Pechl published a novel study detailing folding mechanisms and stabilization of antibodies and development stabilization *in vivo* using enthalpy-entropy plots[129]. Sukenik and company utilized a similar strategy to that of (Figure 4.2) to characterize salt, polyols and polymer stabilization of protein unfoling[107].

Similar to the Sukenik et al study, EE plots were employed to show the addition of concentration effects and unfolding of helices rather than whole peptides. Such work allows for better understanding of excipient stabilization mechanisms of helices in a concentration dependent manner, allowing for robust and improved formulation strategies.

4.2 Methods

CD data from systems 1, 2, and 3 were used to construct enthalpy-entropy plots and assess mannitol, trehalose, and PEG effects on EEC regarding the unfolding of PLL alpha helices. All enthalpy and entropy data were compared to system #1 to determine $\Delta\Delta H$ and $T\Delta\Delta S$ values. For system #2 this involved measuring relative changes in enthalpy/entropy due to increasing additive concentrations. For system #3, stabilizing excipients were added at 0.5M concentrations and tested against chemical denaturation of urea at 0.25, 5.0 and 1M urea.

4.3 Results and Discussion

From Figure 4.3 and Table 4.1 it can be observed that mannitol at low, medium, and high concentrations fall within region II (enthalpic stabilization). The entropy/enthalpy compensation effect with concentration possesses a slope of 0.797± and r^2 of 0.999 (Table 4.2). Trehalose also demonstrated enthalpic stabilization at low, medium, and high concentrations (region II) that

became more pronounced with concentration, possessing a slope of 0.674±0.0202 and r^2 0.948. In the lower concentration ranges, PEG400 demonstrates enthalpic destabilization (region IV), entropic destabilization (region I) in the mid concentration ranges, and entropic stabilization (region II) at 0.75M. Moreover, PEG400 showed a linear relationship with increasing PEG concentration with a slope of 0.764±0.0793 and r^2 0.997. Urea, on the other hand, showed slight enthalpic destabilization, largely offset by entropic stabilization effects at the low concentrations (0.1 and 0.25M), enthalpic destabilization becomes more pronounced from 0.35M and beyond. Entropy/enthalpy slope were very even at 0.924±0.0174 and r^2 of 0.999.

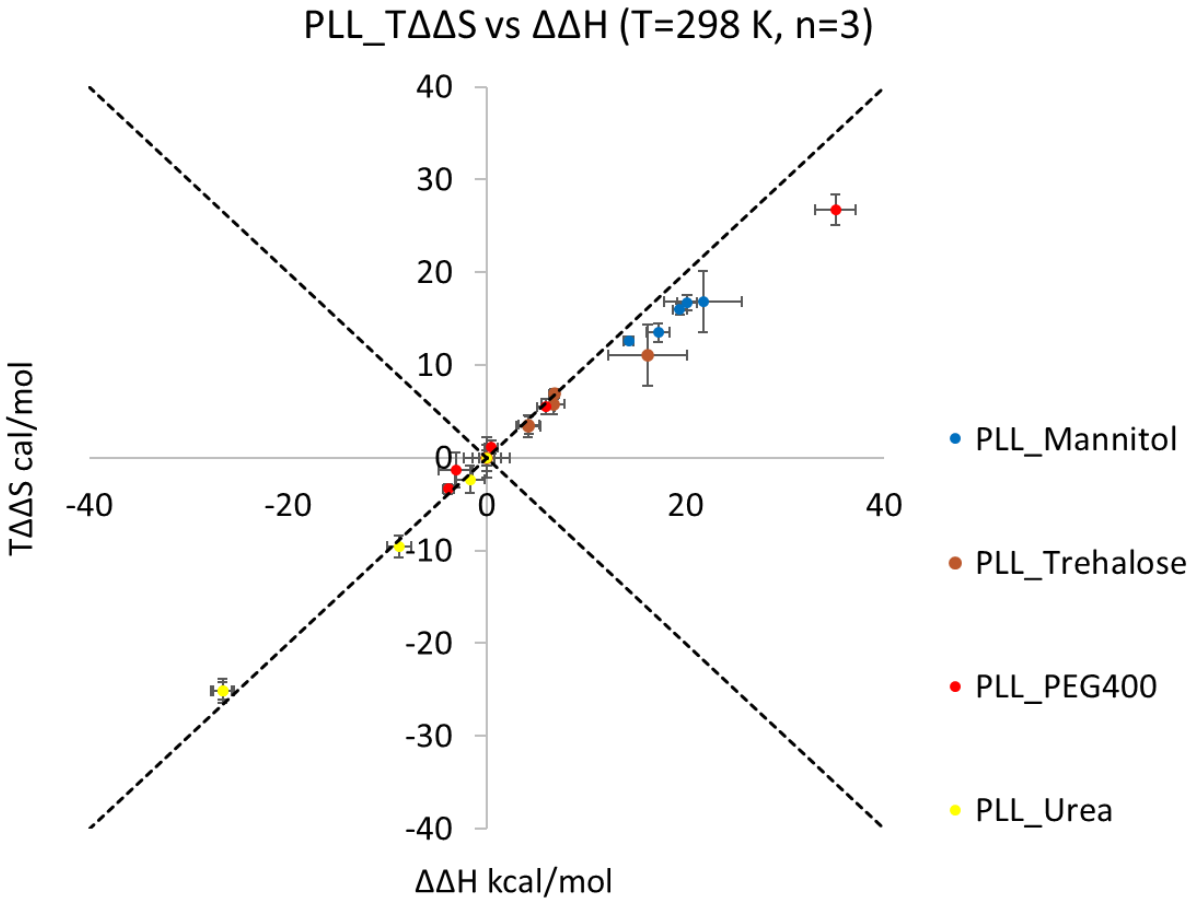

Figure 4.3. EEC plot of PLL. Part a.) an EEC plot at T=298K of PLL in the presence of varying excipient concentrations. In part b.) a table of slope and r^2 values of mannitol, trehalose, PEG400 and urea.

Table 4.1.
EEC classification by excipient and concentration.

Excipient	Concentration	Region
Mannitol	Low	II
	Medium	II
	High	II
Trehalose	Low	II
	Medium	II
	High	II
PEG400	Low	IV
	Medium	III
	High	II
Urea	Low	IV
	High	IV

Table 4.2.
Entropy/enthalpy slope and r^2 for system #2 with CD data.

Excipient	Slope	r^2
Mannitol	$0.707 \pm 1.26 \times 10^{-2}$	0.998
Trehalose	0.681±0.260	0.777
PEG400	0.975±0.575	0.993

When assessing the stabilization mechanisms of mannitol, trehalose and PEG400 from chemical denaturation through increasing urea concentrations, it was found that mannitol enthalpically stabilized PLL from 0.25 to 0.5M urea; however, at the higher urea concentrations,

enthalpic destabilization effects dominate (Figure 4.4 and Table 4.2). The relationship between urea concentration and enthalpy-entropy effect is linear, with a slope of 0.707±0.0126 and r^2 being observed. Trehalose likewise is enthalpically stabilized at low urea concentration but is destabilized at 0.5M and above. Interestingly though, the mechanisms of destabilization switches from entropic to enthalpic at 0.5M and 1M, respectively. Moreover, the changes in enthalpy vs entropy are less linear in nature, possessing a slope of 0.681±0.260 and r^2 of 0.777. PEG400 at 0.5M has little effect on PLL stabilization even without the addition of urea as was observed for system #2 (Figures 3.6 and 3.7); urea concentrations did not change this effect much in the low to mid urea concentrations, though it did affect its urea's location in the EEC plots. Without PEG, urea EEC effects straddled the diagonal between regions III and IV ranging from ~ -1 to -10 kcal/mol entropically and enthalpically, up to 0.25M urea. At 0.35M and above ~ -26 kcal/mol and ~ -25 kcal/mol was observed enthalpically and entropically, respectively, in region IV enthalpically destabilizing PLL alpha helices. However, with the addition of 0.5M PEG400, the magnitude in changes were mitigated with enthalpy and entropy magnitudes ranging from ~ -0.7 to ~ -3 kcal/mol from 0.25M to 1M urea, respectively (Figure 4.4). Moreover, despite having minimal effect on PLL helix thermal stability, PEG400 increased the entropy/enthalpy compensation with increasing urea concentrations as evidenced by the PEG-urea data points nearly straddling regions III and IV of the EEC plot, lowering the overall destabilization effects of urea. Like the other excipients, urea EEC effects had a linear relationship with urea concentration, and was near unity with a slope of 0.975±0.0575 and r^2 0.993 being observed. Comparing Tables 2 and 3, it can be seen that EEC is near unity for urea, while trehalose skews the strongest towards enthalpy (slope 0.574±0.0202) followed by PEG400 and mannitol, and that urea has little to no effect on these slopes; however, when comparing

magnitude of ΔΔH/TΔΔS, urea significantly mutes the change in enthalpy and entropy. For example, in Figure 4.4, trehalose at 0.5M enthalpy is ~ 18 kcal/mol while change in entropy is ~ 13 kcal/mol. In Figure 3.5, at 0.5 trehalose and 0.25 M urea both values are less than 1 kcal/mol.

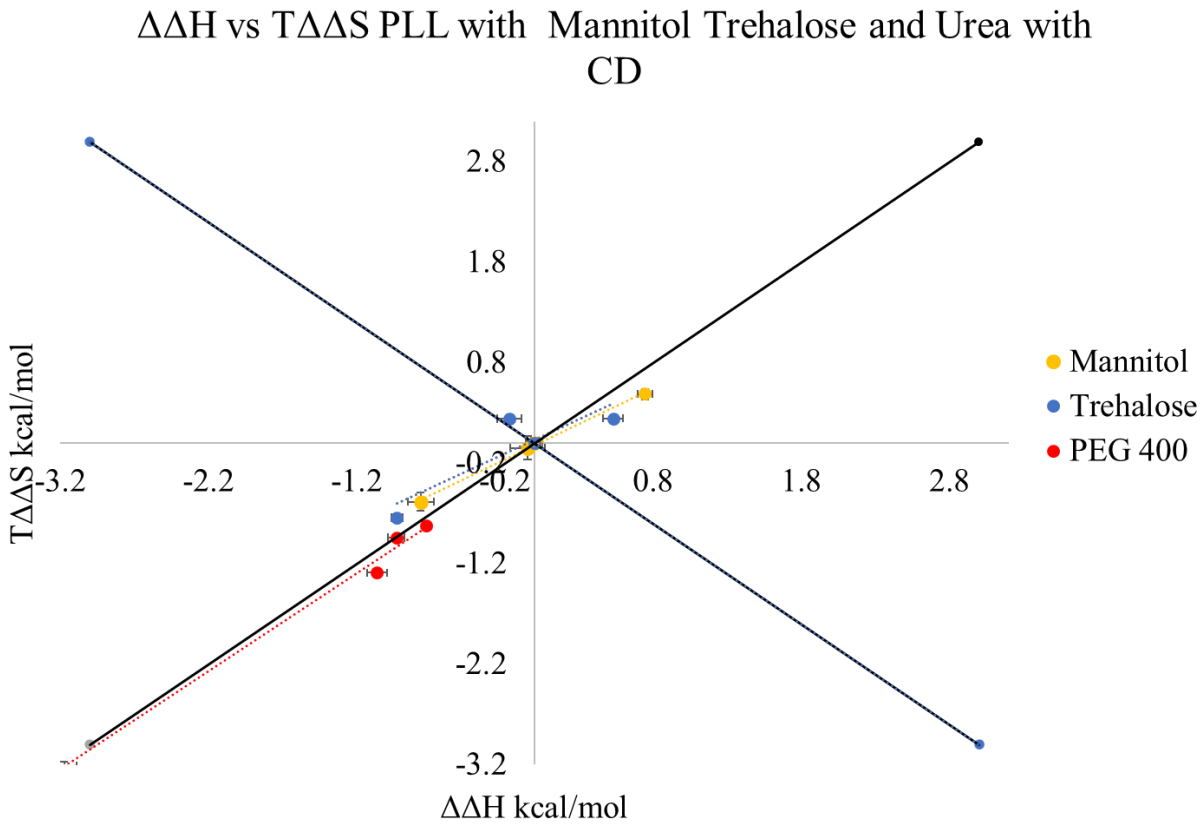

Figure 4.4. EEC plot of PLL helix unfolding in the presence of 0.5 M excipient, and increasing urea concentrations ranging from 0, 0.25, 0.5 and 1M urea. Data was collected via CD and T=298K of the TΔΔS term.

CHAPTER 5: APPLICATION OF PLL MODEL TO MODEL PROTEIN BOVINE SERUM ALBUMIN

5.1 Introduction

Proteins are large, complex macromolecules liable towards deformation, aggregation, and loss of activity. As such, much effort in understanding stresses leading to deformation, how to prevent it, and how to stabilize the structure has been done. Much of this work has gone into identifying problematic sequences, hydrophobic patches, and other liable features. Despite the importance of conformational maintenance in both form and function of protein based biologics, relatively little work has gone into specifically understanding secondary structure stabilization of various excipients. Once more, since peptide/protein based biologics are so fragile, large, and often need to be administered at high concentrations (meaning viscosity, solubility and stability challenges are exacerbated), many excipients are added to aid formulation properties and maintain stability. This means stabilization/destabilization of secondary structure such as helices likely experience a number of forces which can stabilize/destabilize their structure, therefore, a suitable protein containing a large percentage of alpha helices as its overall SS content is desired while also being amenable to thermal denaturation studies as such techniques are mainstays in assessing stability.

5.2 The Model Protein BSA

BSA is a common and a well-studied protein, commonly used as an analog for proteins in general to understand protein behavior such as folding, aggregation, excipient protein interactions, and cellular transport processes, to name a few applications[62, 132-137]. BSA has been extensively studied through thermal denaturation studies[62, 134, 135, 137, 138]. BSA is a large globular protein with a molecular weight of 66,400 kDa, consisting of 584 amino acids, approximately

60% helicity, 10% turn, with the rest random coil/extended chain and no ß-sheet SS[135, 137, 138] (Figure 5.1). The overall shape is oblate consisting of three domains, each stabilized by internal di-sulfide bonds[135]. BSA contains a wide range hydrophilic and hydrophobic regions throughout the molecule[135], further enhancing its suitability as analog to general protein behavior.

In addition to high helical content and varied hydrophilicity, BSA has interesting and well understood thermal denaturation behavior. For instance, thermal unfolding begins with unfolding of short, interconnecting chains of I and IIa and IIb and IIIa, following further unfolding resulting from the loss of alpha helicity of the molecule[135]. Unfolding is fully reversible up to approximately 45-50 ^{o}C[135, 138]; however, for helices, full reversibility extends from 52-60 ^{o}C[135, 139] (FTIR analytical methods). Gel formation and other aggregation phenomena begin to occur above 70 ^{o}C[135]. All loss in helicity is associated with a subsequent increase in beta-sheets and random coil SS features. The former is of interest in that beta-sheet SS is strongly associated with types of aggregation phenomina[135, 140], and may be associated with the observed aggregation and gel-formation behavior of BSA at higher temperatures. Given the folding behavior, high helicity, and varied hydrophobicity of BSA, it makes a suitable test protein to extend the previous peptide model to.

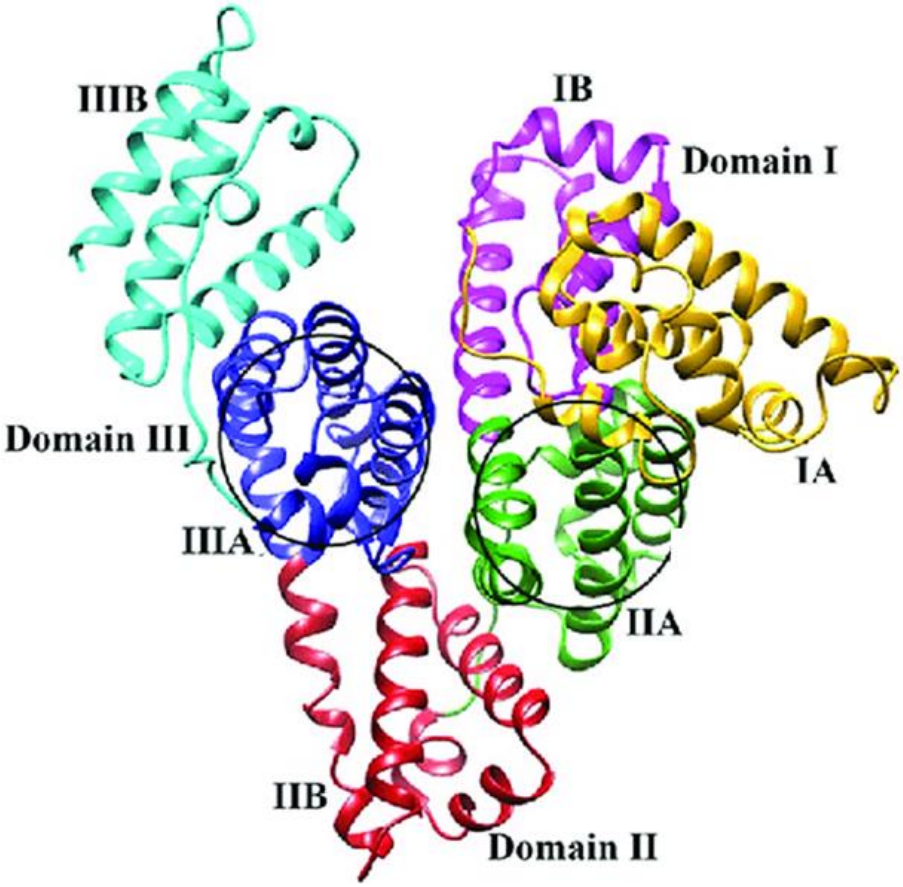

Figure 5.1. X-ray crystallography structure of BSA rbc code: 4F5S (modified in pymol). Here region IIA and IIIA are circled as possible sites of initial helix and short segment unfolding as assessed from FTIR studies[135].

5.3 Materials and Method

BSA (≤95%), mannitol, PEG400, trehalose, urea, phosphate mono/di-basci, NaF and other reagents were purchased from Siga-Aldrich, St. Louis, MO. Jasco. CD methods were the same as that of the previous two chapters when assessing system #1 and #2 to evaluate thermodynamic changes of helix unfolding.

5.3.1 CD Analysis

CD-UV analysis was done on a Jaso-810 CD spectrometer with an attached Peltier and 0.1 cm quartz cuvette. CD spectra were recorded in triplicate with a scan rate of 100 nm/min, 1mm slit

width with excipient/buffer solutions as blanks. HT values did not exceed 600 V for recorded data. Full scan spectra were acquired from 200-260 nm at 25°C to evaluate SS features of BSA. Additional full scans were run at 50, 75, and 90ºC then re-run at 25ºC to assess reversibility of unfolding. Thermal denaturation to calculate free energy of unfolding was carried by ramping the temperature from 25°C to 90°C at a rate of 0.5°C/min.

All data was collected in mdeg then converted to MRE using equation 5.29; fraction helicity was then determined from equation 5.31 while equilibrium constant *K* and free energy ΔG were determined from equations 5.24 and 5.17, respectively, for all data points using Excel 2016. Data was then plotted in Prism 6 using equation 5.36 and fitted with the Levenberg-Marquardt.

5.4 Results and Discussion

5.4.1 CD Analysis of Secondary Structure

At 25ºC BSA displays significant helicity (Figure 5.2) with the characteristic minima at 208 and 222 nm being observed. The helicity decreases as temperature increases, and at 75ºC and above, significant loss in helicity occurs as well, as can be seen in the coil/beta-sheet CD profile in Figure 5.2. Importantly, like PLL, CD is a suitable analytical method to monitor changes in helicity due to thermal denaturation.

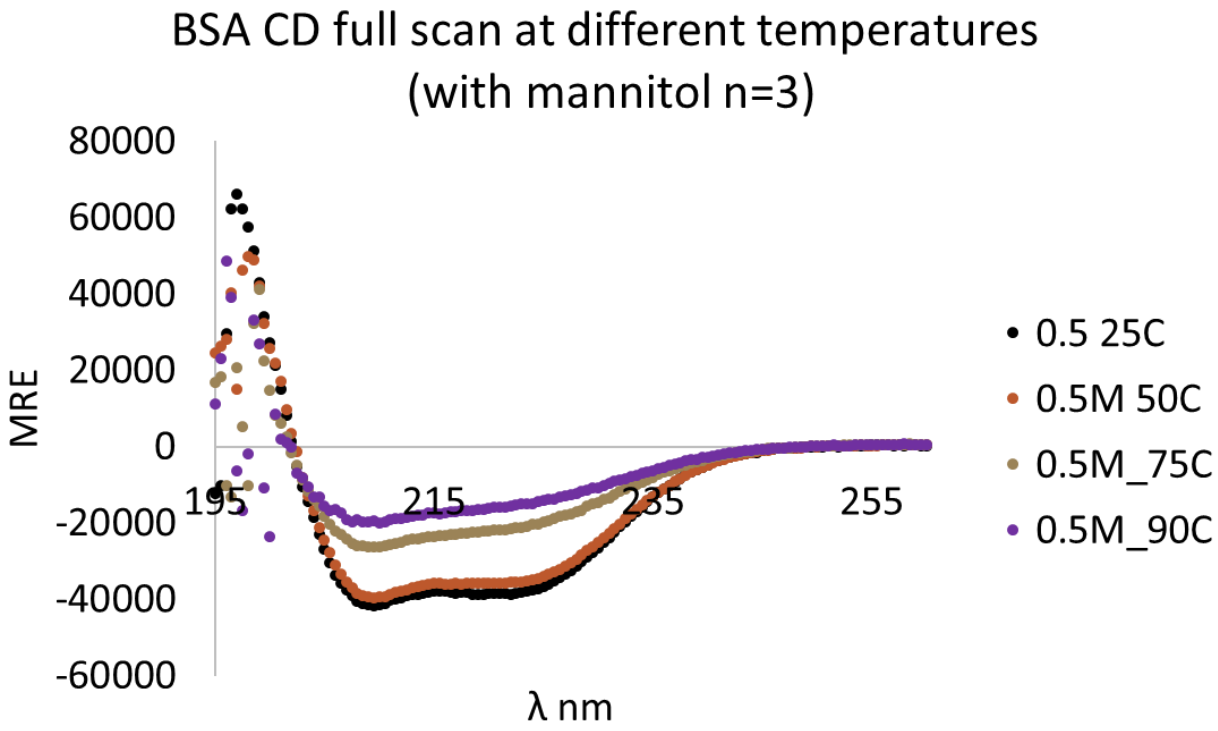

Figure 5.2. Full scan CD spectrum from 195-260 nm of 2 µM BSA in 0.1M PBS and 0.5M mannitol at 25, 50, 75 and 90°C.

5.4.2 Effect of Temperature on BSA MRE and fH

BSA undergoing thermal and chemical challenges causes it to unfold. Monitoring changes in helicity with CD is traditionally done through observing increasing MRE values at 222 nm, which is then correlated to fraction helicity using the mathematical relationships discussed in the methods section of chapter 5. Data for the effect of mannitol concentration on BSA MRE and fH is given in Figure 5.3 as a general example of this behavior. As can be seen, MRE decreases with mannitol concentration in a concentration dependent manner, while the corresponding fH increases as well. It can also be observed that the inflection point of the sigmoidal curves indicating an increase in the T_m values increase with mannitol concentration.

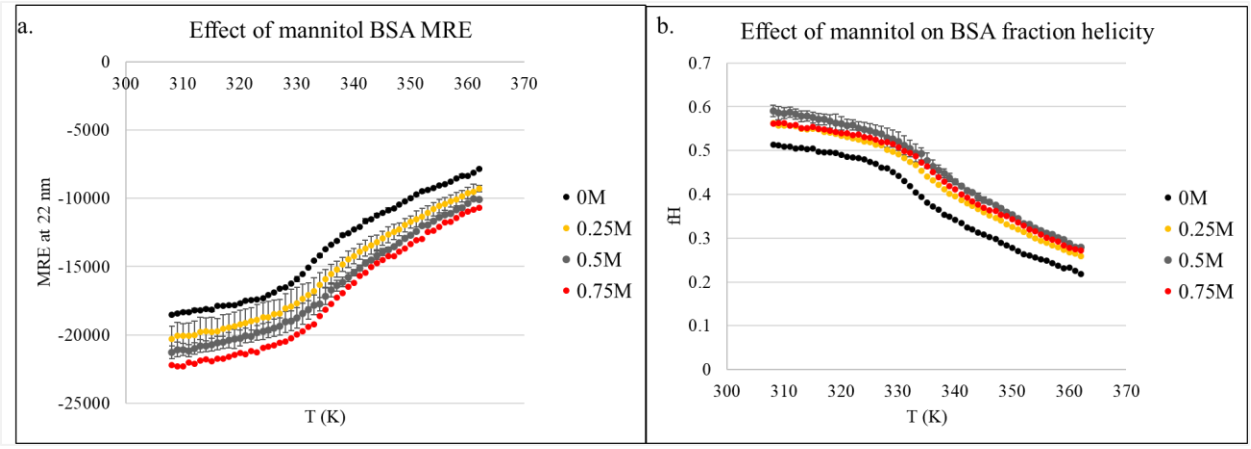

Figure 5.3. Effect of mannitol on BSA MRE (a) and fH (b).

5.4.3 Effect of Thermal and Chemical Denaturation on BSA Unfolding Thermodynamics

Comparing thermodynamic helix stability in the presence and absence of excipients (i.e. system #1 and #2, respectively) yielded several significant findings. Mannitol results are listed and illustrated in Table 5.1, Table 5.2, and Figure 5.4, respectively. Interestingly, at low mannitol concentrations, ΔΔH was slightly negative; however, this was more than compensated entropically with an overall increase in free energy observed at these concentrations. At higher concentrations, ΔΔH becomes positive while entropic stabilization decreases. Overall free energy increases with concentration.

Table 5.1.
ΔΔX of mannitol on BSA.

CONC. [M] (n=3)	ΔΔH	TΔΔS (T=298K)	ΔΔG
0.1	-3.10±1.44	-5.42±2.58	2.32±0.216
0.25	-11.8±1.94	-15.3±3.43	3.53±0.324
0.35	-17.3±1.54	-19.3±2.74	1.95±0.246
0.5	9.30±1.71	-0.652±2.97	-8.65±0.315
0.75	37.6±7.10	25.9±12.4	11.7±1.28
1.0	N/A	N/A	N/A

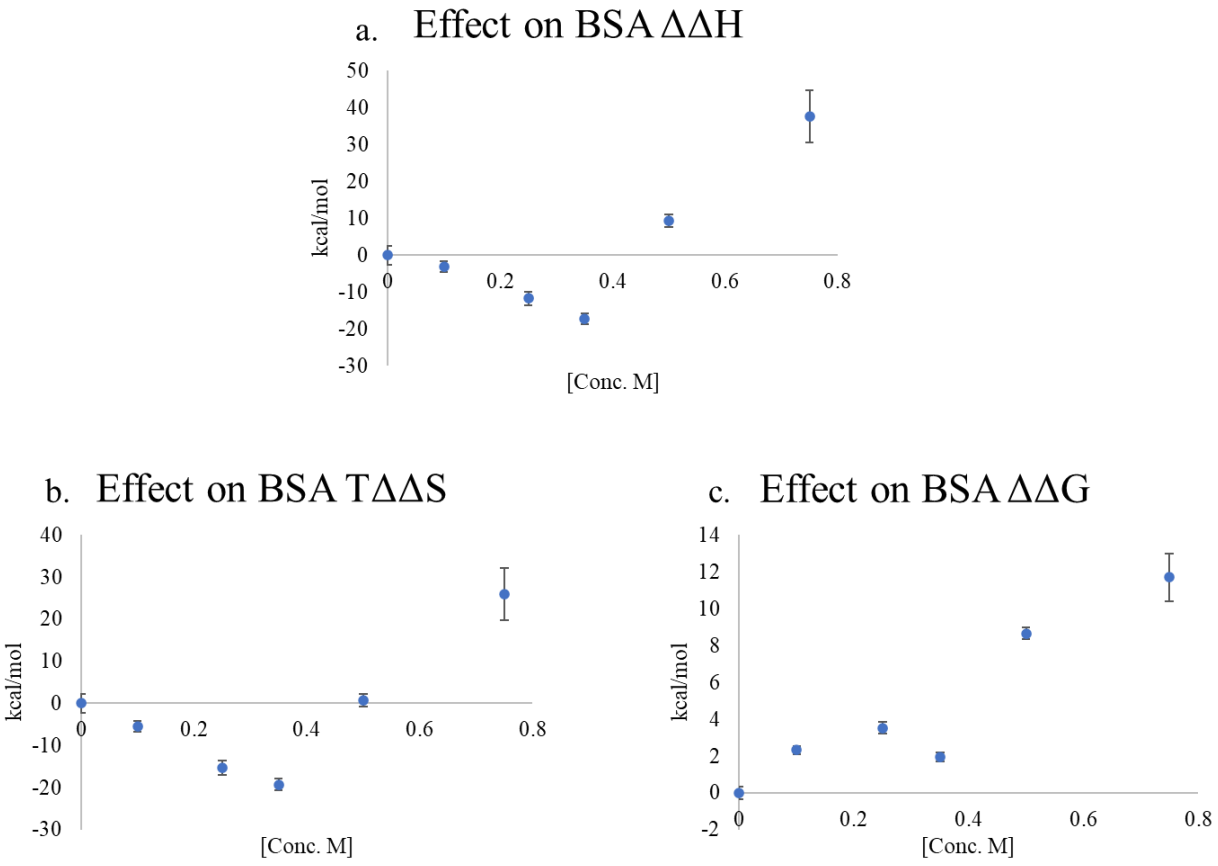

Figure 5.4. ΔΔX effect of mannitol on BSA.

Trehalose on the other hand showed enthalpic stabilization at all concentrations as well as entropic destabilization, offsetting much of the overall stabilization, as can be seen with the relatively flat ΔΔG with concentration (Table 5.1, Table 5.2 and Figure 5.5).

Table 5.2.
ΔΔX of trehalose on BSA.

CONC. [M] (n=3)	ΔΔH	TΔΔS (T=298K)	ΔΔG
0.1	16.3±1.86	14.0±1.71	2.25±0.223
0.25	20.0±4.449	18.0±4.13	2.00±0.517
0.35	75.8±5.63	69.1±5.17	6.74±0.655
0.5	4.80±2.38	2.95±2.18	1.85±0.296
0.75	18.7±3.81	16.7±3.50	2.05±0.443
1.0	N/A	N/A	N/A

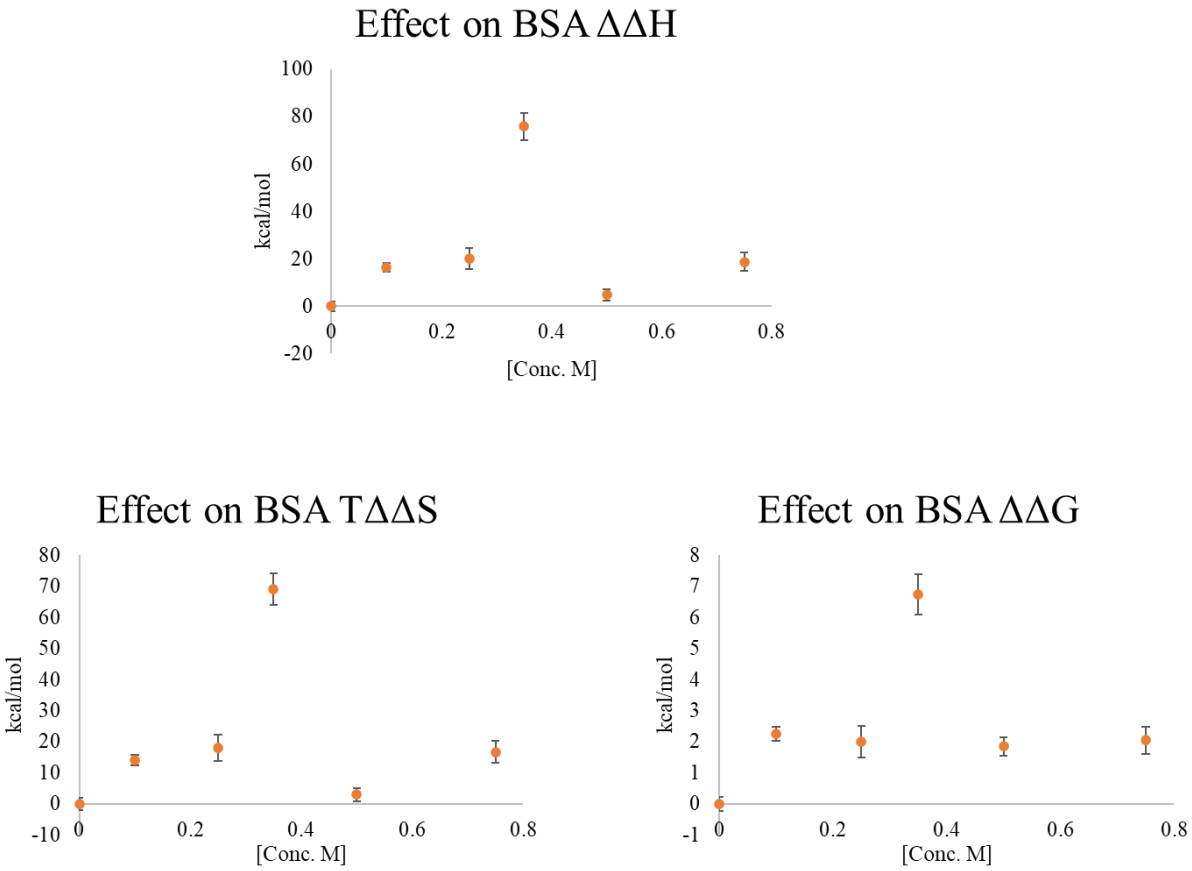

Figure 5.5. Trehalose effect on BSA unfolding ΔΔX.

Results for PEG400 are given in Table 5.1, Table 5.4, and Figure 5.6, respectively. Here, enthalpic destabilization was somewhat offset by entropic stabilization. Overall, there is a slight 0.5-2 kcal/mol destabilization over the 0.1-0.1M PEG400 concentration.

Table 5.3.
ΔΔX of PEG400 on BSA.

CONC. [M] (n=3)	ΔΔH	TΔΔS (T=298K)	ΔΔG
0.1	-2.30±1.83	-1.29±1.74	-1.01±0.129
0.25	-16.5±1.25	-15.5±1.18	-1.00±0.097
0.35	-16.6±1.17	-14.7±1.16	-1.88±0.080
0.5	-18.2±1.18	-16.8±1.12	-1.41±0.088
0.75	-18.9±1.08	-16.9±1.82	-1.96±0.075
1.0	5.73±1.56	6.30±1.65	-0.565±0.126

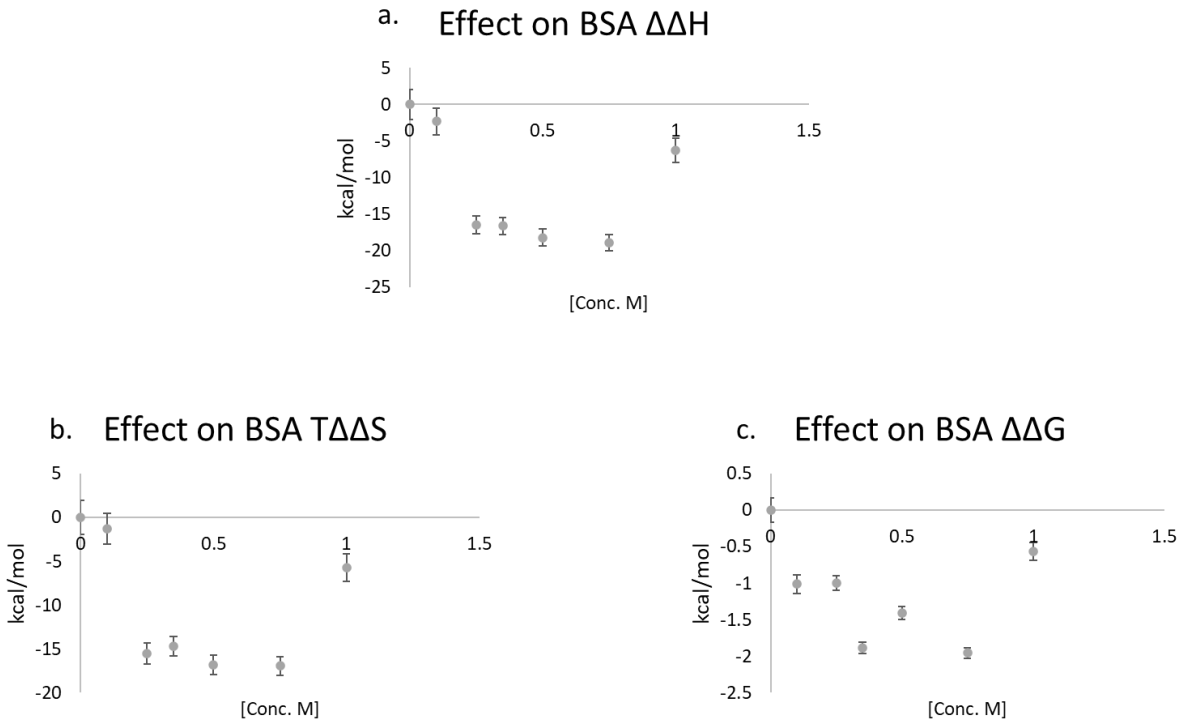

Figure 5.6. PEG400 effect on BSA unfolding ΔΔX.

Interestingly, urea provided entropical stabilization as can be seen in Table 12.4 and Figure 5.7 up to 1.5 M urea with ΔΔH values ranging from 53.9±1.52 kcal/mol at 0.25 M urea

and 1.90±0.196 kcal/mol at 1.5 M urea (Table 5.5 and Figure 5.7). Entropically, it was destabilized up to 1.5 M, with a concentration dependent decrease in destabilization; above 1.5 M it was entropically stabilized. Overall, from 0.1 to 0.5M urea stabilized BSA, with free energy of 7.04±0.267 kcal/mol at 0.25 M urea being observed. Free energy stabilization decreased to 3.14±0.112 kcal/mol at 0.5 M urea, then becoming negative and destabilized at 0.75 M urea with -0.524±0.132 kcal/mol free energy recorded (Table 5.7 and Figure 5.7), ultimately becoming entropically destabilized at said urea concentration. Destabilization appears to be entropically driven at 2 and 4M urea concentrations.

Table 5.4.
ΔΔX of Urea on BSA.

CONC. [M] (n=3)	ΔΔH	TΔΔS (T=298K)	ΔΔG
0.25	53.9±1.52	46.9±1.33	7.04±0.267
0.5	18.1±0.824	15.0±0.721	3.14±0.150
0.75	20.0±0.863	20.5±0.721	-0.505±0.163
1	6.10±0.996	6.71±0.883	-0.610±0.114
1.5	1.90±0.696	2.73±0.616	-0.834±0.161
2	-4.60±0.706	-2.46±0.627	-2.14±0.114
4	-23.4±2.49	-13.6±2.40	-9.75±0.609

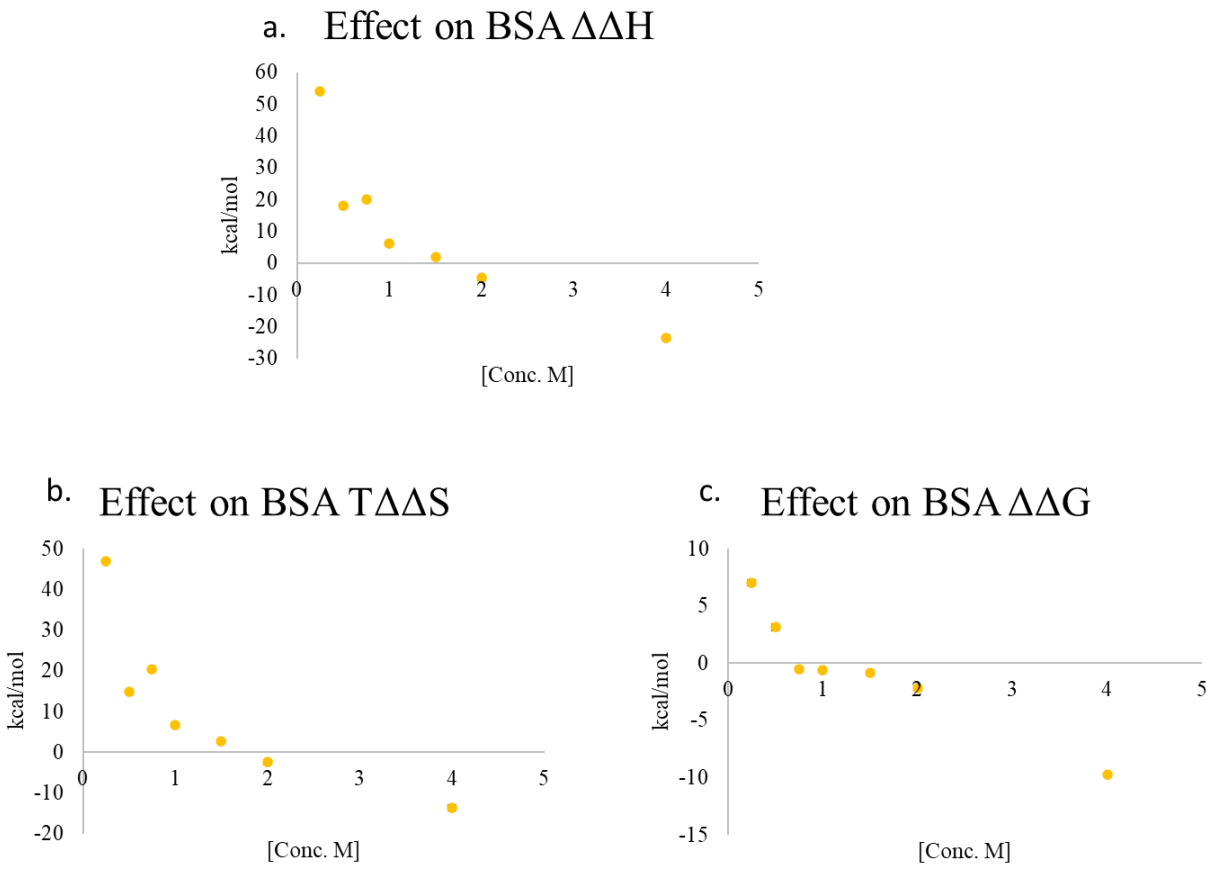

Figure 5.7. Urea effect on BSA unfolding ΔΔX.

Stabilization by urea at the lower concentrations was unexpected. Initially, it was suspected that the low salt concentration of 0.1 M NaCl was insufficient to screen charges and stabilize the protein and that perhaps urea at the low concentrations compensated for the low NaCl concentration. Since the chloride ion absorbs UV light especially at far UV wavelengths[83, 85], it was decided to use NaF as it is a slightly stronger kosmotropic agent and has little effect on CD UV absorption at the desired ranges. Given its stronger kosmotropic properties at similar and higher concentrations, it would be expected that enthalpic stabilization by urea would be reduced. Indeed, this was observed in Figure 5.8 where the ΔΔH was reduced from 53.9 to approximately 25 kcal/mol, while entropic stabilization occurred at lower concentrations. ΔΔG destabilization was much greater and occurred at 0.5 M to 4 M urea concentration.

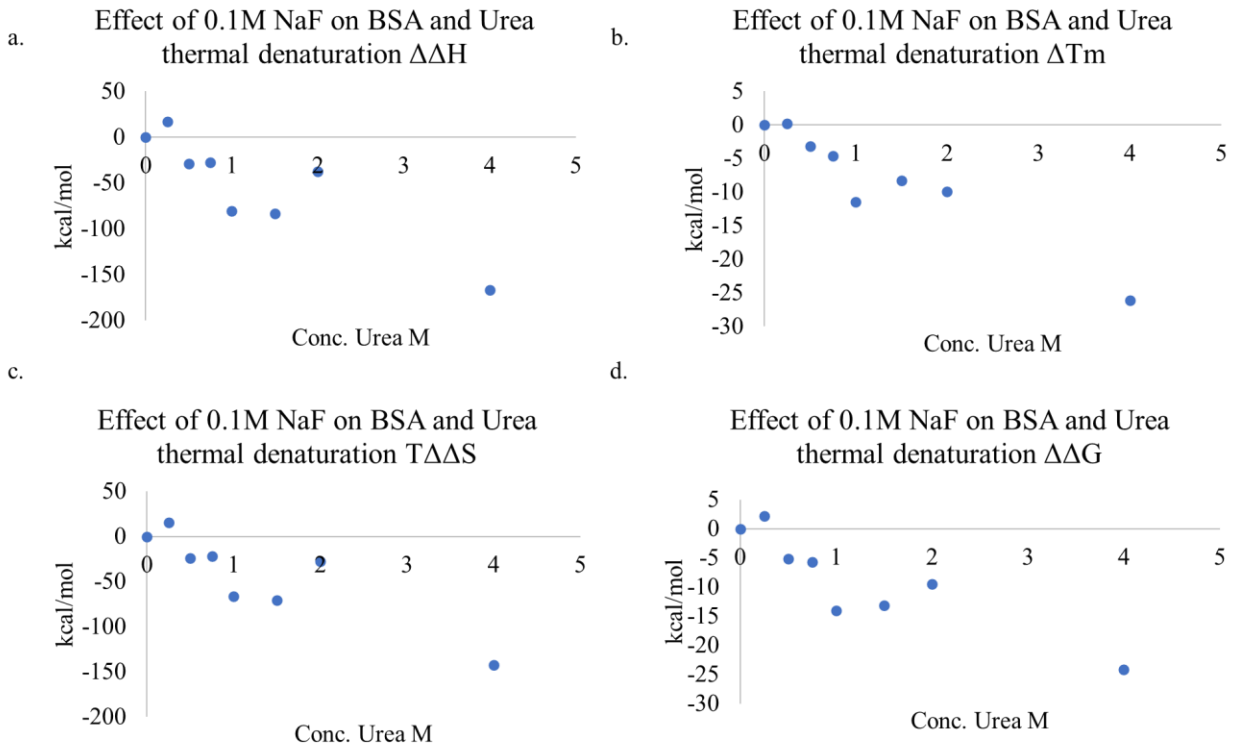

Figure 5.8. NaF effect on ΔΔX on BSA unfolding and increasing urea concentration. Here parts a-d represent changes in enthalpy, T_m, entropy, and free energy, respectively.

Since urea stabilization decreases at 0.1 M NaF relative to 0.1 M NaCl and stabilization was greatest at the lowest urea concentrations, the experiments were repeated with BSA, 0.1M urea and with a NaF concentration gradient of 0.01, 0.1 and 0.2 M NaF. NaF decreases ΔΔH from 26.6±2.29 at 0.01M NaF to a negative value at 0.2M NaF kcal/mol to -0.100±1.80 kcal/mol; additionally, said decreases occur in a linear, concentration dependent manner (Table 5.5 and Figure 5.9). Likewise, TΔΔS stabilization effects decrease with NaF concentration in a linear fashion, becoming destabilizing at 0.2M NaF with a value of -2.73± 0.255 kcal/mol.

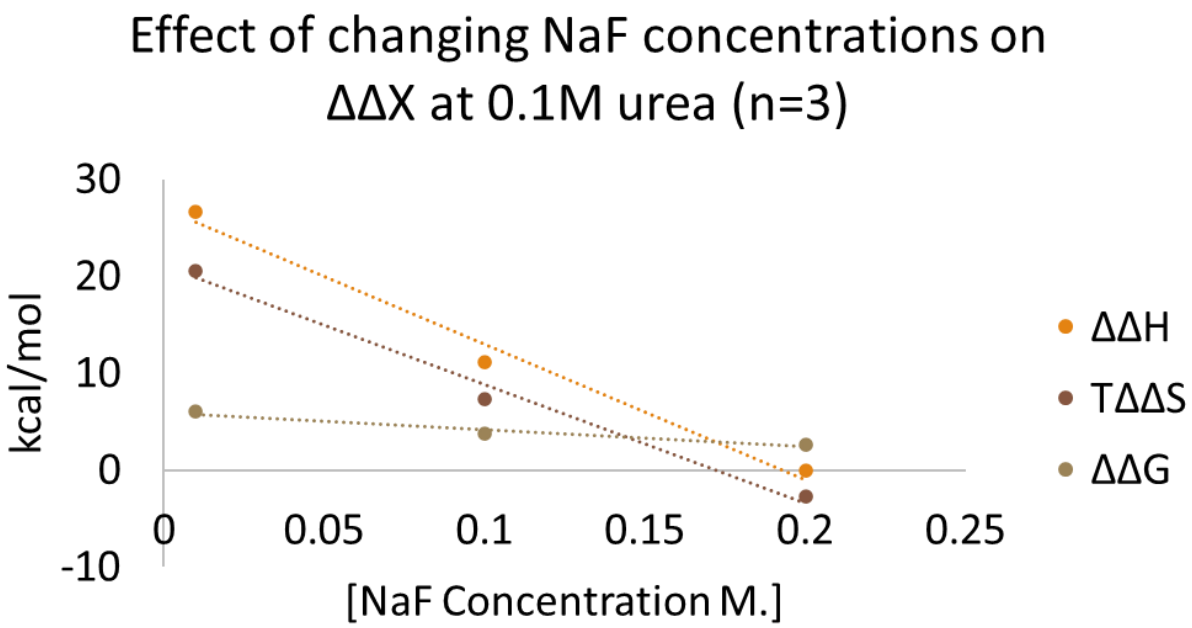

Figure 5.9. Effect of increasing NaF on BSA stability at 0.1M urea.

Table 5.5.
Effect of increasing NaF on BSA stability at 0.1M urea.

Effect of NaF concentration on BSA ΔΔX at 0.1M urea				
NaF [M]	**ΔΔH**	**TΔΔS**	**ΔΔG**	**ΔTm**
0.01	26.6±2.29	20.6±0.173	6.04±0.0298	4.60±0.298
0.1	11.1±2.05	7.38±0.0139	2.63±0.190	4.30±0.0777
0.2	-0.100±1.80	-2.73±0.255	3.72±0.124	3.90±0.136
r^2	0.989	0.989	0.946	0.160

Further exploration of the urea stabilization phenomena revealed numerous literature examples; Shiraga and company explored urea effects of urea on water structure utilizing broad band terahertz NMR to explore its dual kosmotropic and chaotropic nature[141]. It was found that up to 5M concentration, urea had a hydration number of 1.9, indicative of a constrained water by a strong hydrogen exceptor[141], showing kosmotropic properties. The tetrahedral nature of water was preserved, albeit with it possessing a shorter lifetime; however, an increase in non-hydrogen bonding was also observed[141]. Kosmotropic effects were attributed to the -NH_2 urea components, which significantly reduced the dynamics of the system, while chaotropic effects were attributed to the -CO portion responsible for slight water structure perturbance[141].

While urea can have both kosmotropic and chaotropic effects, its interaction with protein is hotly debated[74, 112, 141-144]. In another NMR study, Otting et. al. used the nuclear Overhauoser effect to measure urea binding to a bovine pancreatic trypsin inhibitor[143], discovering that at low temperatures it bound to specific regions; however, at higher temperatures this specificity decreased, instead showing weak hydrogen bonding with the general protein in structure.[143]. While not conclusive, such studies show the potential for favorable urea/protein interactions, that

may explain in part urea's enthalpic stabilization of BSA at low concentration and subsequent enthalpic destabilization at high concentration. In another study addressing urea's stabilizing potential at low concentrations, Gull and company studied the effects of urea on a closely related protein, human serum albumin (HSA), and found that it increased alpha helix content by 8%[145]. It was conjectured stabilization was due to its effect on water structure (i.e. kosmotropic effect[141]) and the lowering of the dielectric constant, thereby increasing the hydrophobic effect enhancing alpha helix content[145].

Given the mild kosmotropic nature of urea, its ability to form weak interactions with protein surface and dielectric effects, it is understandable to see how it may stabilize a protein enthalpically. Additionally, its effect on water structure could explain entropic stabilization. In light of the discussed effects, it is not surprising that a stronger ionic kosmotrope such as NaF could mask and mitigate urea stabilization. Another point of interest is the difference between PLL and BSA. No such stabilization was observed for PLL. This is likely due to PLL already having numerous neutral $-NH_2$ side chains (due to the high pH of 11.7) that would minimize any urea effects.

Plotting $\Delta\Delta H$ vs $T\Delta\Delta S$ (T=298 K) reveals interesting effects of mannitol, trehalose, PEG400, and urea on alpha helices unfolding behavior in BSA (Figure 5.10, Table 5.6). Mannitol provides entropical stabilization (region III) up to 0.35 M mannitol, then becomes enthalpically (region II) stabilized at 0.5 and 0.75M mannitol. This is in opposition to PLL, which was $\Delta\Delta H$ stabilized at all concentrations. It is unclear why this would be the case. One potential reason includes preferential interaction with BSA, which would be possible given the relative heterogeneous nature of BSA compared to PLL. However, this seems unlikely given that no such behavior was observed with trehalose. Trehalose behaves similarly to PLL, in

which ΔΔH stabilization is observed but less in magnitude compared to mannitol, much like what was observed in PLL (Figure 5.10)

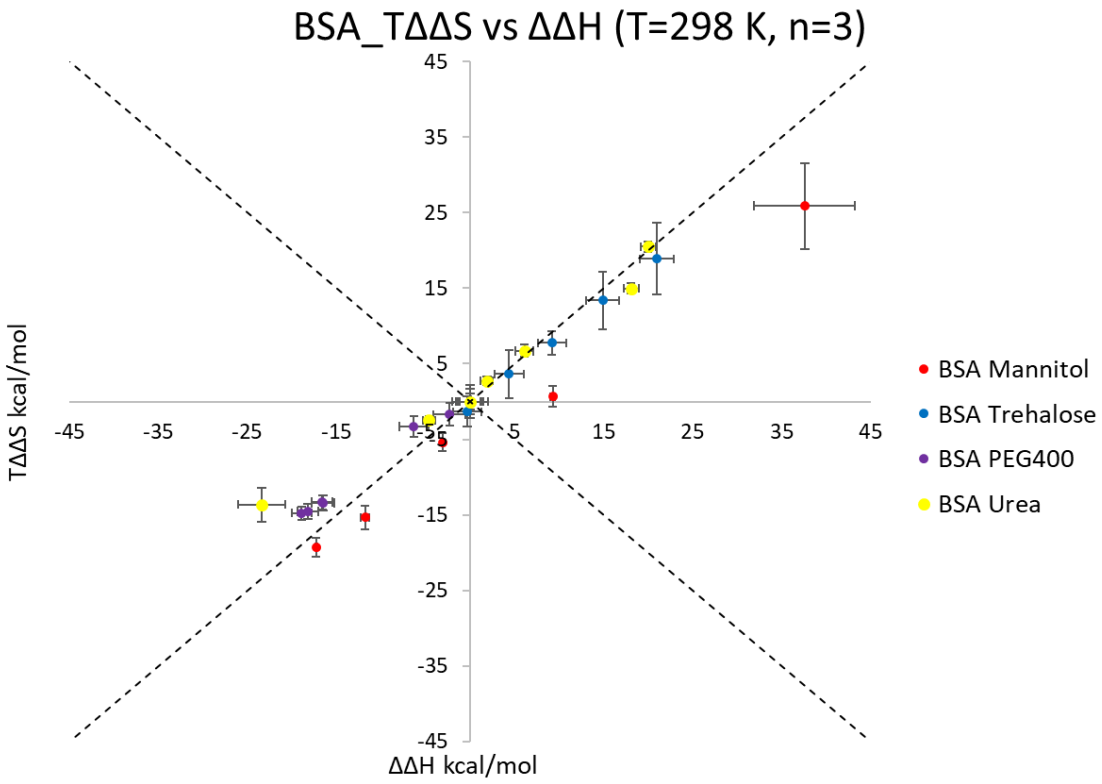

Figure 5.10. EEC plot of BSA in presence of different concentrations of excipients.

Table 5.6.
EEC classification by excipient and concentration.

Excipient	Concentration	Region
Mannitol	Low	III
	Medium	III & II
	High	II
Trehalose	Low	II
	Medium	II
	High	II
PEG400	Low	IV
	Medium	IV
	High	IV
Urea	Low	II
	Medium	II & IV
	High	IV

PEG400 effect on BSA is much like that of PLL, in which enthalpic destabilization (region IV) was observed for all concentrations with the exception of 0.75M, which enthalpically stabilized PLL, but not BSA (Figure 4.8). BSA destabilization through PEG is not without precedent having been noted by Arakawa[6, 7] nearly 40 years ago, where it was hypothesized that the -CH_2- group interacted preferentially with BSA hydrophobic patches.

Urea, as discussed earlier, has complex interactions with both the protein and the solvent. This is further illustrated in the enthalpy-entropy plot (Figure 5.10). At lower concentration

region II (enthalpic), stabilization is observed but shifts to region IV (enthalpic destabilization) at higher concentrations.

Ultimately, BSA alpha helix stabilization follows similar trends to that of PLL, such as similar mannitol and trehalose $\Delta\Delta G$ stabilization magnitudes and similar PEG400 stabilization/destabilization. However, the thermodynamic mechanism differences in mannitol at low concentrations was observed. For PLL, stabilization (at low concentration) was driven enthalpically; BSA stabilization was entropically driven. Reasons for this difference are not clear. Urea difference, i.e. stabilization of BSA at low concentration and no stabilization of PLL at any concentration, is likely explained by the $-NH_2$ side chain of PLL, which would negate the $-NH_2$ kosmotropic stabilization of urea.

CHAPTER 6: GENERAL UNFOLDING OF BSA WITH DSC

6.1 Introduction

In the previous chapter, the effect of excipient on alpha helix stabilization was assessed by directly measuring changes in helicity due to thermal stress using CD analytical methods. Due to its ability to distinguish SS features in a protein, CD is an excellent analytical method to assess thermodynamic effects of excipients on alpha helices located in a protein. However, while BSA is largely composed of helices (coils and turns comprise the rest) it is a large protein in which other stabilizing features such as sulfide bridges, hydrophobic core, and other large and small structural features may factor into the thermodynamics of overall shape deformation. As such, being able to assess excipient effects on overall $\Delta\Delta X$ properties is desirable in order to differentiate between excipient effects on helices and gross structural changes.

In this light, DSC is the analytical method of choice due to its sensitivity to general conformational change. Here, DSC is used to evaluate mannitol, trehalose, and PEG effects on the comparative thermodynamics of BSA unfolding in their absence. There are several ways to treat and model DSC data. In this chapter, a modified Zimm-Bragg model based off work by Seelig and company[39-43] was chosen due to its sequential unfolding methodology and robustness towards a wide range of proteins and peptides[39, 40] , behaving much how BSA does upon thermal denaturation.

6.2 Materials and Methods

All reagents, BSA, PEG400, mannitol, trehalose, mono and dibasic phosphates were purchased from Sigma Aldrich (Mo). All samples were run on a Waters TA Nano DSC. Samples were run from 20^{o}C to 90^{o}C or at 35^{o}C to 90^{o}C (little change was observed between 25-

35ºC and 35ºC was chosen as the starting temperature to expedite analysis) at a 0.5ºC/min temperature gradient. Samples were run at three excipient concentrations of 0.2, 0.5, and 0.75 M in 0.01M phosphate buffer and 0.1M NaCl and a BSA protein concentration of 2 mg/ml.

The extent of unfolding was evaluated using said ZB model equation (5.25). Equation 5.25 is used since BSA is a large protein with more than 500 residues; thus, the matrix method (equation 1.58) can be simplified to 1.65. In 1.65 the value *s* represents the propagation parameter defined by equation (1.61), where *h* is the enthalpy of the elementary unfolding step per residue and is given as 1.1 kcal/mol as that is the estimated enthalpy of formation per helix residue[39, 146]. σ is the nucleation parameter (a penalizing factor for multiple helices in a given sequence) and fitted to the data with values typically ranging from 10^{-4}-10^{-9} while T_m is the melting temperature and *N* is the number of residues in the molecule. The heat capacity at each temperature is calculated through equation Z and fitted to the raw data through adjustment of the parameters discussed. The ΔG is calculated through (equation 1.78) and ΔS and T_m calculated same as discussed previously. Changes in free energy, enthalpy, and entropy are calculated as before, i.e., $\Delta X_{noexp} - \Delta X_{exp} = \Delta\Delta X$. Data is then plotted and compared with CD and NMR studies to deduce stabilization mechanisms through EEC plots.

6.3 Results and Discussion

Samples were run on the Waters Nano DSC as discussed, and below is the DSC thermogram of BSA in the presence of 0.2M mannitol overlaid with the ZB estimated fraction unfolded. As can be seen, the fraction unfolded inflection point matches the T_m of the raw and ZB modeled data.

Mannitol increased $\Delta\Delta H$ but was somewhat offset by $T\Delta\Delta S$ (T=298K) with overall $\Delta\Delta G$ increase of 2-6 kcal/mol from 0.2 to 0.75 M mannitol ΔT_m increased linearly with mannitol

concentration (Figure 6.1). Looking at the EEC plot (Figure 6.5), mannitol net stabilization of BSA is enthalpically driven (region II).

Trehalose, like mannitol, increased BSA stabilization enthalpically (Figure 6.2a) and partially destabilized entropically (Figure 6.2b); a slight linear increase in ΔT_m with respect to trehalose concentration was observed (Figure 6.2c) and overall $\Delta\Delta G$ stabilization of approximately 5.5 kcal/mol. Interestingly, most effects plateaued at the low concentration of 0.2M trehalose, with only slight changes at 0.5 and 0.75 M. As can be seen from the EEC plot (Figure 6.5), trehalose stabilization mechanism is enthalpic (region II).

Much like the CD data, PEG400 effects were muted compared to mannitol and trehalose. However, unlike the CD samples, the $\Delta\Delta H$ effects were slightly positive, though decreasing with PEG concentration. Enthalpic stabilization was slight at 0.2M PEG400, decreasing 0.5M, becoming negative at 0.75M. $T\Delta\Delta S$ (T=298K) destabilization effects were observed for PEG, which is to be expected given its purported crowding effects. Melting temperature decreases with PEG400 concentration in a linear fashion. $\Delta\Delta G$ decreases with PEG400 concentration. Looking at the EEC plot (Figure 6.5) it can be seen that it is slightly enthalpically stabilized (region 2 at low mid concentration); however, it is somewhat destabilized at the higher end through a combination of entropic and enthalpic effects (regions I and IV). As previously stated, Arakawa many years ago noted PEGs have polar and hydrophobic components that may be both repulsive and attractive towards different portions of a protein, complicating analysis of stabilization/destabilization effects[6]. More recent study has looked at the effects of PEG (in this case PEG 20) on the stabilization of ubiquitin[16]. Here, similar trends in enthalpy stabilization were observed. PEG destabilization was observed and overall loss in free energy observed at higher concentrations and decrease in T_m. Additionally it was concluded that PEG is both

preferentially excluded and interacts with ubiquitin[16] making overall stability somewhat destabilized.

There are noticeable differences between CD and DSC. With DSC, changes in energy of native vs denatured state are recorded (which incorporates effects from gross molecular structural changes, salt-bridges etc.); CD only monitors changes in helicity or other secondary structure features. When comparing EEC plots between the two, there are significant differences. For DSC everything is enthalpically stabilized (region I) except PEG400 at high concentration. CD, however, depended both on excipient type and concentration with stabilization/destabilization occurring, happening over a number of different regions depending on concentration. Such differences are important since specific changes in a protein/peptide can have significant effects on aggregation rates and properties that might not be observed in DSC type measurements.

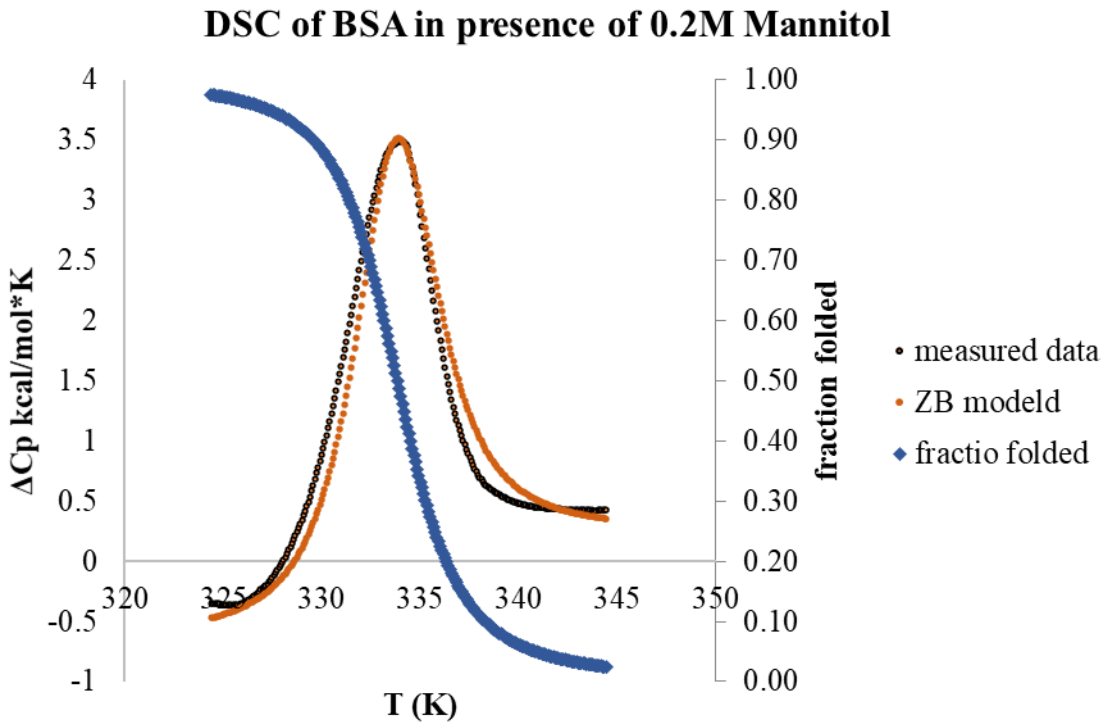

Figure 6.1. DSC scan of 2 mg/ml BSA in presence of 0.5M mannitol. Black line is raw data while the brown line is the ZB modeled data. The blue data line is the ZB modeled estimated fraction folded.

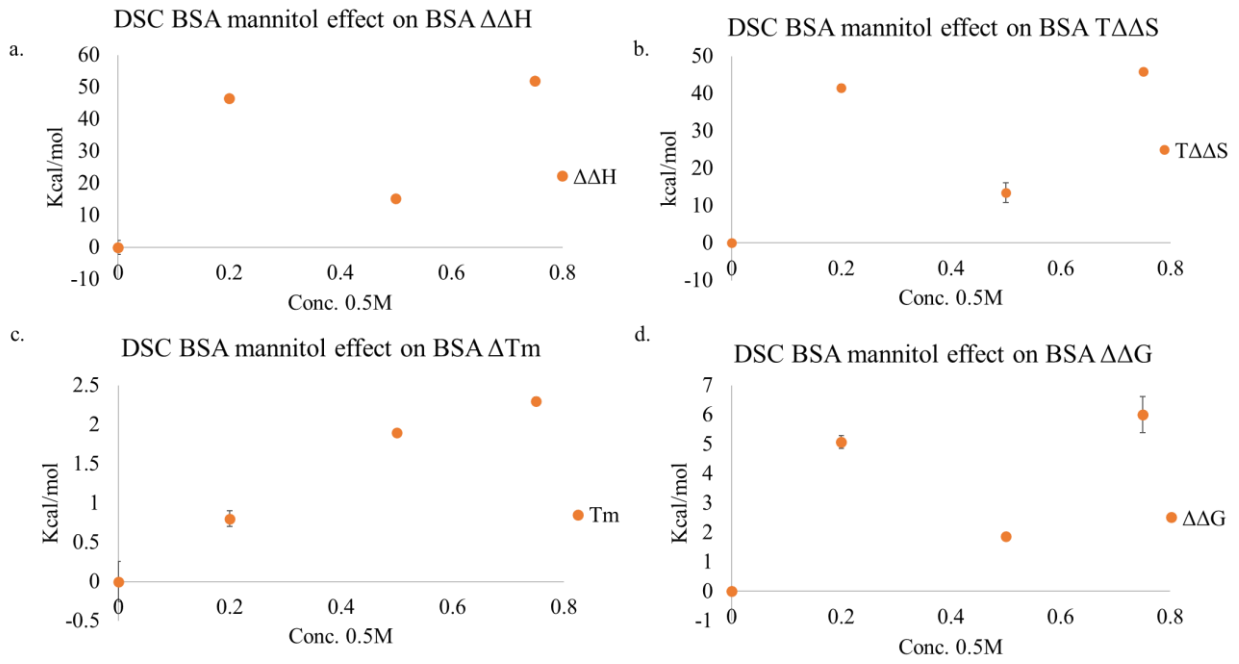

Figure 6.2. Change in ΔΔX parameters determined from DSC analysis of 2 mg/ml BSA in the presence of mannitol at 0.2, 0.5, 0.75M. ΔΔH, TΔΔS (T=298 K), ΔT_m, and ΔΔG is Figure a., b., c., d., respectively.

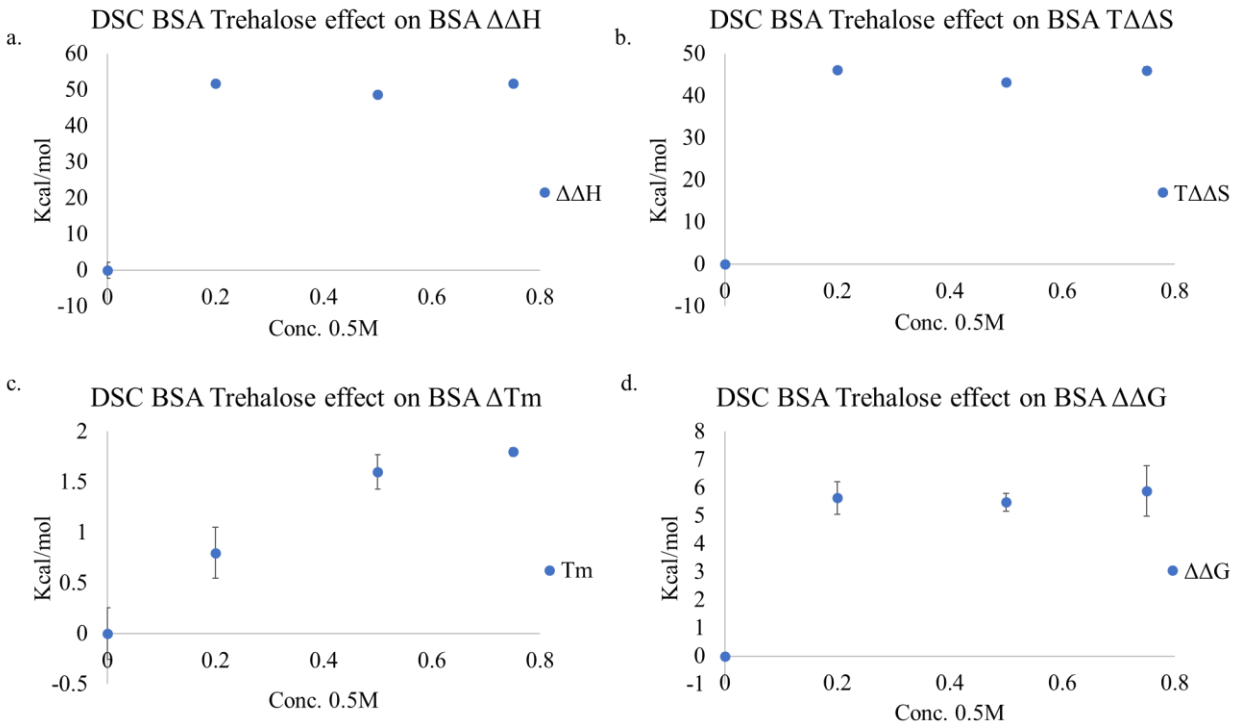

Figure 6.3. Change in ΔΔX parameters determined from DSC analysis of 2 mg/ml BSA in the presence of trehalose at 0.2, 0.5, 0.75M where ΔΔH, TΔΔS (T=298 K), ΔT_m, and ΔΔG is Figure a., b., c., d., respectively.

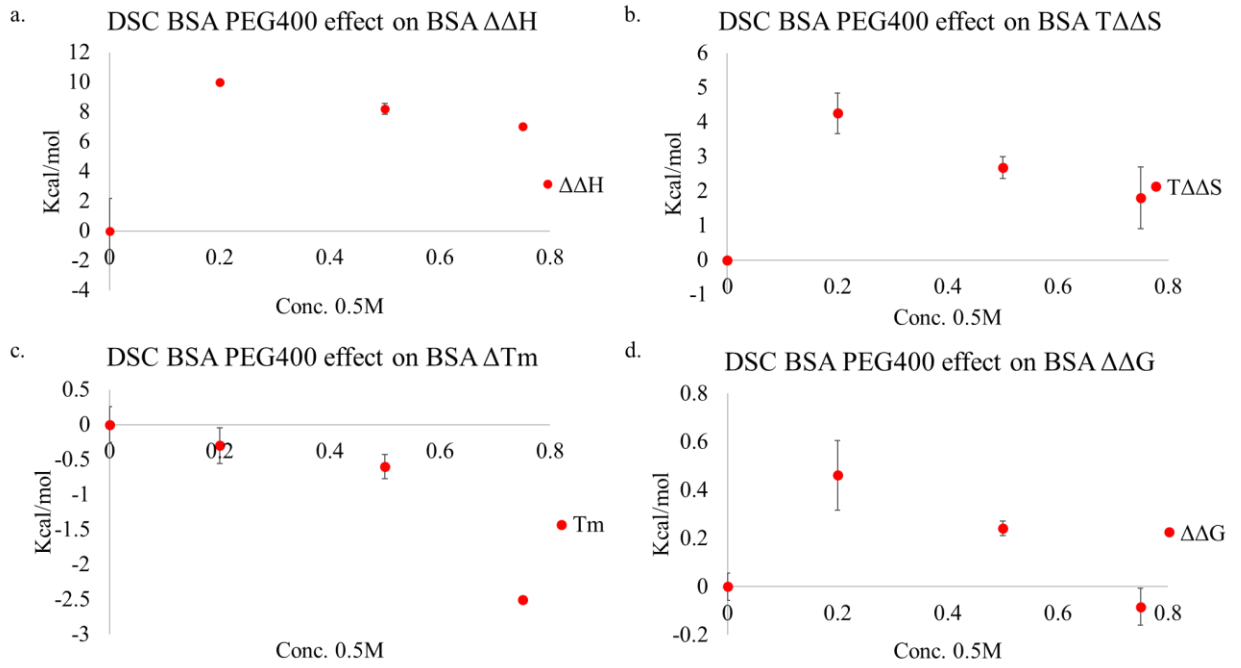

Figure 6.4. Change in ΔΔX parameters determined from DSC analysis of 2 mg/ml BSA in the presence of PEG400 at 0.2, 0.5, 0.75M. where ΔΔH, TΔΔS (T=298 K), ΔT_m, and ΔΔG is Figure a., b., c., d., respectively.

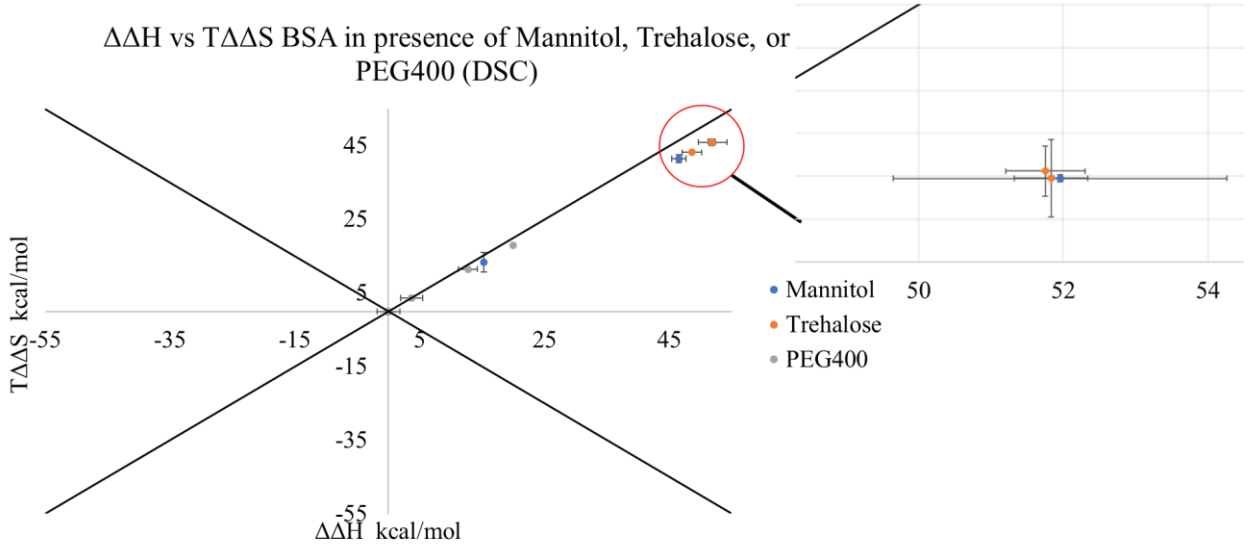

Figure 6.5. DSC EEC plot of BSA in the presence of mannitol, trehalose, and PEG400.

Comparing DSC and CD EEC plots, it can be seen there are similarities and differences in the driving stabilizing/destabilizing mechanisms depending on the tested excipient (Figure 6.6,

Table 6.1). For mannitol, medium and high concentrations show both region II (enthalpic stabilization) while low concentrations differ, regions I/II for CD/DSC, respectively. Trehalose results match across concentration ranges (region II), while PEG400 differ completely, regions IV/I&II, respectively. Unlike PLL, BSA is composed of multiple helices, coils and turns; additionally, it contains a variety of amino acid residue types and is over 20 times larger than the PLL polymer chosen. Moreover, DSC measures calorimetric enthalpy ΔH_{cal}, not ΔH_v, and accounts for overall unfolding, not just helix unfolding, and may account for other global changes not observable in CD. Differences in DSC and CD unfolding measurements allows for excipient effect on helix vs whole protein thermodynamic stabilization/destabilization to be quantified. As can be seen in Figure 6.6 and Table 6.1 DSC values possess larger enthalpic/entropic changes and differ in the driving stabilization/destabilization.

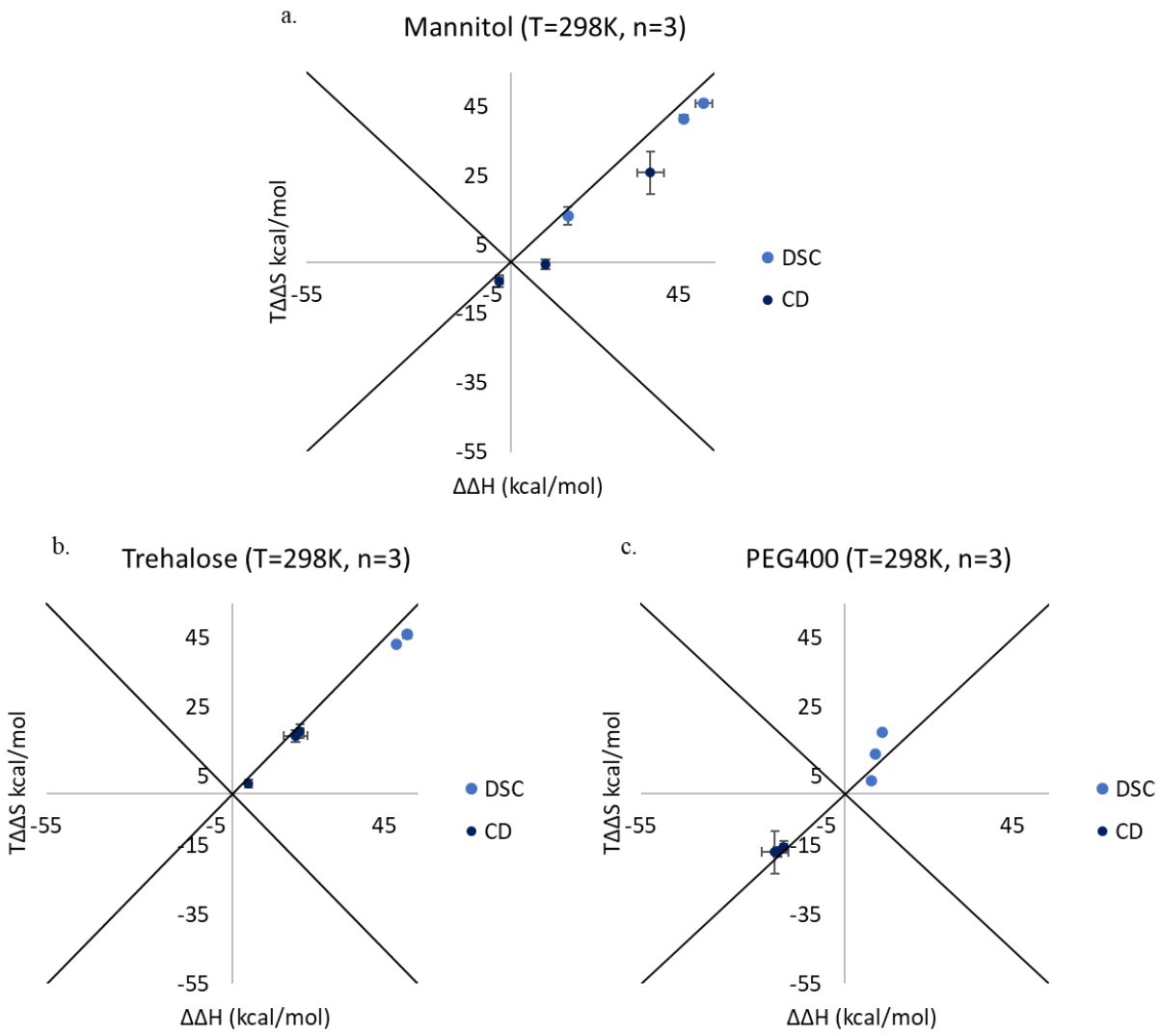

Figure 6.6. BSA EEC plots CD vs DSC

Table 6.1.
BSA EEC plots CD vs DSC

[Conc.]	Mannitol		Trehalose		PEG400	
	CD	DSC	CD	DSC	CD	DSC
Low	III	II	II	II	IV	I
Medium	II	II	II	II	IV	I
High	II	II	II	II	IV	II

CHAPTER 7: EFFECT OF EXCIPIENTS ON THE RECOVERY OF BSA HELICITY AFTER THERMAL DENATURATION

7.1 Introduction

BSA, like nearly all proteins, is subject to aggregation upon denaturation. The greater, or more frequently the native state transitions to the unfolded state, the greater the risk of aggregation. Many studies have reported on this phenomenon, describing the aggregation process to occur due to loss of SS[133, 135] and reduction in hydration layer[147], beta-sheet cross linking[147], and other self-association mechanisms[135, 138]. The beta-sheet susceptibility towards aggregation is particularly germane, given loss of helicity in BSA is converted directly to coils and beta-sheets[135, 139], meaning preservation of helicity through appropriate excipient additives should reduce aggregation and improve structure recoverability after undergoing thermal stress.

As already seen, osmotic, surfactant, and crowding agents can have a dramatic effect not only on the thermodynamics of unfolding but affect SS content as well. In addition to unfolding and SS content, these additives can also alter the protein/peptide size and number and size of aggregates. This has been demonstrated through various DLS studies such as Das's study of trehalose and glycerol on BSA conformation[137], in which BSA in the presence of each excipient exhibited two main species at approximately 10 nm and 200 nm for the monomeric and aggregated species, respectively, in BSA only solutions. Trehalose reduced the monomer to 6.590 nm and 190.3 nm for the aggregated species for 0.5 M trehalose. Interestingly, CD analysis showed a 3-4% increase in total helicity. 20% glycerol (same viscosity as 0.5 M trehalose[137]), however, enlarged both the monomeric and aggregate BSA species. This is unsurprising given the chemical similarity to the PEG400 molecule and its minimal stabilization/destabilization effects observed in CD and DSC studies. BSA aggregation rates and

size increased with temperature, especially after exceeding 60°C[139]. Finally, Kishore et. al, utilizing DSC experiments, noted the inhibition mechanism of osmolytes on BSA aggregation listed here in decreasing inhibition: Hydroxyproline> Sorbitol> Sarcosine> Glycine betaine[148].

Here, CD studies of BSA undergoing thermal denaturation at different temperature increments in the presence of 0.5M mannitol, trehalose, or PEG400 were performed to assess their respective abilities to preserve helical content in BSA after heating. Loss of helicity is assumed to occur through aggregation and irreversible unfolding. Greater preservation of helicity is attributed enhanced stability of helices and other features, which unfold less and aggregate less.

7.2 Materials and Methods

BSA, trehalose, mannitol, PEG400, mono and dibasic sodium phosphate were purchased through Sigma Aldrich (Mo). Samples were run on a Jasco-8 CD using a 0.1 crystal cuvette full scan from 260-195 nm in triplicate, three scans each, at 50 nm/min at 25, 50, 75, and 90°C then rerun at 25°C for the 50, 75 and 90°C. Fraction helicity was calculated at 222 nm as previously discussed for past CD studies and compared to initial BSA 25°C to determine percent recovery.

7.3 Results and Discussion

Here, UV CD full scan of BSA upon heating at different temperatures in the presence of 0.5M mannitol is shown in Figure 7.1. Heating BSA to 50°C had very little effect on helicity and overall secondary structure (dark blue), which is to be expected from both previous CD and DSC studies as well as literature examples[139]. At 75°C, well past the transition temperature, the CD profile changes significantly to one comprising large coil and beta-sheet SS structure content (Figure 7.1). Though not shown here, 50°C rerun at 25°C showed full recovery; however, at 75°C (grey), samples rerun at 25°C had significant loss in fraction helicity and had greater coil

content which was observed from the large negative peak at 205 nm (light blue). Samples run at 90^{o}C (yellow) lost most of the original helicity. Rerunning said samples at 25^{o}C showed little recovery of original helicity.

BSA in the presence of 0.5M trehalose and PEG400 were carried out as well, and percent recovery is shown in Figure 7.2. The BSA rerun after 75^{o}C showed significant decrease in fraction helicity across all samples, with different excipients, with values ranging from 77.6±8.83 for PEG400, 78.2±8.85, buffer only, 84.9±3.29 and 86.3±5.28 for trehalose and mannitol, respectively (Figure 7.2 and Table 7.1). While trehalose and mannitol percent recovery trend higher than buffer and PEG, there is no significance between them and buffer and PEG400. These differences become significant after heating at 90^{o}C with only 58.6±1.12 and 58.2±11.2 for buffer and PEG400, respectively, while mannitol and trehalose 76.7±2.58 and 76.4±4.99, respectively (Table 7.2).

Increased stabilization of helices in BSA from mannitol and trehalose means that there is less helices unfolding and converting to coils/beta sheet SS,[135-137, 144, 147, 149] thereby decreasing the rate of aggregation which bears out in the data presented in Figures 6.1-6.2 and Table 6.

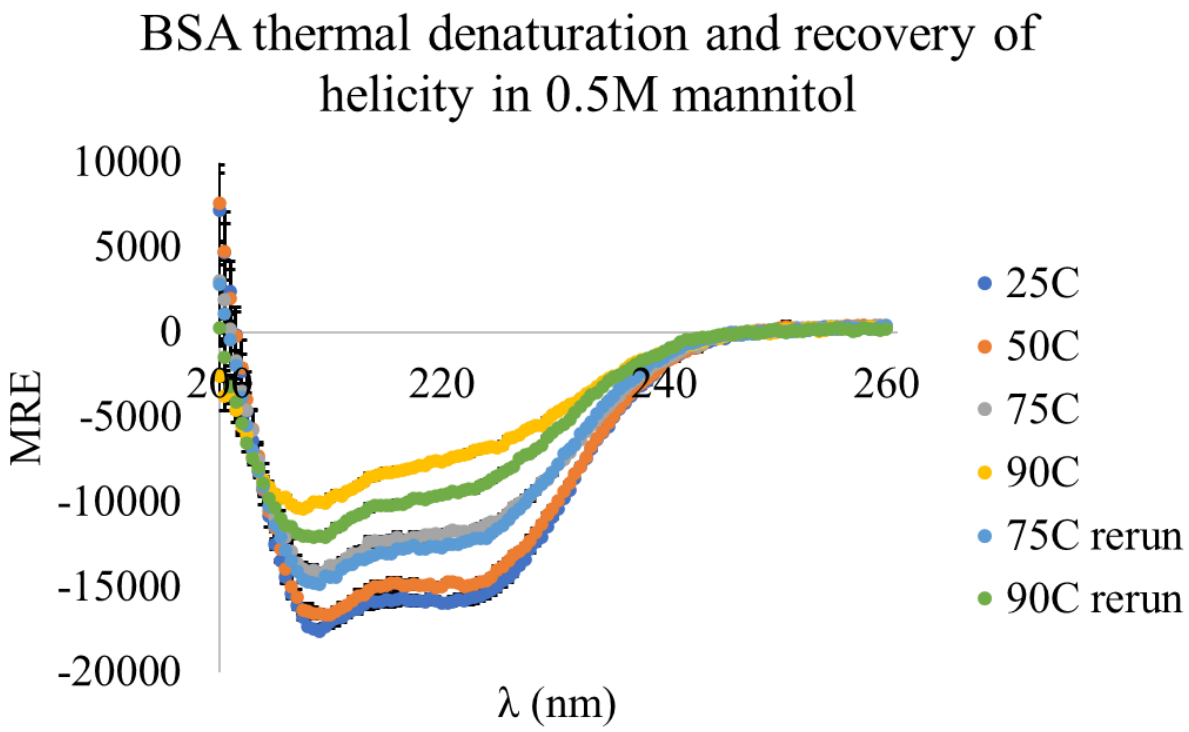

Figure 7.1. Far-UV full scan of BSA in the presence of 0.5M mannitol run at 25, 50, 75 and 90^{o}C increments then rerun at 25^{o}C (n=3).

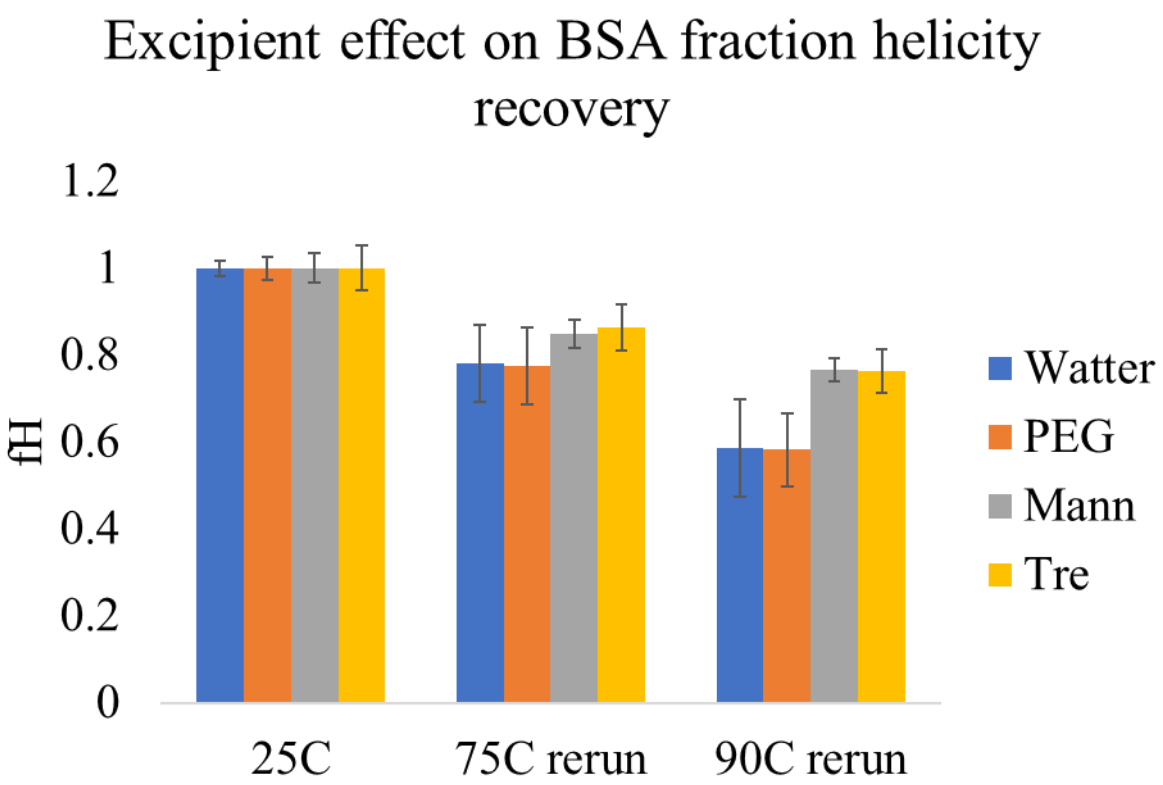

Figure 7.2. Fraction helicity recovered after heating BSA at 75ºC and 90ºC and rerun at 25ºC.

Table 7.1.
Percent recovery of BSA after heating in presence of 0.5M mannitol, trehalose, PEG400.

Temp	Buffer	Mannitol	Trehalose	PEG400
75ºC	78.2±8.85	84.9±3.29	86.3±5.28	77.6±8.83
90ºC	58.6±1.12	76.7±2.58	76.4±4.99	58.6±11.2

7.4 Summary and Conclusion

Stabilization by mannitol and trehalose reduces the concentration of unfolded helices of BSA, thereby reducing the amount of coil present in a given time frame to irreversibly fold into beta-sheet configuration allowing for less denaturation and greater recovery upon cooling. Likewise, PEG400 destabilizes helix structure (from possible interactions with hydrophobic patches of BSA) allowing for more irreversible helix unfolding.

CHAPTER 8: GENERAL DISCUSSION AND CONCLUDING REMARKS

Protein/peptide based biologics are large, complex, fragile molecules that often need to be delivered at high concentrations, need to be highly soluble, maintained at specific and narrow pH ranges, and often have poor shelf-life/transportation stability. As such, many excipients are added to biologic formulations to boost their performance, storage, and compliance profiles. These excipients can have profound effects on stability and performance as a whole and require much time and effort in order to optimize a formulation. Because of such challenges, much effort has gone into better understanding their mechanisms of stabilization of proteins and peptides, which are generally surmised to occur through preferential hydration and volume exclusion mechanisms (in the liquid state). While the general mechanisms are well understood, little effort has gone into understanding how excipients may stabilize individual features such as SS. This is important as SS features are not static elements in a biologic therapeutic, but instead are capable of unfolding and refolding. This is true of helices as well as other SS types and is significant, because upon unfolding, they are more prone to self-association, other aggregation phenomena, and degradation. In the case of helices, the more stabilized it is, the less time it will spend unfolded and will be less likely to degrade or aggregate. Understanding and quantifying mechanisms of stabilization will help expedite and improve the formulation process.

Proteins and peptides stability are largely assessed through thermal and chemical denaturation studies and generally behave similarly one to another under such stresses. Because of this, it was proposed to measure and classify common excipient effects on the thermodynamic unfolding of alpha helices using a model peptide PLL and model protein BSA. PLL is a very simple peptide polymer, that under appropriate pH and room temperature conditions will adapt a

neutral alpha-helix. Given its homopolymer and simple nature, PLL is an excellent model to assess excipient effects on helicity. BSA, is a highly helical protein that possesses a wide variety of amino acid types, hydrophobic/hydrophilic regions, and is also susceptible to aggregation which make it an excellent model protein. Model peptide and protein were tested with three common excipients: mannitol (a sugar alcohol), trehalose (a disaccharide), and PEG 400 (a polyol). All three excipients are ubiquitous in both liquid and solid formulations. All three are purported to protect and interact with peptide/proteins differently. Moreover, all formulations including solid formulations spend time as liquid formulation (reconstitution). Said peptide and protein were then put through various thermal and chemical (urea denaturation) challenges to measure excipient stabilization of alpha helices.

PLL CD studies showed CD could detect the alpha helix component of PLL, and that it could monitor changes in helicity due to thermal stress. Moreover, CD studies on PLL revealed that mannitol and trehalose protected helices enthalpically, with mannitol having a stronger effect than trehalose. These trends were largely observed as well in BSA, with mannitol again showing stronger overall stabilization than trehalose; however, at low concentrations, mannitol appeared to stabilize more through entropic means than enthalpic. PEG effects were similar in both. Not much change was observed in either, other than slight destabilization in both (except at the highest PEG concentrations for PLL). PLL was enthalpically stabilized at 0.75 M PEG400, while BSA was not, but PEG at its highest concentration did have some enthalpic stabilization though it was more than offset by entropic destabilization. Urea, as expected, was enthalpically destabilizing for PLL, but interestingly, at low to intermediate ranges, BSA was stabilized by urea. Studies with NaF at high and low concentrations confirmed that increased salt presence mitigated this stabilization effect. Furthermore, literature searches revealed that

urea possess both kosmotropic (-NH_2) and chaotropic (-CO) components and at low to intermediate concentrations the kosmotrope stabilization can dominate. As to why stabilization of PLL at low to mid urea concentration was not observed, it was attributed to the many -NH_2 on the lysine side chains which may mute the kosmotrope effects of urea -NH_2.

For PLL, the ability of excipients to protect helicity against chemical denaturation was assessed. 0.5M excipient (common concentrations of many formulations) were put with PLL with different urea gradients. It was found that mannitol could protect against chemical denaturation up to 0.5M urea. Trehalose behaved similarly but was less effective than mannitol. When looking at EEC plots, mannitol and trehalose protected initially enthalpically (region II) before becoming destabilized entropically or enthalpically (regions I and IV, respectively). PEG400 had little effect and all PLL samples showed enthalpic destabilization (region IV).

The same experiment was repeated using NMR. For NMR, changes in chemical shift were used to monitor change PLL helicity. Ultimately, it was shown that changes in helicity, as monitored with NMR, trended with those of CD, though change in helicity increased faster with NMR and there was not a perfect correlation with CD.

DSC studies were carried out with BSA due to its sensitivity and comprehensive ability to account for all thermodynamic changes due to conformational change, allowing for differences in alpha helix unfolding relative to general conformational changes. Such differences in measuring thermodynamics of unfolding allow greater elucidation of helix effects on helices. DSC results did indeed differ from those of CD. Mannitol and trehalose enthalpically stabilized BSA at all concentrations while PEG was slightly destabilizing, showing a mixture of Region II and IV stabilization/destabilization, respectively. Such differences are attributed to the additional global features of the protein undergoing thermal denaturation.

Maintaining SS structure in proteins, including helices, is vital in mitigating adverse effects such as aggregation and degradation. Stabilizing excipients can serve in this function. Heating and rerunning samples at 25ºC revealed the ability of mannitol and trehalose to protect BSA helicity while PEG400 and buffer showed greater loss of helicity. Such loss is purported to occur from self-association of beta-sheets formed from helix to coil to beta-sheet transition.

Ultimately, it was shown that the use of a model peptide and protein could be used to measure stabilization of alpha helices by excipients. This work is unique in that no previous studies have specifically addressed alpha helix stabilization by excipients and is of particular importance since it shows stabilization of helices can differ from excipient to excipient and from other general features of a protein. Another important consideration is that of the complicated nature of formulations. Categorizing excipient stabilization mechanisms at different concentrations using EEC plots can be useful strategy while developing formulations.

REFERENCES

1. *EMERGENCE OF PHARMACEUTICAL SCIENCE AND INDUSTRY: 1870-1930*. 2020.
2. *Biologics vs small molecule drugs – what's the difference?* @admescope, 2020. https://www.admescope.com/whats-new/blog/2018/biologics-vs-small-molecule-drugs-whats-the-difference.html.
3. The Biologics Revolution in the Production of Drugs. FraserInstitute: 2016.
4. *Pharmaceutical market size by chemical drugs and biologics worldwide 2014-2023 | Statista*. 2020. https://www.statista.com/statistics/1085563/revenue-chemical-drugs-and-biologics-global-pharmaceuticals/
5. Walker, N. *Biologics: Driving Force in Pharma*. 2020. https://www.pharmasalmanac.com/articles/biologics-driving-force-in-pharma
6. Arakawa, T.; Timasheff, S. N. Preferential interactions of proteins with solvent components in aqueous amino acid solutions. *Arch Biochem Biophys* **1983**, *224* (1), 169-177. From NLM.
7. Arakawa, T.; Timasheff, S. N. The stabilization of proteins by osmolytes. *Biophys J* **1985**, *47* (3), 411-414.
8. Manning, M. C.; Chou, D. K.; Murphy, B. M.; Payne, R. W.; Katayama, D. S. Stability of protein pharmaceuticals: an update. *Pharm Res* **2010**, *27* (4), 544-575. DOI: 10.1007/s11095-009-0045-6 From NLM.
9. Manning, M. C.; Liu, J.; Li, T.; Holcomb, R. E. Rational Design of Liquid Formulations of Proteins. *Adv Protein Chem Struct Biol* **2018**, *112*, 1-59. DOI: 10.1016/bs.apcsb.2018.01.005 From NLM.
10. JF, C.; MJ, P.; BS, C.; TW, R. Rational design of stable lyophilized protein formulations: some practical advice. *Pharmaceutical research* **1997**, *14* (8). DOI: 10.1023/a:1012180707283.
11. Wang, W. Instability, stabilization, and formulation of liquid protein pharmaceuticals. *Int J Pharm* **1999**, *185* (2), 129-188. From NLM.
12. Rees, D. C.; Robertson, A. D. Some thermodynamic implications for the thermostability of proteins. In *Protein Sci*, Vol. 10; 2001; pp 1187-1194. A, L.; S, H.; SS, P. An effective solvent theory connecting the underlying mechanisms of osmolytes and denaturants for protein stability. *Biophysical journal* **2011**, *100* (2). DOI: 10.1016/j.bpj.2010.11.087. Moorthy, B. S.; Schultz, S. G.; Kim, S. G.; Topp, E. M. Predicting Protein Aggregation during Storage in Lyophilized Solids Using Solid State Amide Hydrogen/Deuterium Exchange with Mass Spectrometric Analysis (ssHDX-MS). **2014**, research-article. DOI: 10.1021/mp500005v. Platts, L.; Falconer, R. J. Controlling protein stability: Mechanisms revealed using formulations of arginine, glycine and guanidinium HCl with three globular proteins. *Int J Pharm* **2015**, *486* (1-2), 131-135. DOI: 10.1016/j.ijpharm.2015.03.051 From NLM.
13. Khan, T. A.; Mahler, H. C.; Kishore, R. S. Key interactions of surfactants in therapeutic protein formulations: A review. *Eur J Pharm Biopharm* **2015**, *97* (Pt A), 60-67. DOI: 10.1016/j.ejpb.2015.09.016 From NLM.

14. HX, Z.; G, R.; AP, M. Macromolecular crowding and confinement: biochemical, biophysical, and potential physiological consequences. *Annual review of biophysics* **2008**, *37*, 375-397. DOI: 10.1146/annurev.biophys.37.032807.125817.
15. Politi, R.; Harries, D. Enthalpically driven peptide stabilization by protective osmolytes. *Chemical Communications* **2010**, *46* (35), 6649-6451. DOI: 10.1039/C0CC01763A.
16. Senske, M.; Törk, L.; Born, B.; Havenith, M.; Herrmann, C.; Ebbinghaus, S. Protein Stabilization by Macromolecular Crowding through Enthalpy Rather Than Entropy. *J. Am. Chem. Soc.* **2014**, *136* (25), 9036-9041, research-article. DOI: 10.1021/ja503205y.
17. MitsuhiroHiraiaSatoshiAjitoaMasaakiSugiyamabHirokiIwasecShin-ichiTakatadNobutaka Shimizue, N. I., Anne Martelf, Lionel Porcarf. Molecular crowding effect on protein structure and hydration clarified by using X-ray and neutron scattering. *Physica B: Condensed Matter* **2017**, 1-6. DOI: 10.1016/j.physb.2018.02.020.
18. S, U. Liquid Formulation for Antibody Drugs. *Biochimica et biophysica acta* **2014**, *1844* (11). DOI: 10.1016/j.bbapap.2014.07.016.
19. Moorthy, B. S.; Iyer, L. K.; Topp, E. M. Characterizing Protein Structure, Dynamics and Conformation in Lyophilized Solids. *Curr Pharm Des* **2015**, *21* (40), 5845-5853. From NLM. Arsiccio, A.; Paladini, A.; Pattarino, F.; Pisano, R. Designing the Optimal Formulation for Biopharmaceuticals: A New Approach Combining Molecular Dynamics and Experiments. *J Pharm Sci* **2018**, 1-8. DOI: 10.1016/j.xphs.2018.09.002 From NLM. Arsiccio, A. The Preservation of Lyophilized Human Growth Hormone Activity: how Do Buffers and Sugars Interact? | SpringerLink. **2019**. DOI: 10.1007/s11095-018-2410-9. A, A.; A, P.; F, P.; R, P. Designing the Optimal Formulation for Biopharmaceuticals: A New Approach Combining Molecular Dynamics and Experiments. *Journal of pharmaceutical sciences* **2019**, *108* (1). DOI: 10.1016/j.xphs.2018.09.002.
20. Mensink, M. A.; Frijlink, H. W.; van der Voort Maarschalk, K.; Hinrichs, W. L. How sugars protect proteins in the solid state and during drying (review): Mechanisms of stabilization in relation to stress conditions. *Eur J Pharm Biopharm* **2017**, *114*, 288-295. DOI: 10.1016/j.ejpb.2017.01.024 From NLM.
21. Shukla, D.; Trout, B. L. Interaction of Arginine with Proteins and the Mechanism by Which It Inhibits Aggregation. *J. Phys. Chem. B* **2010**, *114* (42), 13426-13438, research-article. DOI: 10.1021/jp108399g.
22. Li, Y.; Williams, T. D.; Topp, E. M. Effects of excipients on protein conformation in lyophilized solids by hydrogen/deuterium exchange mass spectrometry. *Pharm Res* **2008**, *25* (2), 259-267. DOI: 10.1007/s11095-007-9365-6 From NLM.
23. Anders Liljas (Lund University, S., Lars Liljas (Uppsala University, Sweden), Miriam-Rose Ash (The University of Sydney, Australia), Göran Lindblom (Umeå University, Sweden), Poul Nissen (Aarhus University, Denmark) and Morten Kjeldgaard (Aarhus University, Denmark). *Textbook of Structural Biology | Series in Structural Biology*; 2017. DOI: 10.1142/10102.
24. JS, R. The Anatomy and Taxonomy of Protein Structure. *Advances in protein chemistry* **1981**, *34*, 167-339. DOI: 10.1016/s0065-3233(08)60520-3.
25. Pace, C. N.; Trevino, S.; Prabhakaran, E.; Scholtz, J. M. Protein structure, stability and solubility in water and other solvents. *Philos Trans R Soc Lond B Biol Sci* **2004**, *359* (1448), 1225-1234; discussion 1234-1225. DOI: 10.1098/rstb.2004.1500 From NLM.
26. Zbacnik, T. J.; Holcomb, R. E.; Katayama, D. S.; Murphy, B. M.; Payne, R. W.; Coccaro, R. C.; Evans, G. J.; Matsuura, J. E.; Henry, C. S.; Manning, M. C. Role of Buffers in

Protein Formulations. *J Pharm Sci* **2017**, *106* (3), 713-733. DOI: 10.1016/j.xphs.2016.11.014 From NLM.
27. W, W. Lyophilization and Development of Solid Protein Pharmaceuticals. *International journal of pharmaceutics* **2000**, *203* (1-2). DOI: 10.1016/s0378-5173(00)00423-3.
28. Lee, H. J.; McAuley, A.; Schilke, K. F.; McGuire, J. Molecular origins of surfactant-mediated stabilization of protein drugs. *Adv Drug Deliv Rev* **2011**, *63* (13), 1160-1171. DOI: 10.1016/j.addr.2011.06.015 From NLM.
29. Wang, W.; Roberts, C. J. Protein aggregation - Mechanisms, detection, and control. *Int J Pharm* **2018**, *550* (1-2), 251-268. DOI: 10.1016/j.ijpharm.2018.08.043 From NLM.
30. Cao, W.; Krishnan, S.; Ricci, M. S.; Shih, L. Y.; Liu, D.; Gu, J. H.; Jameel, F. Rational design of lyophilized high concentration protein formulations-mitigating the challenge of slow reconstitution with multidisciplinary strategies. *Eur J Pharm Biopharm* **2013**, *85* (2), 287-293. DOI: 10.1016/j.ejpb.2013.05.001 From NLM.
31. Bedu-Addo, F. K. Understanding Lyophilization Formulation Development. **2018**.
32. Garidel, P.; Kuhn, A. B.; Schafer, L. V.; Karow-Zwick, A. R.; Blech, M. High-concentration protein formulations: How high is high? *Eur J Pharm Biopharm* **2017**, *119*, 353-360. DOI: 10.1016/j.ejpb.2017.06.029 From NLM. Kheddo, P.; Tracka, M.; Armer, J.; Dearman, R. J.; Uddin, S.; van der Walle, C. F.; Golovanov, A. P. The effect of arginine glutamate on the stability of monoclonal antibodies in solution. *Int J Pharm* **2014**, *473* (1-2), 126-133. DOI: 10.1016/j.ijpharm.2014.06.053 From NLM. Quigley, A.; Williams, D. The second virial coefficient as a predictor of protein aggregation propensity: A self-interaction chromatography study. In *Eur J Pharm Biopharm*, Vol. 96; 2015; pp 282-290.
33. Hung, J. J.; Dear, B. J.; Dinin, A. K.; Borwankar, A. U.; Mehta, S. K.; Truskett, T. T.; Johnston, K. P. Improving Viscosity and Stability of a Highly Concentrated Monoclonal Antibody Solution with Concentrated Proline. *Pharm Res* **2018**, *35* (7), 133. DOI: 10.1007/s11095-018-2398-1 From NLM.
34. Kamerzell, T. J.; Esfandiary, R.; Joshi, S. B.; Middaugh, C. R.; Volkin, D. B. Protein-excipient interactions: mechanisms and biophysical characterization applied to protein formulation development. *Adv Drug Deliv Rev* **2011**, *63* (13), 1118-1159. DOI: 10.1016/j.addr.2011.07.006 From NLM.
35. Ohtake, S.; Kita, Y.; Arakawa, T. Interactions of formulation excipients with proteins in solution and in the dried state. *Adv Drug Deliv Rev* **2011**, *63* (13), 1053-1073. DOI: 10.1016/j.addr.2011.06.011 From NLM.
36. Sinko, P., J. *Martin's Physical Chemistry And Pharmaceutical Sciences*; Lippincott Williams & Wilkins, 2011.
37. McQuarrie, D., A.; Simon, J., D. *Physical Chemistry A Molecular Approach*; Viva Books, 2011.
38. Prabhu, N. V.; Sharp, K. A. Heat capacity in proteins. *Annu Rev Phys Chem* **2005**, *56*, 521-548. DOI: 10.1146/annurev.physchem.56.092503.141202 From NLM.
39. Seelig, J. Cooperative protein unfolding. A statistical-mechanical model for the action of denaturants. *Biophys Chem* **2018**, *233*, 19-25. DOI: 10.1016/j.bpc.2017.12.001 From NLM.
40. P, G.; patrick.garidel@boehringer-ingelheim.com; Boehringer Ingelheim Pharma GmbH & Co. KG, I. U., PDB, Biberach an der Riss, Germany.; A, E.; M, B.; J, S.; joachim.seelig@unibas.ch; Biozentrum, U. o. B., Klingelbergstrasse 50/70, Basel,

Switzerland. Thermal and Chemical Unfolding of a Monoclonal IgG1 Antibody: Application of the Multistate Zimm-Bragg Theory. *Biophysical Journal* **2020**, *118* (5), 1067-1075. DOI: 10.1016/j.bpj.2019.12.037.

41. Li-Blatter, X.; Seelig, J. Thermal and Chemical Unfolding of Lysozyme. Multistate Zimm-Bragg Theory Versus Two-State Model. *J. Phys. Chem. B* **2019**, *2019* (123), 10181-10191. DOI: 25413.
42. J, S.; Division of Biophysical Chemistry, B., University of Basel,Klingelbergstrasse 50/70,CH-4056 Basel,Switzerland.; HJ, S.; Schönfeld - Protein Science Consulting, M., DE-79115 Freiburg,Germany. Thermal protein unfolding by differential scanning calorimetry and circular dichroism spectroscopy Two-state model versus sequential unfolding. *Quarterly Reviews of Biophysics* **2020**, *49*. DOI: 10.1017/s0033583516000044.
43. Schulthess, T.; Schönfeld, H.-J.; Seelig, J. Thermal Unfolding of Apolipoprotein A-1. Evaluation of Methods and Models. *Biochemistry* **2015**, *54* (19), 3063-3075, research-article. DOI: 10.1021/acs.biochem.5b00238.
44. S.M. Herbig, J. R. C. Asymmetric-membrane tablet coatings for osmotic drug delivery. *Journal of controlled release* **1995**, *35*, 127-136. Scholtz, J. M.; Marqusee, S.; Baldwin, R. L.; York, E. J.; Stewart, J. M.; Santoro, M.; Bolen, D. W. Calorimetric determination of the enthalpy change for the alpha-helix to coil transition of an alanine peptide in water. *Proc Natl Acad Sci U S A* **1991**, *88* (7), 2854-2858. Kypr, J.; Kejnovská, I.; Renčiuk, D.; Vorlíčková, M. Circular dichroism and conformational polymorphism of DNA. In *Nucleic Acids Res*, Vol. 37; 2009; pp 1713-1725.
45. Chandler, D. Interfaces and the driving force of hydrophobic assembly. *Nature* **2005**, *437* (7059), 640, Special Features. DOI: doi:10.1038/nature04162. N., G. S. What is the role of thermodynamics on protein stability? | SpringerLink. *Biotechnology and bioprocess Engineering* **2018**, *8* (1), 9-18. DOI: 10.1007/BF02932892.
46. Arakawa, T.; Prestrelski, S. J.; Kenney, W. C.; Carpenter, J. F. Factors affecting short-term and long-term stabilities of proteins. *Adv Drug Deliv Rev* **2001**, *46* (1-3), 307-326. From NLM.
47. Timasheff, S. N. Protein-solvent preferential interactions, protein hydration, and the modulation of biochemical reactions by solvent components. **2002**. DOI: 10.1073/pnas.122225399.
48. Arakawa, T.; Timasheff, S. N. Theory of protein solubility. *Methods Enzymol* **1985**, *114*, 49-77. From NLM.
49. Arakawa, T.; Timasheff, S. N. Stabilization of protein structure by sugars. *Biochemistry* **1982**, *21* (25), 6536-6544. From NLM.
50. Kita, Y.; Arakawa, T.; Lin, T.-Y.; Timasheff, S. N. Contribution of the Surface Free Energy Perturbation to Protein-Solvent Interactions. *Biochemistry* **2002**, *33* (50), 15178-15189, research-article. DOI: 10.1021/bi00254a029. Arakawa, T.; Timasheff, S. N. Stabilization of protein structure by sugars. *Biochemistry* **2002**, *21* (25), 6536-6544. DOI: 10.1021/bi00268a033.
51. Arakawa, T.; Bhat, R.; Timasheff, S. N. Why preferential hydration does not always stabilize the native structure of globular proteins. *Biochemistry* **1990**, *29* (7), 1924-1931. From NLM.
52. Okur, H. I.; Hladilkova, J.; Rembert, K. B.; Cho, Y.; Heyda, J.; Dzubiella, J.; Cremer, P. S.; Jungwirth, P. Beyond the Hofmeister Series: Ion-Specific Effects on Proteins and

Their Biological Functions. *J Phys Chem B* **2017**, *121* (9), 1997-2014. DOI: 10.1021/acs.jpcb.6b10797 From NLM.

53. Marcus, Y. Effect of ions on the structure of water: structure making and breaking. *Chem Rev* **2009**, *109* (3), 1346-1370. DOI: 10.1021/cr8003828 From NLM.
54. Sotomayor-Pérez, A.-C.; Subrini, O.; Hessel, A.; Ladant, D.; Chenal, A. Molecular Crowding Stabilizes Both the Intrinsically Disordered Calcium-Free State and the Folded Calcium-Bound State of a Repeat in Toxin (RTX) Protein. *J. Am. Chem. Soc.* **2013**, *135* (32), 11929-11934, research-article. DOI: 10.1021/ja404790f.
55. IM, K.; BY, Z.; L, B.; KK, T.; VN, U. Beyond the excluded volume effects: mechanistic complexity of the crowded milieu. *Molecules (Basel, Switzerland)* **2015**, *20* (1). DOI: 10.3390/molecules20011377.
56. Knowles, D. B.; LaCroix, A. S.; Deines, N. F.; Shkel, I.; Record, M. T. Separation of preferential interaction and excluded volume effects on DNA duplex and hairpin stability. *proceedings of the National Academy of Sciences of the United States of America* **2011**. DOI: 10.1073/pnas.1103382108.
57. Minton, A., P. Excluded volume as a determinant of macromolecular structure and reactivity - Minton - 1981 - Biopolymers - Wiley Online Library. *Biopolymers* **2021**, *20* (10), 2093-2120. DOI: 10.1002/bip.1981.360201006.
58. Akers, M. J. Excipient-drug interactions in parenteral formulations. *J Pharm Sci* **2002**, *91* (11), 2283-2300. DOI: 10.1002/jps.10154 From NLM.
59. Tandon, S.; PM, H. Detergent-assisted refoding of guanidinium chloride-denatured Rhodanese. *J. Biol Chem* **1987**, *262* (10), 4486-4491.
60. Chou, D. K.; Krishnamurthy, R.; Randolph, T. W.; Carpenter, J. F.; Manning, M. C. Effects of Tween 20 and Tween 80 on the stability of Albutropin during agitation. *J Pharm Sci* **2005**, *94* (6), 1368-1381. DOI: 10.1002/jps.20365 From NLM.
61. Bam, N. B.; Cleland, J. L.; Randolph, T. W. Molten globule intermediate of recombinant human growth hormone: stabilization with surfactants. *Biotechnol Prog* **1996**, *12* (6), 801-809. DOI: 10.1021/bp960068b From NLM.
62. Hoffmann, C.; Blume, A.; Miller, I.; Garidel, P. Insights into protein-polysorbate interactions analysed by means of isothermal titration and differential scanning calorimetry. *Eur Biophys J* **2009**, *38* (5), 557-568. DOI: 10.1007/s00249-009-0404-6 From NLM.
63. Kim, Y. S.; Jones, L. S.; Dong, A.; Kendrick, B. S.; Chang, B. S.; Manning, M. C.; Randolph, T. W.; Carpenter, J. F. Effects of sucrose on conformational equilibria and fluctuations within the native-state ensemble of proteins. *Protein Sci* **2003**, *12* (6), 1252-1261. DOI: 10.1110/ps.0242603 From NLM.
64. Arsiccio, A.; Pisano, R. Surfactants as stabilizers for biopharmaceuticals: An insight into the molecular mechanisms for inhibition of protein aggregation. *Eur J Pharm Biopharm* **2018**, *128*, 98-106. DOI: 10.1016/j.ejpb.2018.04.005 From NLM.
65. Williams, D. A. *Foye's Principles of Medicinal Chemistry*; LWW, 2012.
66. Taehun Hong, K. I. Viscosity Control of Protein Solution by Small Solutes: A Review. *Current Protein & Peptide Science* **2018**, *19* (8), 746-758. DOI: 10.2174/1389203719666171213114919.
67. W, W.; S, S.; DL, Z.; K, K.; S, N. Antibody structure, instability, and formulation. *Journal of pharmaceutical sciences* **2007**, *96* (1). DOI: 10.1002/jps.20727.

68. Alam, M.; Barnett, G. V.; Slaney, T. R.; Starr, C. G.; Das, T. K.; Tessier, P. M. Deamidation Can Compromise Antibody Colloidal Stability and Enhance Aggregation in a pH-Dependent Manner. **2019**, research-article. DOI: 10.1021/acs.molpharmaceut.8b01311.
69. Arsiccio, A.; Pisano, R. Stability of Proteins in Carbohydrates and Other Additives during Freezing: The Human Growth Hormone as a Case Study. *J Phys Chem B* **2017**, *121* (37), 8652-8660. DOI: 10.1021/acs.jpcb.7b05541 From NLM.
70. Souillac, P. O.; Middaugh, C. R.; Rytting, J. H. Investigation of protein/carbohydrate interactions in the dried state. 2. Diffuse reflectance FTIR studies. *Int J Pharm* **2002**, *235* (1-2), 207-218. From NLM. Carpenter, J. F.; Crowe, J. H. An infrared spectroscopic study of the interactions of carbohydrates with dried proteins. *Biochemistry* **1989**, *28* (9), 3916-3922. From NLM. Lu, J.; Wang, X.; Liu, Y.; Ching, C. Thermal and FTIR investigation of freeze-dried protein-excipient mixtures. *http://dx.doi.org/10.1007/s10973-006-7598-y* **2006**, research-article. DOI: 8554283437774737.
71. @pharmareview. Excipient selection in biologics and vaccines formulation development. *European Pharmaceutical Review* **2020**.
72. Wang, W. Advanced protein formulations. *Protein Sci* **2015**, *24* (7), 1031-1039.
73. Schneider, C. P.; Shukla, D.; Trout, B. L. Arginine and the Hofmeister Series: The Role of Ion–Ion Interactions in Protein Aggregation Suppression. *J. Phys. Chem B* **2011**, *115* (22), 7447-7458, research-article. DOI: 10.1021/jp111920y.
74. Myers, J. K.; Pace, C. N.; Scholtz, J. M. Denaturant m values and heat capacity changes: relation to changes in accessible surface areas of protein unfolding. *Protein Sci* **1995**, *4* (10), 2138-2148.
75. Tripathi, T. CALCULATION OF THERMODYNAMIC PARAMETERS OF PROTEIN UNFOLDING USING FAR-ULTRAVIOLET CIRCULAR DICHROMISM. *Journal of proteins and proteiomics* **2013**, *4* (2), 85-91.
76. Zimm, B. H.; Bragg, J. K. Theory of the Phase Transition between Helix and Random Coil in Polypeptide Chains. *JChPh* **1959**, *31*, 526-535. DOI: doi:10.1063/1.1730390.
77. Schellman, J. A. The Factors Affecting the Stability of Hydrogen-bonded Polypeptide Structures in Solution. *J. Phys. Chem.* **1958**, *62* (12), 1485-1494. DOI: 10.1021/j150570a005. Lifson, S.; Roig, A. On the Theory of Helix—Coil Transition in Polypeptides. *J. Chem. Phys.* **1961**, *34*, 1963-1974, research-article. DOI: 1.1731802.
78. Scholtz, J. M.; Barrick, D.; York, E. J.; Stewart, J. M.; Baldwin, R. L. Urea unfolding of peptide helices as a model for interpreting protein unfolding. *Proc Natl Acad Sci U S A* **1995**, *92* (1), 185-189.
79. AS, Y.; B, H. Free Energy Determinants of Secondary Structure Formation: I. Alpha-Helices. *Journal of molecular biology* **1995**, *252* (3). DOI: 10.1006/jmbi.1995.0502. AS, Y.; B, H. Free Energy Determinants of Secondary Structure Formation: II. Antiparallel Beta-Sheets. *Journal of molecular biology* **1995**, *252* (3). DOI: 10.1006/jmbi.1995.0503.
80. SM, K.; TJ, J.; NC, P. How to Study Proteins by Circular Dichroism. *Biochimica et biophysica acta* **2005**, *1751* (2). DOI: 10.1016/j.bbapap.2005.06.005.
81. Greenfield, N., J. Applications of circular dichromism in protein and peptide analysis. *Trends in analytical chemistry* **1999**, *18* (4), 236-244.
82. NJ, G. Circular dichroism (CD) analyses of protein-protein interactions. *Methods in molecular biology (Clifton, N.J.)* **2015**, *1278*. DOI: 10.1007/978-1-4939-2425-7_15.

83. Greenfield, N. J. Using circular dichroism spectra to estimate protein secondary structure. *Nat Protoc* **2006**, *1* (6), 2876-2890. DOI: 10.1038/nprot.2006.202.
84. Y, W.; AA, T.; RA, L. Protein helical structure determination using CD spectroscopy for solutions with strong background absorbance from 190 to 230nm. *Biochimica et biophysica acta* **2014**, *1844* (12). DOI: 10.1016/j.bbapap.2014.10.001.
85. Greenfield, N. J. Using circular dichroism collected as a function of temperature to determine the thermodynamics of protein unfolding and binding interactions. *Nat Protoc* **2006**, *1* (6), 2527-2535. DOI: 10.1038/nprot.2006.204.
86. Bayat, M.; Gourabi, H.; Khammari, A.; Ahmad, F.; Saboury, A. A. A comparative study of structure, stability and function of sc-tenecteplase in the presence of stabilizing osmolytes. *J Biotechnol* **2018**, *280*, 1-10. DOI: 10.1016/j.jbiotec.2018.05.014 From NLM. Nicholas E. Shepherd; Huy N. Hoang; Giovanni Abbenante, a.; Fairlie*, D. P. Single Turn Peptide Alpha Helices with Exceptional Stability in Water. *J. Am. Chem. Soc.* **2005**, *127* (9), 2974-2983, research-article. DOI: 10.1021/ja0456003.
87. Correcirc, D. H. A.; a; Ramos, C. H. I. The use of circular dichroism spectroscopy to study protein folding, form and function. *African Journal of Biochemistry Research* **2009**, *3* (5), 164-173, Full Length Research Paper. DOI: 15798EB10962.
88. Nicklassson, M. Robust and convenient analysis of protein thermal and chemical stability - Niklasson - 2015 - Protein Science - Wiley Online Library. *Protein Sci* **2021**, *24* (12), 2055-2062. DOI: 10.1002/pro.2809.
89. Skoog, D., A.; Holler, J., F.; Nieman, T., A. *Principles of Instrumental Analysis*; 1998.
90. GEROTHANASSIS, I. P.; TROGANIS, A.; EXARCHOU, V.; BARBAROSSOU, K. NUCLEAR MAGNETIC RESONANCE (NMR) SPECTROSCOPY: BASIC PRINCIPLES AND PHENOMENA, AND THEIR APPLICATIONS TO CHEMISTRY, BIOLOGY AND MEDICINE. **2002**, *3* (2), 229-252. DOI: 10.1039/B2RP90018A.
91. McQuarrie, D., A.; Simon, J., D. Physical Chemistry. 1998; pp 547-576.
92. MP, W.; T, A.; E, N.; M, D. A method for the calculation of protein alpha-CH chemical shifts. *Journal of biomolecular NMR* **1992**, *2* (1). DOI: 10.1007/BF02192802.
93. DS, W.; DA, C. Use of Chemical Shifts in Macromolecular Structure Determination. *Methods in enzymology* **2001**, *338*, 35-81. DOI: 10.1016/s0076-6879(02)38214-4.
94. Szilágyi, L. Chemical shifts in proteins come of age. *Progresss in Nuclear Magnetic Resonances Spectroscopy* **1995**, *27* (4), 325-443.
95. Edelhoch, H. Spectroscopic Determination of Tryptophan and Tyrosine in Proteins*. **1967**. DOI: 10.1021/bi00859a010.
96. Baxter, N. J.; Williamson, M. P. Temperature dependence of 1 H chemical shifts in proteins. *Journal of Biomolecular NMR* **2020**, *9* (4), 359-369, OriginalPaper. DOI: doi:10.1023/A:1018334207887.
97. SP, M.; VV, K. Characterization of protein secondary structure from NMR chemical shifts. *Progress in nuclear magnetic resonance spectroscopy* **2009**, *54* (3-4). DOI: 10.1016/j.pnmrs.2008.06.002.
98. Szilágyi, L.; Jardetzky, O. α-Proton chemical shifts and secondary structure in proteins. *Journal of Magnetic Resonance* **1988**, *83* (3), 441-449. DOI: doi.org/10.1016/0022-2364(89)90341-7
99. Iwadate, M.; Asakura, T.; Williamson, M. P. Cα and Cβ Carbon-13 Chemical Shifts in Proteins From an Empirical Database. *Journal of Biomolecular NMR* **2021**, *13* (3), 199-211, OriginalPaper. DOI: doi:10.1023/A:1008376710086.

100. Abzalimov, R. R.; Kaplan, D. A.; Easterling, M. L.; Kaltashov, I. A. Protein conformations can be probed in top-down HDX MS experiments utilizing electron transfer dissociation of protein ions without hydrogen scrambling. *J Am Soc Mass Spectrom* **2009**, *20* (8), 1514-1517. DOI: 10.1016/j.jasms.2009.04.006 From NLM. Wei, H.; Mo, J.; Tao, L.; Russell, R. J.; Tymiak, A. A.; Chen, G.; Iacob, R. E.; Engen, J. R. Hydrogen/deuterium exchange mass spectrometry for probing higher order structure of protein therapeutics: methodology and applications. *Drug Discov Today* **2014**, *19* (1), 95-102. DOI: 10.1016/j.drudis.2013.07.019 From NLM. Gessner, C.; Steinchen, W.; Bédard, S.; Skinner, J. J.; Woods, V. L.; Walsh, T. J.; Bange, G.; Pantazatos, D. P. Computational method allowing Hydrogen-Deuterium Exchange Mass Spectrometry at single amide Resolution. *Scientific Reports* **2017**, *7* (1), 1-10, OriginalPaper. DOI: doi:10.1038/s41598-017-03922-3. Oganesyan, I.; Lento, C.; Wilson, D. J. Contemporary hydrogen deuterium exchange mass spectrometry. *Methods* **2018**, *144*, 27-42. DOI: 10.1016/j.ymeth.2018.04.023 From NLM.

101. Cieslik-Bockzula, K. Alpha-helix to beta-sheet transition in long-chain poly-l-lysine: Formation of alpha-helical fibrils by poly-l-lysine. *Biochime* **2017**, *137*, 106-114. DOI: doi: 10.1016/j.biochi.2017.03.006.

102. Boczula-Cieslik, K.; Rospenk, M. Interaction of anesthetic molecules with α-helix and polyproline II extended helix of long-chain poly-l-lysine. *Spectrochimica Acta Part A: Molecular and Biomolecular Spectroscopy* **2018**, *189* (2018), 436-442. DOI: 10.1016/j.saa.2017.08.045.

103. Ma, L.; Hong Zhenmin, H.; Sanford, A. UV resonance Raman studies of the NaClO4 dependence of poly-L-lysine conformation and hydrogen exchange kinetics. *The Journal of Physical Chemistry B* **2011**, *116*, 1134-1142. DOI: 10.1021/jp208918n. Lu Ma, Z. A., and Sanford A. Asher. UV Resonance Raman Study of Side Chain Electrostatic Control of Poly-L-Lysine Conformation. *The Journal of Physical Chemistry B* **2011**, *115*, 4251-4258. DOI: 10.102/jp2005343.

104. Davidson, B.; Fasman, G., D. The Conformational Transitions of Uncharged Poly-L-lysine. α Helix-Random Coil-β Structure. *Biochemistry* **1967**, *6* (6), 1616-1629. DOI: doi.org/10.1021/bi00858a008.

105. Bekard, I. B.; Barnham, K. J.; White, L. R.; Dunstan, D. E. α-Helix unfolding in simple shear flow. **2010**. DOI: 10.1039/C0SM00692K.

106. Kaushik, J. K.; Bhat, R. Why is trehalose an exceptional protein stabilizer? An analysis of the thermal stability of proteins in the presence of the compatible osmolyte trehalose. *J Biol Chem* **2003**, *278* (29), 26458-26465. DOI: 10.1074/jbc.M300815200 From NLM.

107. S, S.; L, S.; R, G.-P.; D, H. Diversity in the mechanisms of cosolute action on biomolecular processes. *Faraday discussions* **2013**, *160*. DOI: 10.1039/c2fd20101a.

108. Knowles, D. B.; Shkel, I. A.; Phan, N. M.; Sternke, M.; Lingeman, E.; Cheng, X.; Cheng, L.; O'Connor, K.; Record, M. T. Chemical Interactions of Polyethylene Glycols (PEGs) and Glycerol with Protein Functional Groups: Applications to Effects of PEG and Glycerol on Protein Processes. *Biochemistry* **2015**, *54* (22), 3528-3542, research-article. DOI: 10.1021/acs.biochem.5b00246.

109. Ionova Y, W. L. Biologic excipients: Importance of clinical awareness of inactive ingredients. In *PLoS One.*, 2020; Vol. 15, p (6):e0235076.

110. Rational Selection of Sugars for Biotherapeutic Stabilization: A Practitioner's Perspective - BioProcess International. 2018.

111. Olsson, C.; Jansson, H.; Swenson, J. The Role of Trehalose for the Stabilization of Proteins. *Physical Chemistry B* **2016**, *120* (20), 4723-4731, research-article. DOI: 10.1021/acs.jpcb.6b02517.
112. Canchi, D. R.; Rensselaer Polytechnic Inst, T., NY, USA; Jayasimha, P.; Rensselaer Polytechnic Inst, T., NY, USA; Rao, D. C.; NICHHD, N. I. o. H., Bethesda, MD, USA; Makhatadze, G. I.; Rensselaer Polytechnic Inst, T., NY, USA; Garcia, A. E.; Rensselaer Polytechnic Inst, T., NY, USA. Molecular Mechanism for the Preferential Exclusion of Osmolytes from Protein Surfaces. *Biophysical Journal* **2013**, *104* (2), 189a. DOI: 10.1016/j.bpj.2012.11.1065.
113. D. J. F.; M. Thomas Record, J., #,‡. Thermal and Urea-Induced Unfolding of the Marginally Stable Lac Repressor DNA-Binding Domain: A Model System for Analysis of Solute Effects on Protein Processes†. *Biochemistry* **2003**, *42* (7), 2202-2217, research-article. DOI: 10.1021/bi0270992.
114. Subramanian, S.; Golla, H.; Divakar, K.; Kannan, A.; Sancho, D. d.; Naganathan, A. N. Slow Folding of a Helical Protein: Large Barriers, Strong Internal Friction, or a Shallow, Bumpy Landscape? *J. Phys. Chem. B 2020* **2020**, *124* (41), 8973-8983, research-article. DOI: 10.1021/acs.jpcb.0c05976.
115. TM, D.; M, C.; M, S.; V, M. The effect of electrostatics on the marginal cooperativity of an ultrafast folding protein. *The Journal of biological chemistry* **2010**, *285* (45). DOI: 10.1074/jbc.M110.154021.
116. DS, W.; BD, S.; FM, R. Simple techniques for the quantification of protein secondary structure by 1H NMR spectroscopy. *FEBS letters* **1991**, *293* (1-2). DOI: 10.1016/0014-5793(91)81155-2.
117. Perczel, A.; Hollosi, M.; Tusnady, G.; Fasman, G. D. Convex constraint analysis: a natural deconvolution of circular dichroism curves of proteins. *Protein Eng* **1991**, *4* (6), 669-679. From NLM.
118. Myer, Y. P. The pH-Induced Helix-Coil Transition of Poly-L-lysine and Poly-L-glutamic Acid and the 238-mμ Dichroic Band. *Macromolecules* **2002**, *2* (6), 624-628. DOI: 10.1021/ma60012a012.
119. Xuan, Y.; Jiang, G.; Li, Y.; Yang, L.; Zhang, X. Biodegradable oligo (poly-L-lysine) as a high-performance hydration inhibitor for shale. *RSC Advances* **2015**, *5*, 84947-. DOI: 10.1039/C5RA16003K.
120. Blanco, F. J.; Herranz, J.; Gonzalez, C.; Jimenez, M. A.; Rico, M.; Santoro, J.; Nieto, J. L. NMR chemical shifts: a tool to characterize distortions of peptide and protein helices. *J. Am. Chem. Soc* **2002**, *114* (24), 9676-9677. DOI: 10.1021/ja00050a067.
121. WÜTHRICH, A. P. G. W. K. Protein conformation and proton nuclear-magnetic-resonance chemical shifts - PARDI - 1983 - European Journal of Biochemistry - Wiley Online Library. *European Journal of Biochemistry* **1983**, (137), 445-454. DOI: 10.1111/j.1432-1033.1983.tb07848.x.
122. Cavalli, A.; Salvatella, X.; Dobson, C. M.; Vendruscolo, M. Protein structure determination from NMR chemical shifts. **2007**. DOI: 10.1073/pnas.0610313104. Hong, J.; Jing, Q.; Yao, L. The protein amide (1)H(N) chemical shift temperature coefficient reflects thermal expansion of the N-H...O=C hydrogen bond. *J Biomol NMR* **2013**, *55* (1), 71-78. DOI: 10.1007/s10858-012-9689-3 From NLM.

123. Chauhan, V., M.; Zhang, H.; Dalby, P., A.; Aylott, J., W. Advancements in the co-formulation of biologic therapeutics. *J. Control Release* **2020**, (327), 397-405. DOI: 10.1016/j.jconrel.2020.08.013.
124. Lumry, R.; Rajender, S. Enthalpy–entropy compensation phenomena in water solutions of proteins and small molecules: A ubiquitous properly of water - Lumry - 1970 - Biopolymers - Wiley Online Library. *Biop* **1970**, (9), 1125-1227. DOI: 10.1002/bip.1970.360091002. Litian, F.; Freire, E. On the Origin of the Enthalpy and Entropy Convergence Temperatures in Protein Folding. *Proceedings of the National Academy of Sciences of the United States of America* **2021**, *89* (19), 9335-9338. and, B. L.; Kromhout, R. A. Statistical Mechanical Approach to the Conformational Heat Capacity and Enthalpy of Biomolecules. *J. Phys. Chem. B* **1999**, *1999* (103), research-article. DOI: 10.1021/jp9923724. L, L.; C, Y.; QX, G. A study on the enthalpy-entropy compensation in protein unfolding. *Biophysical chemistry* **2000**, *84* (3), 11122-11130. DOI: 10.1016/s0301-4622(00)00130-7.
125. Dragan, A. I.; Read, C. M.; Crane-Robinson, C. Enthalpy–entropy compensation: the role of solvation. *European Biophysics Journal* **2016**, *46* (4), 301-308, ReviewPaper. DOI: doi:10.1007/s00249-016-1182-6.
126. L, L.; C, Y.; QX, G. A study on the enthalpy-entropy compensation in protein unfolding. *Biophysical chemistry* **2000**, *84* (3). DOI: 10.1016/s0301-4622(00)00130-7.
127. Mills, E. A.; Plotkin, S. S. Protein Transfer Free Energy Obeys Entropy-Enthalpy Compensation. *J. P* **2015**, *119* (44), 14130-14144, research-article. DOI: 10.1021/acs.jpcb.5b09219.
128. Fox, J. M.; Zhao, M.; Fink, M. J.; Kang, K.; Whitesides, G. M. The Molecular Origin of Enthalpy/Entropy Compensation in Biomolecular Recognition. *https://doi.org/10.1146/annurev-biophys-070816-033743* **2018**, *47*, 223-250, review-article. DOI: 10.1146/annurev-biophys-070816-033743.
129. Prechl, J. Thermodynamic projection of the antibody interaction network: The fountain energy landscape of molecular interaction systems. *F1000Research 2018 6:1675* **2018**, *6* (1675), text. DOI: doi:10.12688/f1000research.12614.2.
130. TS, O.; JE, L.; WR, P.; MA, W. Extent of enthalpy-entropy compensation in protein-ligand interactions. *Protein science : a publication of the Protein Society* **2011**, *20* (9). DOI: 10.1002/pro.692.
131. Zhao, T., Miao, Z., Wang, Z., Xu, Y., Wu, J., Liu, X., You, Y., Li, J. CARMA3 overexpression accelerates cell proliferation and inhibits paclitaxel-induced apoptosis through NF-κB regulation in breast cancer cells. *Tumor Biology* **2013**, *34* (5), 3041-3047. DOI: 10.1007/s13277-013-0869-x.
132. Wen, L.; Zheng, X.; Wang, X.; Lan, H.; Yin, Z. Bilateral Effects of Excipients on Protein Stability: Preferential Interaction Type of Excipient and Surface Aromatic Hydrophobicity of Protein. *Pharm Res* **2017**, *34* (7), 1378-1390. DOI: 10.1007/s11095-017-2152-0 From NLM. P, B.; A, K. Thermodynamic investigations of protein's behaviour with ionic liquids in aqueous medium studied by isothermal titration calorimetry. *Biochimica et biophysica acta* **2016**, *1860* (5). DOI: 10.1016/j.bbagen.2015.08.022.
133. Borzova, V. A.; Markossian, K. A.; Kleymenov, S. Y.; Kurganov, B. I. A change in the aggregation pathway of bovine serum albumin in the presence of arginine and its derivatives. *Sci Rep* **2017**, *7* (1), 3984. DOI: 10.1038/s41598-017-04409-x From NLM.

134. Giancola, C.; De Sena, C.; Fessas, D.; Graziano, G.; Barone, G. DSC studies on bovine serum albumin denaturation. Effects of ionic strength and SDS concentration. *Int J Biol Macromol* **1997**, *20* (3), 193-204. From NLM.
135. K, M.; M, T. Heat-induced secondary structure and conformation change of bovine serum albumin investigated by Fourier transform infrared spectroscopy. *Biochemistry* **2004**, *43* (36), 11526-11532. DOI: 10.1021/bi0489154.
136. Hédoux, A.; Willart, J.-F.; Paccou, L.; Guinet, Y.; Affouard, F.; Lerbret, A.; Descamps, M. Thermostabilization Mechanism of Bovine Serum Albumin by Trehalose. *J. Phys. Chem. B* **2009**, *113* (7), 6119-6126, research-article. DOI: 10.1021/jp900330r.
137. Das, A.; Basak, P.; Pattanayak, R.; Kar, T.; Majumder, R.; Pal, D.; Bhattacharya, A.; Bhattacharyya, M.; Banik, S. P. Trehalose induced structural modulation of Bovine Serum Albumin at ambient temperature. *Int J Biol Macromol* **2017**, *105* (Pt 1), 645-655. DOI: 10.1016/j.ijbiomac.2017.07.074 From NLM.
138. Takeda, K.; Wada, A.; Yamamoto, K.; Moriyama, Y.; Aoki, K. Conformational change of bovine serum albumin by heat treatment. *Journal of Protein Chemistry* **1989**, *8* (5), 653-659, OriginalPaper. DOI: doi:10.1007/BF01025605.
139. Adel, A.; Nadia, M.; Mohamed, O.; Abdelhafidh, G. Study of thermally and chemically unfolded conformations of bovine serum albumin by means of dynamic light scattering. *Materials Science and Engineering C* **2008**, *28* (28), 594-600.
140. SP, R.; KG, D. K. A model for the denaturation and aggregation of beta-lactoglobulin. *European journal of biochemistry* **1994**, *226* (3). DOI: 10.1111/j.1432-1033.1994.00883.x.
141. Shiraga, K.; Ogawa, Y.; Tanaka, K.; Arikawa, T.; Yoshikawa, N.; Nakamura, M.; Ajito, K.; Tajima, T. Coexistence of Kosmotropic and Chaotropic Impacts of Urea on Water As Revealed by Terahertz Spectroscopy. *J. Phys. Chem. B* **2018**, *122* (3), 1268-1277, research-article. DOI: 10.1021/acs.jpcb.7b11839.
142. MY, K.; SK, A.; S, H. Urea-induced structural transformations in bovine serum albumin. *Journal of biochemistry* **1987**, *102* (2), 313-317. DOI: 10.1093/oxfordjournals.jbchem.a122056.
143. Liepinsh, E.; Otting, G. Specificity of Urea Binding to Proteins. *J. Am. Chem Soc.* **1994**, *116* (2), 9670-9674. DOI: 10.1021/ja00100a036.
144. Itri, R.; Caetano, W.; Barbosa, L. R. S.; Baptista, M. S. Effect of urea on bovine serum albumin in aqueous and reverse micelle environments investigated by small angle X-ray scattering, fluorescence and circular dichroism. *Brazilian Journal of Physics* **2004**, *34* (1), 58-63. DOI: 10.1590/S0103-97332004000100009.
145. N, G.; P, S.; None, K.-U.-D.; RH, K. Effect of physiological concentration of urea on the conformation of human serum albumin. *Journal of biochemistry* **2007**, *141* (2), 261-268. DOI: 10.1093/jb/mvm027.
146. Privalov, G.; Kavina, V.; Freire, E.; Privalov, P. L. Precise Scanning Calorimeter for Studying Thermal Properties of Biological Macromolecules in Dilute Solution. *Analytical Biochemistry* **1995**, *232* (1), 79-85. DOI: doi.org/10.1006/abio.1995.9957.
147. VA, B.; KA, M.; NA, C.; SY, K.; NB, P.; KO, M.; VA, S.-M.; VV, S.; DI, M.; BI, K. Kinetics of Thermal Denaturation and Aggregation of Bovine Serum Albumin. *PloS one* **2016**, *11* (4). DOI: 10.1371/journal.pone.0153495.

148. M, D.; N, K. Selective inhibition of aggregation/fibrillation of bovine serum albumin by osmolytes: Mechanistic and energetics insights. *PloS one* **2017**, *12* (2). DOI: 10.1371/journal.pone.0172208.
149. Takeda, K.; Wada, A.; Yamamoto, K.; Moriyama, Y.; Aoki, K. Conformational change of bovine serum albumin by heat treatment. *Journal of Protein Chemistry* **2021**, *8* (5), 653-659, OriginalPaper. DOI: doi:10.1007/BF01025605.